MAMMALIAN MODELS OF DUCHENNE MUSCULAR DYSTROPHY: AN INVESTIGATION ON THE NEUROMUSCULAR JUNCTION AND CARDIAC FUNCTIONALITY

A Dissertation

by

SETH GREGORY HADDIX

Submitted to the Office of Graduate and Professional Studies of
Texas A&M University
in partial fulfillment of the requirements for the degree of

DOCTOR OF PHILOSOPHY

Chair of Committee,	Mark Zoran
Committee Members,	Wesley J. Thompson
	Joe N. Kornegay
	Uel J. McMahan
	Peter Nghiem
Interdisciplinary Program Chair,	Michael Smotherman

December 2019

Major Subject: Neuroscience

ABSTRACT

Duchenne muscular dystrophy (DMD) is muscle wasting disease that leads to early mortality in humans. It results from the absence of the protein dystrophin at the membrane, specifically the contractile cells of skeletal and heart muscle. Due to the lack of dystrophin, skeletal and cardiac myocytes have an increased susceptibility to contraction-related injury, bringing about cycles of degeneration and regeneration. With disease progression, regeneration fails and muscle is replaced by fibrotic and adipose tissue, which ultimately leads to muscle weakness. Investigations of skeletal muscle in DMD have generally ignored the neuromuscular junction (NMJ). The synapse is essential in proper skeletal muscle contraction. The NMJ in dystrophy is abnormal. The synapse forms non-continuous "islands" or fragments as compared to normal pretzel-like structures. Whether these fragmented NMJs are causative in disease progression has yet to be resolved and may represent a therapeutic target for disease amelioration. My studies extend understanding of DMD models by investigating the NMJ abnormalities in dystrophic mice and dogs, as well as cardiac muscle function in the former.

The work in presented provides a comprehensive description of NMJ morphological features in mdx, a murine DMD model, and golden retriever muscular dystrophy (GRMD), a canine model. Using confocal microscopy, I compare the normal architecture and pathophysiology of diseased NMJs to normal. Junction structural changes are progressive with age in mdx, paralleling overall disease progression and severity and are similar to GRMD synapses. Using a technique that measures the

replacement of acetylcholine receptors (ACHRs) via their in vivo labeling, I show that receptor replacement is correlated with NMJ remodeling. I also report that dystrophic NMJ remodeling is initiated by muscle injury near the synaptic area. Isometric contraction force recording measurements of various muscles in geriatric mdx mice suggests that contractile function is unperturbed even in the face of synaptic remodeling. The cardiac function, as assessed by echocardiography and speckle tracking is dysfunctional in geriatric mdx hearts. I conclude that arresting NMJ remodeling caused by muscular dystrophy is not a viable therapeutic approach, but that the process is likely held in all mammals that lack dystrophin, including DMD boys.

DEDICATION

To my mentor Wesley J. Thompson, PhD

December 10th, 1947 – March 26th, 2019

It would be impossible to ask for a better person to have worked with than Wes. He wasn't able to see this project at its completion, but spent immeasurable hours toiling on it. He kept me from completely abandoning the project on multiple occasions when it seemed nothing would come of the work, always pressing me to look at the research from a different perspective. Not only was he an exceptional scientist, intellectual, and mentor, he was a better friend. Fridays in the Thompson Lab weren't so much about wrapping up the weeks work, but more in having Wes regale us with his views on the world, music and film, and generally banter with the lab until it was time to go home. Cultural Fridays. He was truly a renaissance man and is sorely missed.

ACKNOWLEDGEMENTS

I would like to thank my current committee chair, Dr. Mark Zoran, my former committee chair, Dr. Wesley J. Thompson, and my committee members Drs. Joe N. Kornegay, Uel Jackson McMahan, and Peter Nghiem for their feedback and insight during the progression from experiment proposal to dissertation write up.

I would also like to thank my lab-mates and friends, Dr. Young il Lee, Ian Smith, Ryan Massopust, and Robert Louis Hastings for their support and help in conducting this research, as well as their personal friendship.

Thanks to the Texas A&M Institute for Neuroscience for acceptance into their program and introducing me to a community of excellent neuroscientists.

Finally, thank you to my family, but especially to my mother and father, who have been there not only through the ups and downs of my graduate school career but ups and downs of 30 years of life, and who instilled in me a desire to ask questions and a measure of self-reliance.

CONTRIBUTORS AND FUNDING SOURCES

Contributors

This work was supervised by a dissertation committee of Professors Mark Zoran, Wesley J. Thompson, and Uel Jackson McMahan of the Biology Department, and Professors Joe N. Kornegay and Peter Nghiem of the Department of Veterinary Integrative Biosciences.

Experimental design for all sections was discussed between Dr. Wesley J. Thompson and Seth Haddix, with invaluable input from the dissertation committee as well as lab members Dr. Young il Lee, Ian Smith, Ryan Massopust, and Robert Louis Hastings.

Confocal images presented in Sections 2 and 4 were in part collected by Drs. Wesley J. Thompson and Young il Lee. Force recordings in Section 4 were in part collected by Drs. Wesley J. Thompson and Young il Lee. Echocardiography presented in Section 4 was collected in concert with Julia Popp and Ryan Massopust. Tissue for analysis of canine neuromuscular junctions in Section 2 was graciously provided by Dr. Joe N. Kornegay.

Sections 2 and 3 have previously been published (Haddix SG, Lee Yi, Kornegay JN, Thompson WJ [2018] Cycles of myofiber degeneration and regeneration lead to remodeling of the neuromuscular junction in two mammalian models of Duchenne muscular dystrophy. PLoS ONE 13(10): e0205926. https://doi.org/10.1371/journal.pone.0205926), and are presented here in a modified format.

All other work conducted for the dissertation was completed by Seth Haddix independently.

Funding Sources

A 3-year Heep Fellowship was awarded to fund this research, through Texas A&M University. This work was also supported by National Institute of Health grant numbers R01 NS020480 and 1S10RR028951-0, and funds from Wesley J. Thompson's start up package awarded by Texas A&M University.

NOMENCLATURE

AChR	Acetylcholine receptor
AP	Action potential
DGC	Dystrophin glycoprotein complex
DI	Dispersion index
DMD	Duchenne muscular dystrophy
ECM	Extracellular matrix
EDL	Extensor digitorum longus
EF	Ejection fraction
EPP	Endplate potential
FS	Fractional shortening
GRMD	Golden retriever muscular dystrophy
mdx	Murine X-chromosome linked muscular dystrophy
MEPP	Miniature endplate potential
NMJ	Neuromuscular junction
P"number"	Postnatal day "number"
SOL	Soleus
STM	Sternomastoid
tSC	Terminal Schwann cell
UGC	Utrophin glycoprotein complex
WT	Wild type

TABLE OF CONTENTS

Page

LIST OF FIGURES

Page

LIST OF TABLES

Page

1. INTRODUCTION

1.1. Duchenne muscular dystrophy and animal models

The most common and extensively researched muscular dystrophy is Duchenne muscular dystrophy (DMD). The disease is X-linked, affecting about 1: 3,500 boys, and is caused by a genetic mutation in the *DMD* gene, which prevents the dystrophin protein expression from beneath the muscle sarcolemma where it is normally localized (Hoffman et al., 1987; Bonilla et al., 1988). Dystrophin is a large, 427 kDalton protein, that links the contractile apparatus of a muscle cell to the surrounding extracellular matrix (ECM) through a complex of proteins, called the dystrophin glycoprotein complex (DGC) or the dystrophin-associated protein complex. In myofibers, dystrophin binds to F-actin in the cytosol and β-dystroglycan, a muscle transmembrane protein. β-dystroglycan, in turn, complexes with α-dystroglycan on the extracellular side of the myofiber. α-dystroglycan binds to other components of the ECM surrounding the myofiber, specifically laminins (Figure 1.1). Muscles that lack dystrophin fail to properly localize the components of the DGC to the muscle membrane, and consequently, the critical linkage between muscle fibers' contractile apparatus and the ECM laminins is compromised. A milder disease, Becker's muscular dystrophy, occurs due to in frame *DMD* gene mutations, allowing dystrophin to be expressed in a truncated form that is still semi-functional and able to connect components of the muscle cytosol to the sarcolemmal membrane and ECM.

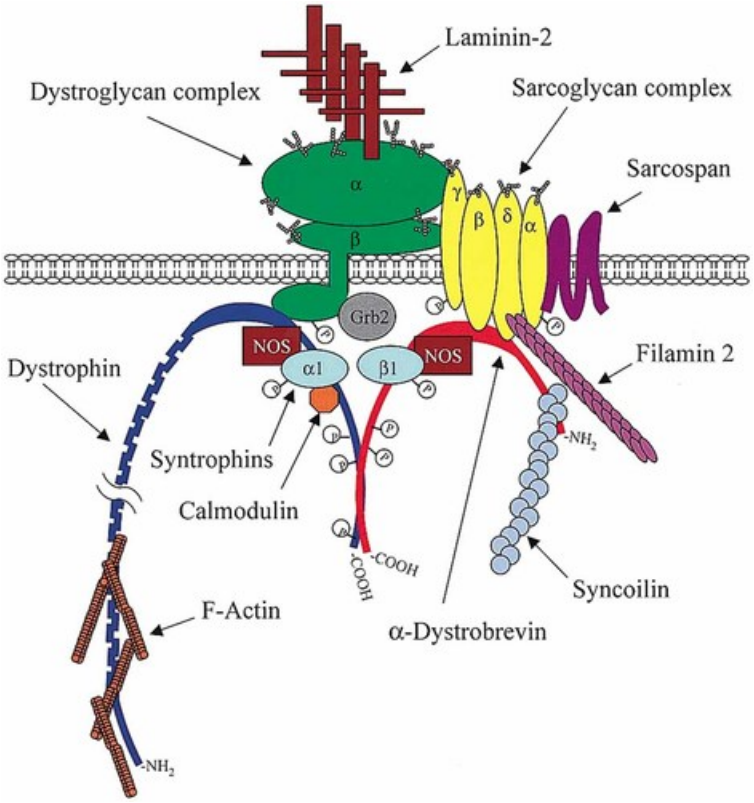

Figure 1.1. The Dystrophin Glycoprotein Complex.
Reprinted from (Rando, 2001). Dystrophin (dark blue) is located on the cytosolic side of the myofiber membrane, and links the contractile cytoskeletal machinery, through F-actin (brown), to laminin proteins of the ECM (red), through beta and alpha-dystroglycan (green).

In dystrophic muscle diseases, the breakdown in cytoskeleton-to-ECM linkage leads to a loss of tensile strength at the muscle fiber surface which results in increased myofiber damage due to eccentric contraction (Moens et al., 1993). This myofiber damage causes a cycle of degenerative and regenerative events in the muscle fiber and a subsequently heightened inflammatory response. Boys affected by DMD eventually lose the regenerative ability provided to skeletal muscles by satellite cells, the resident stem

cells of skeletal muscle fibers. The impact of continued muscle necrosis, in the absence of satellite-derived regeneration, is the replacement of contractile muscle tissue with adipose and fibrotic tissue causing weakness, cardiorespiratory deficiencies, cardiomyopathy, and early mortality. Despite knowing the genetic cause of DMD for 30+ years, there is still no cure for the disease and treatments are purely palliative (Emery and Muntoni, 2003).

There are many animal models for DMD ranging from *Drosophila melanogaster* to porcine, which vary in their similarity to DMD, and are thusly useful for understanding the disease in different ways. Two of the most commonly used models are the murine X chromosome-linked Muscular Dystrophy (mdx) mouse and the Golden Retriever Muscular Dystrophy (GRMD) dog. Like the human disease, both are X-linked and arise from spontaneous mutations in the *DMD* gene, although at different loci (Sicinski et al., 1989; Sharp et al., 1992). Both mutations are out-of-frame mutations resulting in a premature stop codon within the gene, and the full-length functional dystrophin protein is not produced. Additionally, both models show evidence of muscle fiber degeneration, but with differing severity.

1.1.1. Mdx mouse model

Although the majority of DMD related research has focused on the murine model, the mdx mouse has long been considered significantly limited in its usefulness. Early research into this line of mice indicated that damage to their muscles is much less severe, and they do not suffer from fibrotic and adipose tissue deposition until very advanced

ages. While the C57BL/10 (BL10) background is the most commonly used mouse model, it has been noted that genetic background does have an effect on disease progression. Dystrophic mice in a DBA/2 background were noted to display a more intense and earlier onset of disease state than those in a BL10 background (Coley et al., 2015). The lifespan of mdx mice is truncated (Chamberlain et al., 2007), and the mice begin to display signs of dilated cardiomyopathy in adulthood starting at about 6 months of age (Van Erp et al., 2010), a phenomena noted in DMD as well. The muscles of mdx mice are said to suffer from an early life "crisis period" starting at about three post-natal weeks and stabilizing at about twelve weeks, after which the level of myofiber degeneration and regeneration decreases as shown in the tibialis anterior limb muscle (Dangain and Vrbova, 1984). Other limb muscles, such as the soleus (SOL) and extensor digitorum longus (EDL), show continued low levels of myofiber degeneration following the crisis period (Pastoret and Sebille, 1995). Whether all non-respiratory muscles undergo a crisis period in this model will be addressed further in this dissertation.

It is evident that some dystrophic muscles are more prone to damage than others. For example, the extraocular muscles are largely spared from damaging incidents (Porter et al., 2003), while the diaphragm is highly affected and displays even earlier fibrotic tissue replacement than limb muscles (Stedman et al., 1991). The reasons for the sparing of some muscles and not others are not well understood, but are suggested to be the consequence of the frequency and rigor of muscle use (Edwards et al., 1984; Nguyen et al., 2002a). Sparing of the extraocular eyes has been suggested to be a result of the constitutive properties of the extraocular myofibers. These myofibers appear to be in a

developmentally immature state, which protects them from degenerative events (Porter et al., 2003). Functionally, mdx muscle does not suffer a decrease in general force production, and in fact may produce more force than its wildtype (WT) counterpart (Dangain and Vrbova, 1984). However, specific force is decreased and fatigability is increased in mdx muscles (Coulton et al., 1988b; Dellorusso et al., 2001; Chan et al., 2007). Histological examination of mdx limb muscles shows that before 3 weeks of age muscle fibers of dystrophic animals are indistinguishable from WT animals. Thus, prior to the crisis period of the mdx model, limb muscles appear normal despite a lack of dystrophin expression. However, beginning at around postnatal day 21 (P21) sites of muscle necrosis and inflammatory cell (monocellular and neutrophil) infiltration are evident (Tanabe et al., 1986; Carnwath and Shotton, 1987). This is likely in response to ruptures found in muscle membranes, called delta lesions, which can be appreciated by viewing the accumulation of membrane impermeable dyes in dystrophic fibers. When ruptured, dye enters the muscle fiber, but is excluded from intact fibers with uncompromised membranes (Hamer et al., 2002). Following the onset of necrosis, foci of small, basophilic muscle fibers become more frequent. These fibers are regenerating muscle fibers. On the other hand, in the diaphragm muscle, replacement of muscle fibers with areas of endomysial fibrosis and adipose tissue replacement become increasingly evident with disease progression. This pathological event, however, is not appreciable in limb or trunk muscles until the end stages of the mouse disease at about 18 months of age (Chamberlain et al., 2007).

Dystrophic fibers follow a similar regenerative pathway to that of damaged WT muscles. Following necrosis and the infiltration of macrophages, satellite cells (resident stem cells of the musculature) become activated. Activation and proliferation of the satellite cells is initiated by cytokines eluted from macrophages following a switch from a pro-inflammatory to an anti-inflammatory state (Chazaud et al., 2009). Satellite cells then fuse forming a multinucleated syncytial cell, and begin to express myosin heavy chain (MHC) isoforms, part of the contractile machinery of a mature myofiber. Initially, neonatal and embryonic isoforms are expressed, which are indicative of newly regenerated fibers. As the myofibers mature they begin to express fast or slow MHC isoforms depending on their innervation by fast or slow type motor neurons (Ciciliot and Schiaffino, 2010). The activity of satellite cells following muscle injury is similar to how progenitor muscle cells behave during the developmental process, in that they activate, fuse into a single multinucleated cell (syncytial cell), mature, and express various time specific genes such as the MHCs. As mentioned before, muscles eventually lose their regenerative capacity as they age, and in DMD this is thought to likely be due to failures in satellite cell function; however, this may not be the case in mdx (Sacco et al., 2010; Boldrin et al., 2015). There is a theory that satellite cell exhaustion is dictated by telomere length. In mdx satellite cells, telomeres are not shortened as the animals age, and correspondingly there is no satellite cell exhaustion. However, when a telomerase enzyme that maintains telomer length is absent in mdx mice, muscles undergo a more progressive muscle wasting disease, ultimately due to satellite cell senescence (Sacco et al., 2010).

While changes to force generation are largely attributed to loss of contractile tissue, it is possible that some of the changes in behavior are due to changes in the peripheral synapse that controls muscle contraction, the neuromuscular junction (NMJ). This synapse has been noted to have changes to its structure in mdx mice (Lyons and Slater, 1991; Pratt et al., 2015a) and will be discussed further below.

Regardless of a perceived inability to mimic the human disease state, the mdx mouse model has been instrumental in investigating disease mechanisms and muscle regenerative processes, as well as helping to develop potential therapeutics such as exon skipping (Mann et al., 2001; Lu et al., 2003; Fletcher et al., 2007). Few of these techniques have translated into human patients, but there is significant research and excitement in the potential of CRISPR/Cas9 technology, a genetic editing technique, which has shown excellent efficacy in mdx mice (Xu et al., 2016; Bengtsson et al., 2017), and is now being advanced in canine models of the disease (Amoasii et al., 2018). Additionally, gene replacement strategies, in which forced expression of truncated but functional forms of dystrophin are deliver to diseased muscle, also have the ability to restore functionally to skeletal muscles (Harper et al., 2002). Use of these truncated dystrophins has already been advanced into humans to treat DMD.

1.1.2. GRMD dog model

The GRMD model is appealing in that it more faithfully mimics the human disease. Affected dogs show appendicular muscle weakness as well as postural changes, both features in DMD boys. However, like mdx mice, the progression of the disease seems to

plateau in adulthood, but results in early mortality of affected animals. Unlike mdx mice, the GRMD model manifests itself at birth (Nguyen et al., 2002a), and the period of muscle instability is much longer (Valentine et al., 1986). Similar to both humans and mice lacking functional dystrophin, in GRMD small foci of necrotic muscle fibers and regenerating fibers are evident early in the disease state. Perhaps the most clearly identifiable histopathological feature in GRMD is large, rounded fibers, that occur either in small groups or as isolated muscle fibers. These have been termed hyaline or hypercontracted fibers and are considered a marker of muscle fiber necrosis. Hyaline fibers are evident from 4 months of age to 8 months of age, indicating, at least in this time period, that degeneration is ongoing. At early time points, pale areas are also evident and indicate empty basal lamina sheaths from which contractile tissue has been removed, some with invading monocellular cells. Surrounding these degenerating fibers are small regenerating muscle fibers. At later time points, these markers are still evident, but there is also an increased infiltration of inflammatory cells into the degenerating muscle, along with fibrotic tissue deposition (Valentine et al., 1986). These markers are hallmarks of DMD that are not as evident in the mdx model, especially fibrotic tissue deposition in the limb muscles.

As in the murine model, specific muscles in GRMD animals respond to lack of dystrophin in distinct manners. Like mdx muscles, the extraocular muscles in GRMD are largely spared from injury and dystrophic pathology; however, muscles such as the tongue and diaphragm suffer from the events described above with varying severity. Interestingly, the cranial sartorius of GRMD animals is truly hypertrophied at 4-10

months, in that it becomes larger in volume and there is an early increase in contractile tissue and, only later, fibrotic and adipose tissue deposition (Kornegay et al., 2003). Muscle hypertrophy in GRMD is thought to contribute to joint contractures of the limb muscles, also a characteristic of human DMD.

Like DMD patients and mdx mice, GRMD dogs display decrements in skeletal muscle force production (Kornegay et al., 1999). An intriguing trend is that flexor muscles are affected early in life, while extensors display decreases in force production later in life (Nguyen et al., 2002a). This is largely thought to be a consequence of the time course of muscle usage during development. Flexor muscles are used for the crawling behaviors of puppies. As dogs mature, they must support more body weight and extensor muscles become activated. As the muscles contract, they incur damage due to dystrophin loss and associated membrane instability, which leads to decreases in maximal force production. Membrane injury and force reduction becomes especially evident when GRMD muscles are subjected to eccentric contractions (Tegeler et al., 2010). In addition, NMJ morphology of GRMD animals is also abnormal when compared to WT controls, similar to that seen in mdx (Haddix et al., 2018). Whether NMJ changes in GRMD specifically have an effect on muscle function has not been studied.

1.2. Structure and function of the neuromuscular junction

The NMJ is the site of communication between the peripheral nervous system and skeletal muscles. Its purpose is to transmit neural signals to muscle fibers, thereby

initiating body movements. The synapse is tripartite. It consists of the postsynaptic acetylcholine receptor (AChR) aggregate on the surface of muscle fibers, the presynaptic terminal branches of motor axons, and terminal Schwann cells (tSC) that interact with pre- and postsynaptic cells (Sanes and Lichtman, 1999). The neuromuscular synapse has a highly reliable physiology and a distinct morphological structure that compliments its function.

The mammalian NMJ has been studied extensively in rodents and, as such, much is known about its morphology and development. The excitatory neurotransmitter of mammals released from motor neurons on to skeletal muscle fibers is acetylcholine. Tens of thousands of single AChRs are clustered upon the muscle fiber surface in mature NMJs in a specific area of close apposition to the nerve terminal, called the endplate. The role of the endplate is to detect and respond to neurotransmitter release. The microscopic morphology of the endplate's AChR aggregate is described as "pretzel-like" (Figure. 1.2A). Long, continuous ribbons of AChR are aggregated in the muscle fiber plasma membrane, or sarcolemma, and are ultimately responsible for receiving signals from the motor axon and converting them into electrical changes across the muscle membrane, which in turn result in muscle contraction. The motor axon terminal resides directly above the aggregation of receptors, in a branching pattern that closely follows that of the pretzel itself (Figure 1.2B). This nerve terminal-end plate connection is maintained by bindings to the synaptic ECM, by both muscle and neuron, through laminins, fibronectin, and other ECM components (Sanes et al., 1986; Chipman et al., 2010). The receptors themselves are heteromeric structures consisting of five subunits

that compose a cation channel containing binding sites for acetylcholine (Popot and Changeux, 1984). Activation of the AChRs by the binding of acetylcholine molecules results in the receptor channel opening, depolarization of the sarcolemma and, ultimately, excitation-contraction coupling (Catterall, 1991).

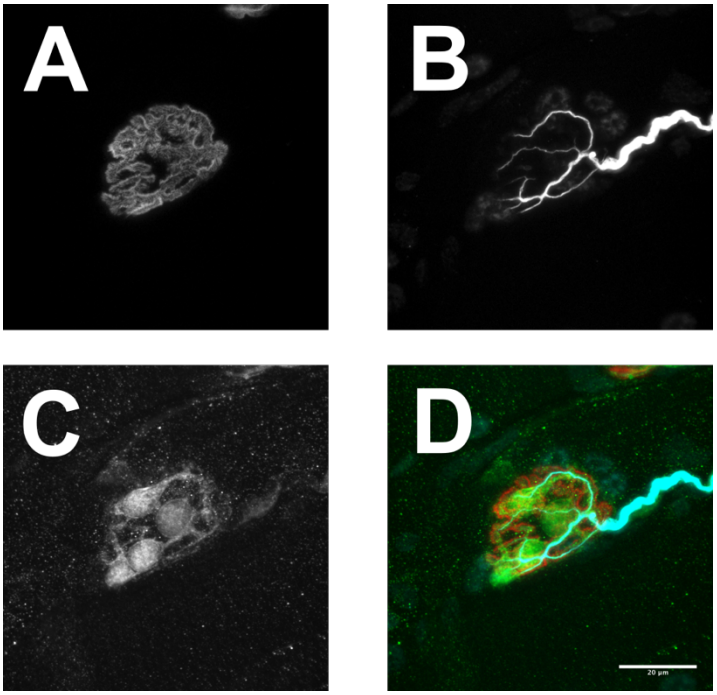

Figure 1.2. The structure of a mature NMJ.
Maximum projection confocal micrographs. Canine tissue. A) AChRs are arranged in a continuous pretzel-like morphology on the surface of the muscle fiber. B) The motor axon run along the ribbons of the receptor aggregate, while C) the tSCs cover and cap the structure. D) Composite. Red = AChR. Cyan = Axon. Green = tSC. Scale bar = 20 μm.

Electron microscopic techniques have been used to detail the NMJ ultrastructure. These investigations revealed that in mature NMJs, the motor axon rests within a minor indentation upon the muscle fiber, called a gutter. Under the axon, the muscle membrane further projects inward forming so called junctional folds. At the crests of the folds, directly apposing vesicle fusion sites in the axon terminals, AChRs are deposited (Salpeter and Harris, 1983). In the bottoms of the folds, there is an accumulation of voltage-gated sodium channels that are responsible for eliciting action potentials (APs) in the muscle, as well as components of the DGC (Sanes and Lichtman, 1999). When labeled using immunohistochemistry, dystrophin can be seen to localize to both the sarcolemma and the NMJ (Figure 1.3). At the crest of the folds a homolog to dystrophin, utrophin, recruits largely the same proteins as that of the DGC, but is intimately involved in the development of the NMJ. The utrophin glycoprotein complex (UGC), is concentrated in muscle at the endplate and the myotendinous junction and also provides a linkage from muscle fiber to ECM (Khurana et al., 1991).

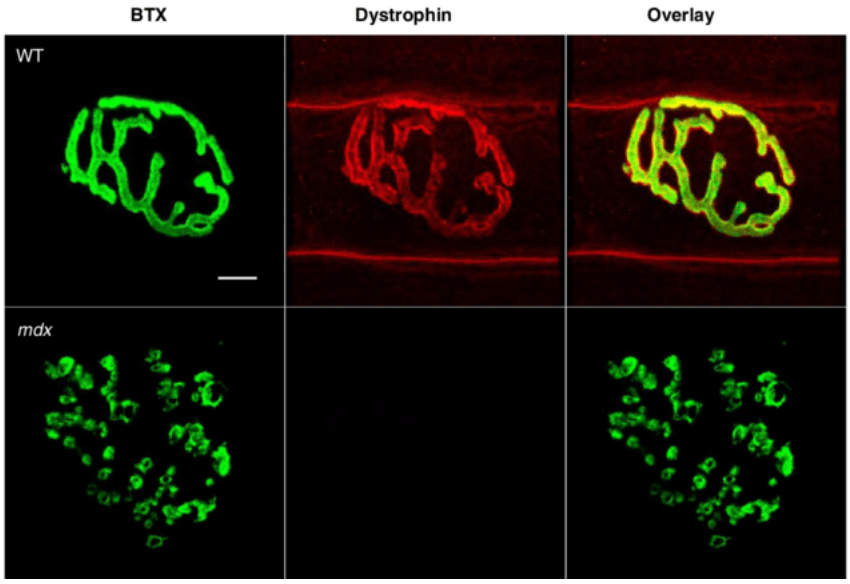

Figure 1.3. Dystrophin is highly expressed at the NMJ.
Reprinted from (Pratt et al., 2015a). WT mice express dystrophin both at the NMJ, labeled via α-bungarotoxin (BTX), and below the sarcolemma. Mdx animals do not express dystrophin at either location. Note the continuous nature of the WT AChR aggregate and the fragmented nature of the mdx. Colocalization of BTX (green) and dystrophin (red) is pseudocolored yellow. Scale bar = 10 μm.

Capping the NMJ endplate structure are the non-myelinating tSCs (Figure 1.2C), which provide trophic support and maintenance to the synapse (Reddy et al., 2003; Feng and Ko, 2008b; Feng and Ko, 2008a). In rodents, there are typically 3-5 tSCs associated with each NMJ. The somata of the tSCs lie along the motor terminal, while the small processes of tSCs extend to cover the axon branches. As tSCs do not create myelin sheaths they have no role in saltatory conduction. They are, however, able to respond to purinergic and muscarinic signaling from the motor neuron, and may play a role in determining neurotransmission efficiency (Georgiou et al., 1999; Rousse and Robitaille, 2006).

Although neuromuscular synapses are often referred to as tripartite in nature, a fourth aspect of the NMJ should be noted, the synaptic basal lamina. This is a composite of signaling and structural components that reside in the synaptic cleft, the small gap between the pre- and postsynaptic cells. This cleft is densely filled with extracellular matrix, including collagen, laminin and agrin, and is critical for NMJ development and function (Slater, 1990). In healthy synapses, the synaptic cleft is a 50 nm gap that can be viewed with transmission electron microscopy (TEM) following osmium tetroxide precipitation (Smith et al., 2013). This synaptic cleft's electron density is generated by the protein components of the ECM and DGC, which keeps the synapse from becoming displaced following muscle contraction or damage to the NMJ (Betz and Sakmann, 1973).

Also present in the synaptic cleft is an enzyme acetylcholine esterase (AChE) derived from the muscle cells and tethered to the ECM. AChE is responsible for hydrolyzing acetylcholine into its constitutive parts, choline and acetate, to allow the neurotransmitter byproducts to be recycled back into the neuron. Hydrolyzation of the neurotransmitter prevents both receptor desensitization and neurotoxicity. The enzyme also localizes at the endplate region of the muscle in the same morphology as the AChR cluster (Brimijoin, 1983). Taken together, the NMJ synaptic cleft and its associated ECM, DGC, enzymes, signaling molecules and scaffolds constitute an essential and often overlooked player in the structure and function of this synapse. The NMJ cleft's necessity in skeletal muscle function and its role in diseases such as DMD may require a more modern view of NMJ as a quadripartite synapse.

Within an animal group, or even a genus, NMJ morphology can be vastly different. In an invertebrate (*Drosophila*) system, the variance in fly NMJ morphology is striking and cannot be explained by genetic drift, nor body size of the insect (Campbell and Ganetzky, 2012). Importantly, the shape of the presynaptic terminus in flies does not have an effect on neuromuscular performance. Neither the frequency or the amplitude of MEJPs (miniature excitatory junctional potentials), nor excitatory junctional potentials amplitudes were different among species of *Drosophila*. Still, the motor axon terminals and NMJ morphology, which resemble beads on a string, differed significantly. Therefore, the form of the NMJ does not necessarily dictate its overall synaptic function. In some vertebrates, such as the frog for example, motor nerve terminals have long continuous protrusions that extend laterally across the myofiber. Even between mammals there are distinct differences in the terminal structure of the NMJ. Rodents, as mentioned before, the terminal branches into ribbon a like structure within the defined pretzel structure of the endplate. In humans, the terminal is smaller and made up of small bulbous varicosities along thinner axonal ribbons (Slater, 2008; Jones et al., 2017). Postsynaptic accumulation of receptor (glutamate receptors for flies, AChR for vertebrates) mirrors that of the presynaptic morphology. Between rodent and humans, this translates as the difference between a continuous receptor aggregate and a more fragmented morphology, respectively. Junctional fold length and number beneath the nerve terminal are also different between species. Frogs have relatively few, short invaginations, while humans have many, longer ones. There is an inverse relationship between the complexity of postsynaptic folding and the size of the endplate. These

changes manifest themselves functionally as well. The amount of acetylcholine released by the axon terminal is typically much more than is necessary to bring a muscle fiber to threshold and induce a muscle contraction. This overabundance of acetylcholine release is termed the safety factor, and plays a role in maintaining synaptic function over a wide array of physiological conditions (Wood and Slater, 2001). Postsynaptic folding of the muscle membrane is thought to play a role in determining the safety factor. The folds create a path of increased resistance to the voltage gated sodium channels that are clustered at the depths of the folds, essentially channeling depolarizing current to these channels (Martin, 1994). In theory, endplates with longer postsynaptic folds should have increased resistance and therefore a higher safety factor. This may not be the whole story, however, as muscles with similar folding morphologies can display different safety factors (Wood and Slater, 1997).

The conservation of synaptic function, even among vastly different NMJ morphologies, is of particular interest in neuromuscular disease. As mentioned above, the morphology and structure of dystrophic NMJs is distinct from that of non-diseased synapses. The question then arises in light of the fact that synaptic function is not much perturbed between species with different NMJ morphologies— are the changes noted in DMD models due to homeostatic adaptations to preserve synaptic integrity?

1.3. Development and maintenance of the neuromuscular junction

While in adulthood the synaptic structure is quite static, the NMJ goes through distinct changes in morphology during development. At buirth birth (P0) in rodents the AChR are clustered into a "plaque". Axons terminals of many motor neurons as situated just opposite it. By postnatal day 14 (P14), the AChR aggregate has matured into its pretzel-like morphology, progressing through distinct intermediates as its structure changes over time (Marques et al., 2000). This rearrangement of postsynaptic structure is coincident with synapse elimination via the withdrawal of the terminals of motor axons, until the terminals of only one axon remain per endplate. Nonetheless, most motor neurons innervate multiple muscle fibers, which allows all connected muscle fibers to contract as a collective. A single motor neuron and the many muscle fibers it innervates have been termed a motor unit. All muscle fibers that make up a single motor unit are noted to have the same myofiber subtype (I, IIa, IIb, etc.), and it has been determined that the motor neuron dictates these myofibers' contractile and metabolic properties (Buller et al., 1960; Stålberg, 2004).

The cues for maturation of the postsynaptic apparatus to the pretzel shape come from all aspects of the NMJ (muscle, neuron, tSC, and basal lamina). Activity of the presynaptic neuron (Balice-Gordon and Lichtman, 1994; Busetto et al., 2000), as well as stresses imposed by phagocytic tSCs, drive synapse elimination (Smith et al., 2013). Additionally, there are factors secreted from the motor axon into the synaptic cleft that are known to promote synaptic maturation. One of these factors, neural agrin, is directly involved in the clustering of AChR aggregate (McMahan, 1990). Agrin binds to a low-

density lipoprotein receptor-related protein 4 (LRP4) which in turn causes transphosphorylation of muscle-specific kinase (MuSK). The MuSK/LRP4 complex is tethered to the sarcolemma and extends into the synaptic cleft (Kim et al., 2008). MuSK activation results in AChR clustering is contingent upon LRP4 biding to agrin (Zong et al., 2012). MuSK expression is implicated not only in the physical aggregation of AChRs but also with the elevated synaptic transcription of AChR subunits (Jones et al., 1999; Yang et al., 2001). An adapter protein, downstream of tyrosine kinase (Dok7), acts as an enhancer proteins for MuSK phosphorylation and the activation of receptor clustering activity (Okada et al., 2006). Downstream of the agrin/MuSK/LRP4 complex is Rapsyn, which binds AChRs and is also necessary for clustering (Apel et al., 1997; Moransard et al., 2003). AChR expression, however, is not contingent on Rapsyn (Gautam et al., 1995). The MuSK/LRP4 complex may also have a role in the development, and specialization, of the presynaptic apparatus. In cell culture experiments, it was determined that LRP4 acts as a retrograde signal to motor terminals directing the formation of active zones, release sites at areas of apposition to AChRs (Yumoto et al., 2012).

Agrin surely acts as AChR clustering and postsynaptic maturation signal secreted from the motor neuron, but there is evidence that clustering can occur without innervation, and therefore in the absence of neural agrin. The developmental clustering of AChRs before the motor neuron innervates them has been termed pre-patterning. Muscle derived agrin is not responsible for this phenomenon, as it lacks portions of the protein that result in clustering ability through MuSK/LRP4 binding (Ruegg et al., 1992;

Ferns et al., 1993). The maturation of secondary myotubes may provide an explanation. Secondary myotubes form near the center of the developing muscle and express high levels of AChR subunit transcripts (Yang et al., 2001) as well as a number of transcription factors. Myogenin is one such factor involved in muscle maturation (Babiuk et al., 2003), and also AChR subunit expression. It should be noted however that myogenin's effects on AChRs is dependent on electrical activity in the myotube (Dutton et al., 1993). Increased receptor expression at this central area, due to the high concentration of muscle precursor cells, could give rise to the pre-patterned clusters. Additionally, MuSK expression is elevated in the secondary myotubes at the central band region (Kim and Burden, 2008). Forced self-activation of MuSK through dimerization not only causes the clustering of receptors but also increased expression of the subunit transcripts, and may be involved in pre-patterning (Jones et al., 1999; Yang et al., 2001). As the nerve contacts the muscle and the central band region, agrin is released, resulting in further clustering and stabilization of the post-synaptic apparatus. In fact, the agrin/MusK/LRP4 complex may act as a stop signal for axon growth. The nerves of agrin knockouts grow well past the pre-patterned clusters along the muscle fibers (Campagna et al., 1995; Gautam et al., 1996).

Interestingly acetylcholine release plays a role in AChR clustering at the endplate site. In the absence of acetylcholine release or agrin, NMJs form normally and in fact the number and size of innervated clusters increases (Misgeld et al., 2005). Additionally, acetylcholine agonists have the ability to cause endocytosis of AChR in cell culture when agrin is not present (Misgeld et al., 2005).

Regardless of whether the cues for synaptic maturation are derived from primarily the neuron or the muscle (as suggested by pre-patterning), if key members of the signaling complex are missing NMJs do not form or form abnormally (e.g. agrin, MuSK, LRP4, Dok7, or Rapsyn).

In dystrophy, there is evidence that the development of the NMJ, from the plaque morphology to the mature pretzel, is accelerated (Minatel et al., 2003). Not only is postsynaptic maturation altered, the synapse reaches a single innervated state earlier than WT animals. There is perhaps a role in dystrophy in the initial development of the NMJ, and it is certainly implicated in rearrangement of the mature endplate structure following muscle fiber injury caused by its loss.

1.4. Neuromuscular regeneration

Unlike the central nervous system, the mammalian peripheral nervous system has potent capacities for regeneration following injury. As mentioned above, the regeneration of damaged muscle cells is contingent upon satellite cell activation, fusion, and maturation into viable myofibers. Following muscle fiber ablation in the frog, the nerve terminal remains at the synaptic location, even in the absence of the postsynaptic muscle fiber (Yao, 1988; Dunaevsky and Connor, 1995, 1998). During the regenerative process of the muscle, a new NMJ is formed in the same area as the old with receptor deposited under the motor terminal (Burden et al., 1979). Even if both muscle and nerve are damaged, following the regeneration of both cells, a synapse at the location of the old is reconstituted (Marshall et al., 1977).

Motor neuron terminals act differently in the rodent model. Following muscle fiber necrosis, the motor neuron follows one of two paths. Either the motor neuron remains at the synaptic site, likely tethered to the basal lamina, or the terminal retracts from the synaptic site. This difference in response may be explained by the severity and type of damage incurred by the muscle fiber. Following muscle crush near the synaptic area, the nerve terminal retracts from the synapse following muscle fiber necrosis (Rich and Lichtman, 1989a). It should be noted that while the experimental procedure used to care not to damage the nerve, there was no way to fully guarantee it wasn't also crushed with the muscle. If damaged the nerve would retract from the muscle fiber skewing results. Following myofiber ablation via focal laser ablation, the nerve terminal remains during the subsequent regenerative process (Li and Thompson, 2011). Regeneration of the muscle also results in the establishment of a new NMJ, at the site of the previous synapse. In some cases, the morphology of the postsynaptic apparatus changes little, if any, upon successful reestablishment of the contact between muscle and nerve. In other cases, small branches are added to the regenerated synapse, while in other cases such as those associated with DMD and other diseases, a vast morphological change is evident. The structural reorganization of the postsynaptic apparatus seen in damaged and dystrophic synapses is part of a phenomenon called NMJ remodeling, which will be defined in further detail in subsequent sections of this dissertation.

The axon of the lower motor neuron also has a great capacity for regeneration. If injured, the motor terminal degrades below the site of injury and the proximal stump retracts. After some time, depending on the degree of injury and the distance from the

muscle, an axon (originating from either the initial neuron that connected to the muscle fiber or a foreign neuron) regrows from a proximal stump using the endoneurial tube and Schwann cells to the muscle fiber. This axon makes contact at the extant synaptic site on the muscle and extends branches into the gutters of the receptor aggregate (Rich and Lichtman, 1989b; Nguyen et al., 2002b).

Contingent on this regenerative capacity of motor neurons is the activity of Schwann cells, both myelinating and non-myelinating. Schwann cells, the multifunctional glia of the periphery, are responsible for the myelination of the axons of alpha motor neurons and therefore responsible for saltatory conduction. Upon insult to the peripheral nervous system the Schwann cells provide two distinct roles. A population of the glia adopt phagocytic characteristics and begin to digest cellular debris associated with axonal degeneration, namely myelin and axonal cellular components (Kang and Lichtman, 2013). The Schwann cells also provide the track that the regenerating motor neurons will use to reinnervate muscles. During the degeneration process the Schwann cells and the surrounding endoneurium remain in place. They create Bands of Büngner that act as a bridge for the growing axon to navigate the injury site on the muscle fiber to the NMJ (Arthur-Farraj et al., 2012). As the neuron reaches the endplate, branches of the terminal re-enter the gutter of the postsynaptic apparatus without morphological rearrangement of the synapse.

During partial denervation, such as that created by crushing only a section of a nerve, newly denervated NMJs may be adjacent to neighboring muscle fibers with innervated NMJs. As the nerve terminal is removed following damage, tSCs will extend

processes from the denervated endplate in a seemingly stochastic manner. If a process grows to an innervated endplate, then the terminal Schwann cell can provide a bridge upon which the axon sprouts from the innervated NMJ can grow. Ultimately, the axon can reinnervate the denervated junction, growing into the gutters that the previous axon occupied (Son and Thompson, 1995). This reinnervation process, in turn, changes the muscle fibers that are part of that motor unit. It is possible that the reinnervated muscle fiber's contractile properties, based on the isoform of MHC expressed, may also change if the new neuron is of a different type (fast or slow) than the old. In mdx mice it is quite evident that there are changes to the pre- and postsynaptic structure, likely caused by myofiber damage.

1.5. Neuromuscular junction remodeling

It is well established that as animals age the morphology of the NMJ changes as well. This is a normal and necessary maturation that relies upon both pre- and postsynaptic factors. While the adult NMJ morphology is very stable, there is irrefutable evidence that NMJ remodeling can occur in certain instances. Some of the best-recognized examples are in advanced age, muscle injury, and diseases such as DMD.

In aging, the postsynaptic apparatus has a clear morphological shift from a continuous pretzel to a more fragmented appearance (Li et al., 2011). Additionally, in extremely advanced age there is a granularization of the receptor aggregate (Valdez et al., 2010). At these geriatric ages, there is also evidence of motor axon die back, where the motor terminal vacates the endplate area. Axonal die-back causes tSCs from adjacent

endplates to sprout to the denervated endplate. Axons from innervated endplates then grow along these tSC tracks to re-innervate the recently vacated endplate as in peripheral nervous system damage (Connor et al., 2002). The concepts of NMJ remodeling and endplate fragmentation, in combination with NMJ age, are central to the current dissertation research.

Vital imaging experiments demonstrate that fragmentation of AChR aggregates can be initiated by muscle fiber degeneration and regeneration. Indeed, when a single muscle fiber is damaged with a high intensity laser near the endplate area, a once continuous AChR aggregate is transformed into a fragmented one (Li and Thompson, 2011). It is possible that similar processes are taking place in aging myofibers, as aged muscles are more susceptible to injury. The same phenomenon has been suggested for muscular dystrophies (Lyons and Slater, 1991). Just as seen in aging and muscle damage experiments, dystrophic NMJs are clearly abnormal. AChR aggregates are fragmented from an early age in dystrophic mice. There is also a coincident change in the morphology of the innervating motor neuron and a proliferation of tSCs in mdx mice (Pratt et al., 2015a). However, there is little evidence of ultra-terminal (originating from the endplate) axon sprouting to adjacent endplates suggesting little to no denervation in these animals, at least in early adulthood (Lyons and Slater, 1991). The NMJ remodeling process in the context of dystrophy will be elaborated on in Sections 2, 3, and 4 of this report.

It is likely that the regeneration process of the muscle also causes a rearrangement of the synaptic basal lamina, which would have a role in the remodeling

process of NMJs. Basal lamina changes are suggested by a widening of the synaptic cleft and the loss of secondary fold under some terminals in muscular dystrophy (Law et al., 1983; Lyons and Slater, 1991). The increased width of the synaptic cleft is suggested to be a result of ECM elution from the regenerating muscle fiber, which is added to the existing ECM retained during myofiber necrosis. The continued build-up of ECM could not only widen the cleft but also flatten ECM projections at the endplate. So upon full regeneration secondary folds would be lost. Agrin, which is tethered to the basal lamina, distribution may then be altered following ECM build up. Subsequent reconstitution of the NMJ could be affected as the myofiber expands and touches only some areas of agrin deposition. Alternatively, agrin that initially provided a clustering signal may not ever bind to the newly expressed MuSK/LRP4 complex on the regenerated myofiber. The new ECM could mask binding epitopes of the receptors. In this case newly released agrin from the rearranged motor terminal could instruct NMJ remodeling. A distributional change of these signaling molecules has not been investigated, but there is evidence of changes to the basal lamina in muscle fiber regeneration (Gulati et al., 1983) and dystrophy (Patton et al., 1999).

There is, however, evidence of NMJ remodeling even in the absence of myofiber necrosis and regeneration. TSC activity itself seems able to remodel junctions. When the activity of tSCs is elevated via motor neuron overexpression of Type III NRG1, receptor aggregates become fragmented in appearance (il Lee et al., 2016). In fact, the AChR morphology is indistinguishable from muscle injury models. It is evident that this remodeling is independent of myofiber necrosis and regeneration. A hallmark sign of

myofiber regeneration is the appearance of nuclei running through the center of a myofiber, sometimes in small segments and sometimes in long chains (Figure 1.4). In uninjured, mature muscles, myonuclei run in a spiral around the periphery of the syncytia directly under the sarcolemma (Bruusgaard et al., 2003). When myofibers regenerate their nuclei localize to the center of the cell and remain there for up to 6 months (Wada et al., 2008).

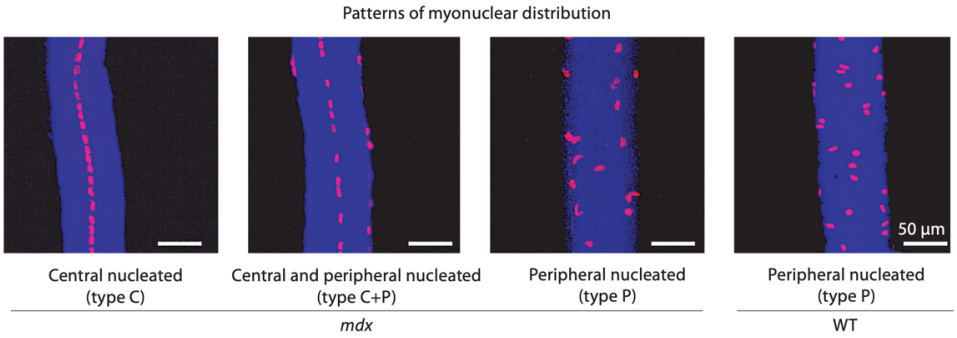

Figure 1.4. Examples of peripheral and central myonuclei.
Reprinted from (Terada et al., 2010). Isolated muscle fibers from WT and mdx labeled with propidium iodide. Mdx myofibers display both central (left most panel) and peripheral nuclei, while WT myonuclear distribution is predominantly peripheral.

When tSC activity is increased genetically, there is no evidence of central nuclei in myofibers. So, it is likely that the fibers remain intact and that it is purely presynaptic influence that remodels the junction. Whether tSCs play a role in remodeling NMJs in damaged muscle fibers remains to be investigated.

1.6. Physiology of remodeled NMJs

It is evident that aging, disease, and muscle damage all have a role in NMJ remodeling from a continuous, pretzel morphology to an aberrant, fragmented morphology. However, the consequence of this change in appearance on the function of the synapse is a contested subject in the field. Aged, fragmented junctions are equally as efficient at neuromuscular transmission as middle-aged ones (Willadt et al., 2016). It must be noted that although this experimental protocol did not investigate specifically remodeled NMJs, the ages of mice examined make it likely that most synapses were abnormal in their morphology.

Muscles damaged by eccentric contractions have also been shown to have force deficits following lengthening. While this has traditionally been hypothesized to occur as a result of breaking the cross-bridge connections between the actin and myosin filaments in sarcomeres, or potentially excitation-contraction uncoupling at t-tubules, there may also be a deficit in neuromuscular transmission (Warren et al., 1999; Deschenes et al., 2000).

The effects of NMJ remodeling in disease, specifically DMD, is also unclear. Analysis of NMJ performance in mdx animals, where it is known the NMJ is abnormal, is sparse. However, there is evidence of slight changes in neuromuscular transmission in the mdx model. A finding corroborated on human studies is a depressed mean resting potential of dystrophic muscle fibers (Carlson and Roshek, 2001). This is possibly due to changes in ion channel properties, or membrane permeability to sodium and calcium, both of which could compromise NMJ transmission. Additionally, it has been reported

that mdx mice display changes in miniature endplate potential (MEPP) characteristics, features associated with altered spontaneous synaptic transmission, or AChR properties. Notably MEPP amplitude is smaller and more variable than WT animals, but MEPP frequency is unaltered (Nagel et al., 1990; Carlson and Roshek, 2001; van der Pijl et al., 2016). This does not, however, seem to correspond with changes in action potential-evoked endplate potential (EPP) amplitude (van der Pijl et al., 2016). Interestingly, there may be changes to the receptor density (Nagel et al., 1990), but this finding is contested (Lyons and Slater, 1991). Other studies have recorded variability in twitch force in nerve-stimulated muscle responses (Personius and Sawyer, 2006), which might stem from the muscles varied ability to respond to acetylcholine. It is unlikely that dystrophic muscle fibers' variable responses to nerve stimulation has much or any pathological effect, and overall loss of contraction force is due more in part to myofiber degeneration. Neuromuscular transmission deficits may play a role in dystrophic muscles increased fatigability during tetanic stimulation, as EPP values fall with repetitive stimulation (van der Pijl et al., 2016).

When neuromuscular performance is assessed in GRMD dogs, some notable differences can be found compared to WT. These affected dogs also have abnormal NMJs, as noted in their mdx counterparts which will be discussed in Section 2. Specifically, using single fiber EMG, both GRMD dogs and DMD boys show increased jitter and fiber density (Kornegay et al., 2012). Jitter in single fiber EMG indicates a variation in muscle fibers of the same motor unit generating action potentials in comparison to other muscle fibers in the motor units. In normal systems, muscle fibers

within the same motor unit will activate with a clearly defined (but very short) time interval between them (Figure 1.5a). In some cases, however, the delay between action potential generation is increasingly variable, as is seen in dystrophic and myasthenic muscle (Figure 1.5b). In fact, sometimes complete failure to activate the myofiber is noted in a phenomenon called blocking (Figure 1.5c).

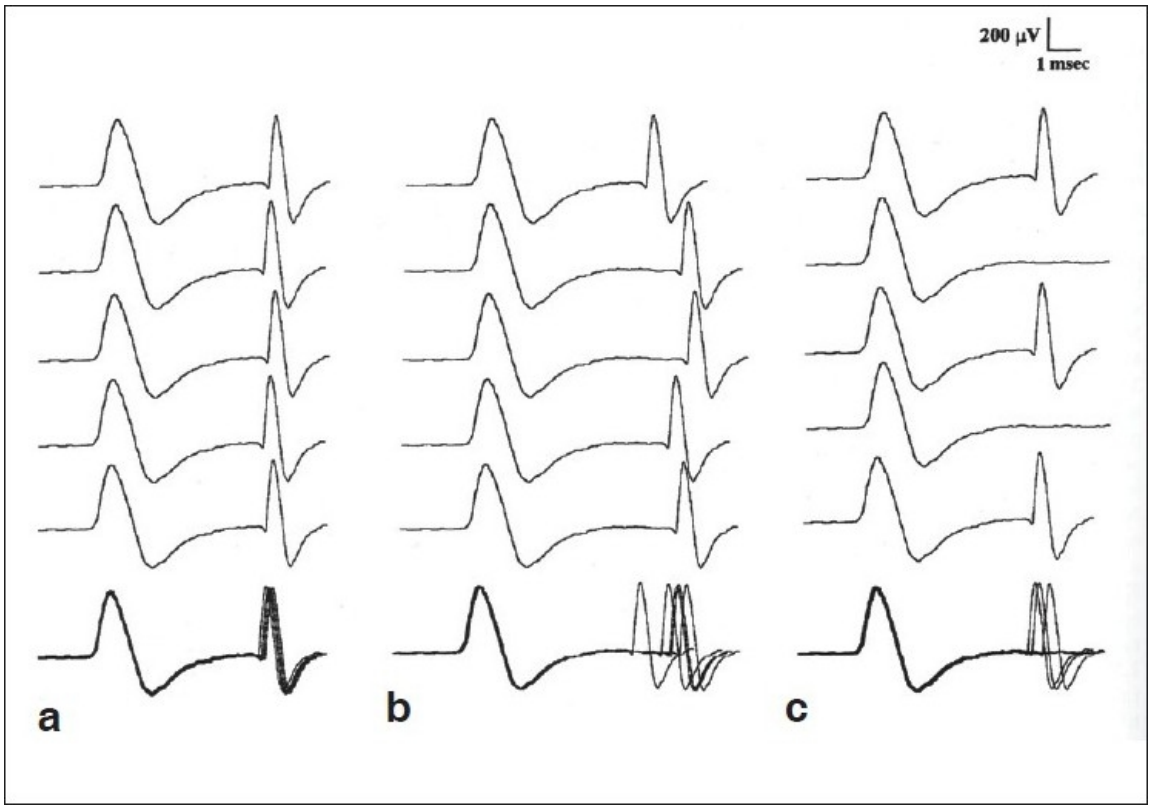

Figure 1.5. Single fiber EMG jitter recordings.
Reprinted from (Selvan, 2011). Variation in the timing of muscle fiber activation within the same motor unit is defined as jitter, and indicative of changes to neuromuscular transmission. Low jitter indicates reliable neuromuscular transmission, while increased jitter or blocking indicates discrepancies or failures. a) Normal jitter. b) Increased jitter. c) Increased jitter with blocking as seen in second and fourth traces from top. Above traces are from myasthenic muscle but increased jitter is noted in DMD and GRMD muscle.

The increased fiber density, or the recording of multiple APs via single fiber EMG, is indicative of regenerating myofibers in the vicinity of the recording electrode probe. However, it is likely that these slight differences in neuromuscular transmission are not responsible for the drops in force noted in GRMD muscles. More probable is that, as in mdx mice, specific force drops seen in dystrophic dogs result from myofiber injury and in the case of dystrophic dogs, replacement of contractile tissue with fibrotic and adipose tissue.

1.7. Dystrophic cardiomyopathy

Advances in respiratory therapy have significantly lengthened the lifespan of DMD patients, extending life into their third or fourth decade. However, with these important life extensions come concomitant complications in cardiac function and additional contributing factors in disease pathology. Indeed, dilated cardiomyopathy accounts for 20-30% of DMD mortalities as treatment has ameliorated respiratory complications that accounted for earlier mortality (Eagle et al., 2002; Passamano et al., 2012).

Dystrophic cardiac involvement begins early in life, but does not manifest clinically until later years (Figure 1.6). Lack of dystrophin in the cardiomyocytes is also the cause of this heart dysfunction and has similar myofiber impacts as dystrophin loss from skeletal muscle. That is to say, decreased cellular membrane integrity leads to increased damage of the heart cells (Danialou et al., 2001), inflammatory cell infiltration into cardiac tissue (Mavrogeni et al., 2010), and gradual and progressive fibrosis of the heart (Frankel and Rosser, 1976). These disease processes result in decreased cardiac

function due to diminished contractile tissue, but unlike skeletal muscle, the heart does not have resident stem cells for tissue regeneration.

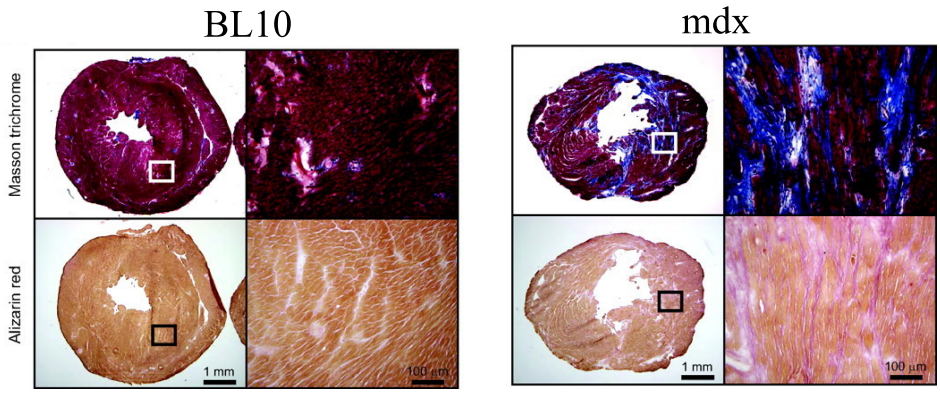

Figure 1.6. Dilated cardiomyopathy associated with muscular dystrophy. Adapted from (Bostick et al., 2008). Cross section of left and right ventricle of mouse heart. Masson trichome stain in blue indicates connective tissue, while alizarin red labeling shows calcium deposition. Note the increase in connective tissue and calcified areas of the mdx heart at 21 months. The left ventricle also becomes dilated in comparison to the BL10 heart, indicating dilated cardio myopathy.

The standard diagnostic technique for cardiomyopathies is echocardiography and cardiac MRI (Buddhe et al., 2016). Decreases in ejection fraction and fractional shortening, measurements of the contractility of the left ventricle, are indicative of decreased cardiac function in DMD. Additionally, more advanced methods of echocardiography, such as speckle tracking or Doppler tissue imaging (techniques that measure the elasticity of the myocardium), are more sensitive to changes and contrasts between a DMD and normal heart, and can predict the development of clinical cardiomyopathy before patients present overt symptoms (Ogata et al., 2007).

Dystrophic dogs also display an advancing cardiomyopathy associated with dystrophin loss (Valentine et al., 1989; Moise et al., 1991; Fine et al., 2011; Guo et al., 2019). When conscious echocardiography is used as a diagnostic, systolic function is significantly decreased in older, affected dogs as compared to younger ones. Like DMD boys, using speckle tracking and evaluating myocardial strain decreases has been shown to be a sensitive strategy to predict the development of dilated cardiomyopathy in affected dogs (Guo et al., 2019).

The mdx mouse model presents similar dilated cardiomyopathies and decreased left ventricular function. These dystrophic mice also have a reduced life span, but the cause has not been attributed to cardiac malfunction. Few echocardiographic studies have investigated the progression of cardiac involvement at near-death time points (i.e. +18 months), with most ending at 12 months. In these cases, fibrosis is increased and strain analysis via speckle tracking reveals cardiac dysfunction (Spurney et al., 2011). The severity of cardiomyopathy in mdx mice has been investigated and discussed in this research project.

1.8. Research focus

While DMD is a vastly researched disease, there is comparatively minimal investigation in to how the synapse is responsible for voluntary motion or how the NMJ develops, functions, and degrades in dystrophic disease. While it is generally agreed upon that the NMJ remodels due to myofiber degeneration and regeneration at the endplate region, direct evidence for this phenomenon in muscular dystrophy is scarce. In the forthcoming

chapters, a more accurate description of the NMJ remodeling process due to muscular dystrophy in mouse and dog models is given. Focus is also centered on the function of these remodeled synapses. I find, in agreement with the majority of literature, that remodeling of the NMJ does occur in this mdx model, and that it is due to myofiber damage at the endplate site and under direct control of the innervating motor axon. In addition, I provide an updated view of the mdx mouse's value as a model of DMD, and give evidence that remodeling of the NMJ is a shared attribute of mammals lacking the dystrophin protein. I report on the efficiency of neuromuscular transmission in muscular dystrophy and the potential role of receptor aggregate fragmentation. Finally, a brief investigation of cardiomyopathies in mdx mice is described.

2. MORPHOLOGICAL ABNORMALITIES OF THE DYSTROPHIC NMJ[1]

2.1. Research impetus

As mentioned in Section 1, there is a repertoire of evidence that dystrophic NMJs are abnormal in appearance (Lyons and Slater, 1991; Minatel et al., 2003; Pratt et al., 2015a). Much attention has been given to the postsynaptic AChR aggregate, which has been described as fragmented into non-continuous clusters of receptors, as compared to the continuous pretzel formation of healthy synapses. Aside from the fragmentation, other noticeable changes to dystrophic NMJs have been reported including morphological changes to the presynaptic components. Using an mdx mouse model that expresses fluorescent proteins in both the motor axon and Schwann cells, I sought to make rigorous measurements and analyze the pre- and postsynaptic structure of NMJs in mdx mice, including the innervating motor axon and tSCs, and to describe how the synaptic rearrangements progress with age in mdx. Furthermore, while the murine mdx model of Duchenne muscular dystrophy has been extensively described at the NMJ level, that for other mammalian models has not been. To fill this void, I analyzed morphological aspects of canine GRMD NMJs to discover if NMJ remodeling is a characteristic of all mammalian dystrophic synapses.

---

[1] The research presented below is adapted from Haddix SG, Lee Yi, Kornegay JN, Thompson WJ (2018) Cycles of myofiber degeneration and regeneration lead to remodeling of the neuromuscular junction in two mammalian models of Duchenne muscular dystrophy. PLoS ONE 13(10): e0205926

2.2. Materials and methods

2.2.1. Mouse strains

C57BL/10ScSn-*Dmd*^{mdx}/J mice (mdx, RRID:IMSR_JAX:001801) were purchased from Jackson Laboratory and mated with transgenic mice expressing both a green fluorescent reporter expressed in Schwann cells, (B6:D2-Tg(s00B-EGFP)1Wjt/J, RRID:IMSR_JAX:005621) and a cyan fluorescent reporter expressed in motor axons (B6.Cg-Tg(Thy1-CFP)23Jrs/J, RRID:IMSR_JAX:003710). Use of these mice has been previously reported and all mice are available from Jackson Laboratories. Mdx mice were crossed into fluorescent mice, and progeny back crossed into mdx for 8 generations to ensure a C57BL/10 congenic background in fluorescent mdx mice. A pool of 4 -7 male mice per genotype and age were used for each experiment, for a total of 111 mice in Sections 2 and 3. Experimental procedures in the formation and maintenance of neuromuscular synapses (2016-0158 or 2019-0179) protocol were approved by Texas A&M University IACUC.

2.2.2. Mouse muscle preparation

Mice were killed via I.P. injection of 0.15 mL of Euthasol. The sternomastoid muscle (STM) was dissected, pinned at resting length to a sylgard dish and fixed using 4% phosphate buffered paraformaldehyde (PFA) for 20 minutes. After fixation the muscles were washed three times with phosphate buffered saline (PBS) and labeled with α-bungarotoxin conjugated to Alexa Fluor™ 647 (ThermoFisher Scientific, Cat# 35450)

for 5 minutes (BTX, diluted 2 μg/mL in PBS). In some cases Fasciculin II (FasII) conjugated to AlexaFluor™ 647 was applied to muscles for 2 hours to label AChE (diluted 0.5 μg/mL in standard blocking solution). DAPI (Thermo Fisher Scientific Cat# D3571, RRID:AB_2307445) was used to label nuclei (diluted 0.5 μg/mL in PBS). After three PBS washes, a longitudinal "filet" from across the surface of the muscle was dissected from distal tendon to proximal tendon and mounted on a microscope slide in anti-fade fluorescence mounting medium.

2.2.3. Image acquisition, and NMJ characterization and analysis

Confocal micrographs were collected on either a Leica TPS II SP5 or a Zeiss LSM 780 microscope using a 40X Oil objective (NA 1.4). Step size was set between 300-500 nm. Laser lines 405 nm, 458 nm, 488 nm, 563 nm, and 633 nm were used as necessary. Images were analyzed in ImageJ (ImageJ, RRID:SCR_003070) by creating maximum intensity projection images from collected stacks. Junctional area was calculated by thresholding the BTX labeled channel using the Auto Threshold tool provided by ImageJ. A polygon shaped region of interest was then circumscribed around the thresholded signal and the region of interest's area measured. Receptor area was measured as the thresholded area of the BTX label within the circumscribed region of the AChR. Dispersion Index was calculated as receptor area/junctional area. The number of AChR fragments (fragmentation) was measured using the objects counter in ImageJ by setting the minimum area for counts as 5 μm^2. This measurement protocol does not consider fragments in separate z-planes, as they may be superimposed in our maximum

intensity projections. Thus, these measurements are a conservative estimate of fragmentation, in that the actual number of fragments for both WT and mdx is likely underestimated. TSC counts were made by counting only fluorescently labeled Schwann cells in proximity to the endplate having coincident nuclear label via DAPI. Axon branch points were measured by creating 3D rotations of the confocal images of fluorescently labeled motor neurons, and then counting the number of times the axon splits. Small varicosities of the motor terminal were not counted as branches.

2.2.4. Canine use

Dogs were used and cared for in accordance with the National Research Council's Guide for the Care and Use of Laboratory Animals and housed at Texas A&M University. Procedures used were approved by university IACUC protocol, Standard Operating Procedures-Canine X-Linked Muscular Dystrophy (2012-052 or 2015-0110). Ages of dogs ranged from 1 to 6 years. Two male and one female wild-type (WT) controls, two females hemizygous for the GRMD mutation (carriers), seven male GRMD dogs, and one myostatin heterozygote/GRMD (MSTN/GRMD) female were used for a total of 13 animals. The animals used in these studies were undergoing necropsy for other purposes and the tissues shared. These dogs were part of a colony owned and maintained by Texas A&M University for research purposes.

2.2.5. Canine muscle preparations

Following euthanasia for non-related procedures via I.V. injection of Euthasol, the middle portion of cranial tibial muscles was dissected and placed in 4% PFA for 20 minutes. After fixation, the muscles were washed three times with PBS. Muscle fiber fascicles were dissected from the section and labeled with BTX conjugated to Alexa Fluor™ 555 overnight in PBS (BTX, diluted to 2 μg/mL). Labeled fascicles were washed in PBS three times and then examined under a fluorescence dissecting microscope to identify the endplate band. A small portion of the fascicle containing the endplate band was cut from the fascicle and embedded in a 3% agarose gel. 40 μm longitudinal sections (parallel to the long axis of muscle fibers) were prepared using a vibratome. These sections were blocked using standard blocking solution (0.2% bovine serum albumin, 0.3% Triton 100X, 0.1% sodium azide in PBS) and labeled via mouse monocolonal antibodies to neurofilament (SMI-31, Covance, RRID:AB_531793, diluted 4 μg/mL in standard blocking solution), synaptic vesicles (DSHB Cat# SV2, RRID:AB_2315387, diluted 4 μg/mL in standard blocking solution) and rabbit polyclonal antibodies to Schwann cells (S100, Dako Cat# Ga504, diluted 4 μg/mL in standard blocking solution) in PBS overnight. After three PBS washes, goat anti-rabbit secondary antibodies conjugated to AlexaFluor™ 647 (Thermo Fisher Scientific Cat# A-21245, RRID:AB_2535813), and goat anti-mouse secondary antibodies conjugated to AlexaFluor™ 488 (Thermo Fisher Scientific Cat# A-11001, RRID:AB_2534069) were applied for two hours in PBS (diluted 2.5 μg/mL in standard blocking solution), along with BTX conjugated to AlexaFluor™ 555 (diluted 2 μg/mL in standard blocking

solution) and in some cases FasII conjugated to AlexaFluor™ 647 to label AChE (diluted 0.5 μg/mL in standard blocking solution). DAPI was used to label nuclei (diluted 0.5 μg/mL in standard blocking solution). Following three additional PBS washes, the sections were mounted on microscope slides using an anti-fade mounting medium.

2.2.6. Statistics

Mice: For analysis of mouse confocal images, STMs from 3-5 individuals of each group were used. Animals were grouped by approximate age and genotype (P38 WT, P38 mdx, etc). Five - 20 NMJs were imaged per muscle. NMJs were pooled for statistical analysis of confocal measurements. P38 animals were 38 ± 3 days old, P66 animals were 66 ± 3 days old, and P450 animals over 450 days old at the time of death. Measurements were averaged and a Student's t-test preformed to assess for significant differences between genotypes. Within genotypes but among ages, 2-Way ANOVA with Bonferroni post-hoc tests were used. The degrees of freedom (df) for each measurement is reported in text as t(df) = t-value, P-value. For t-tests performed on these measurements, the sample size n (number of pooled individual NMJs) was calculated as df + 2.

Canine: For measurements of dog confocal images, muscle preparations from two male and one female WT controls, two female carriers, seven male GRMD dogs, and one GRMD/MSTN female were used for a total of 13 animals. Twenty-50 NMJs were imaged per individual and measurements were made as described above in "Image acquisition and analysis". These measurements were pooled by genotype. A 1-Way

ANOVA with a post-hoc Tukey's test was performed between genotypes on averages of each measurement. The degrees of freedom for each measurement is reported in text as q(df) = q-value, p-value. Statistical analyses were performed using Prism GraphPad 5 software, and statistical significance was set at $P < 0.05$. In figures and text, results are presented as means with SEM, unless otherwise noted.

2.3. Results

2.3.1. Mdx mice undergo progressive fragmentation of their AChR rich endplate

Using fluorescence confocal microscopy, I found changes to NMJ morphology in mdx mice similar to those reported previously (Lyons and Slater, 1991; Minatel et al., 2003; Pratt et al., 2015a). I imaged mdx muscles near the onset of necrosis (P38) and onward. These changes were present in the youngest animals examined. Morphological differences were seen in older adult versus younger mdx animals, matching disease progression. When labeled with fluorescently tagged BTX, a highly specific ligand for the AChRs, the receptors at most individual mdx NMJs were fragmented into discontinuous aggregates. This differs from the pretzel-like receptor aggregates of WT animals, which are arranged into continuous branches (Figure 2.1A). Junctions with this abnormal clustering of AChRs have been classified as fragmented. Instead of continuous tracks of receptor accumulation, AChRs cluster into discrete islands (Lyons and Slater, 1991; Kong and Anderson, 1999; Pratt et al., 2015a). Maximum intensity

projections of confocal stacks were evaluated for the number of AChR fragments they contained. Mdx NMJs had more fragments than WT at all ages (Figure 2.1B. Fragmentation: 336% increase at P38 $t(32) = 7.974$, $P < 0.001$, 77% increase at P66 $t(75) = 4.756$, $P < 0.001$, and 445% increase at P450, $t(19) = 7.186$, $P < 0.001$, t-tests). Notably, at P38 in mdx, there was a population of both fragmented (56.7%) and continuous junctions. I think it is likely, as others have postulated (Minatel et al., 2003), that dystrophic junctions remodel from continuous to fragmented as the animals age, that this remodeling is stochastic in its occurrence, and that this process is irreversible. The irreversibility is suggested by two observations. First, the proportion of junctions that are fragmented increases as mdx mice age and does not fall. At early time points (P14), WT and mdx animals have roughly the same proportion of adult-like, continuous junctions (Minatel et al., 2003), but from P66 on nearly all the AChR aggregates at mdx NMJs are fragmented in appearance. Additionally, the degree of fragmentation becomes more severe as dystrophic animals age, with the number of fragments increasing from 7.3 in P38 mdx animals to 13.0 in P450 mdx animals (Fig 2.1B. $t(90) = 5.460$, $P < 0.001$, 2-Way ANOVA, Bonferroni post-hoc test). In WT animals, no such increase from P38 to P450 was evident, and the average number of fragments at all ages was less than five.

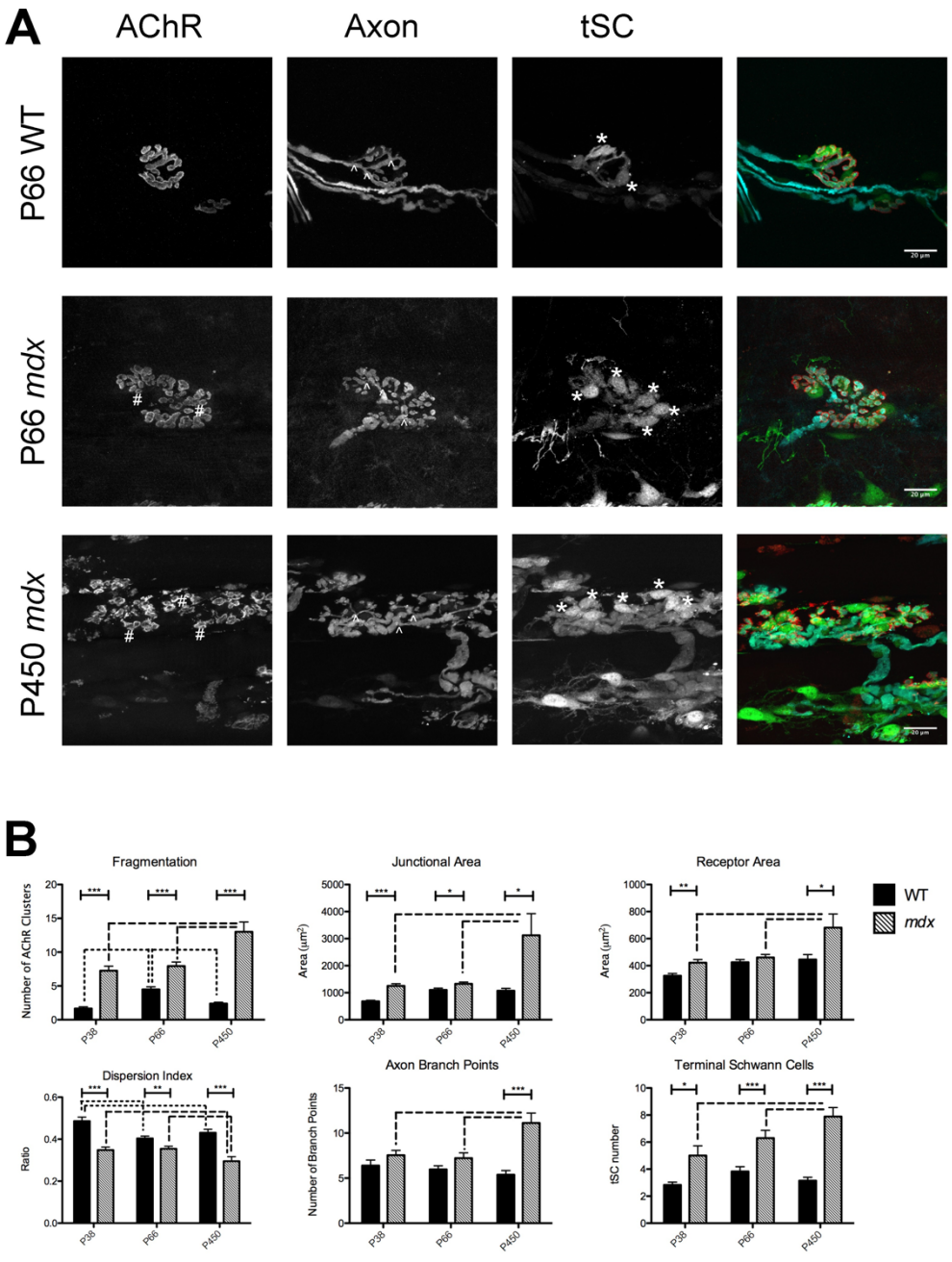

Figure 2.1. WT and mdx NMJs.
(A) Maximum intensity projection confocal images of P66 WT, P66 mdx and P450 mdx NMJs. Images from left to right: AChR, motor axon terminal arbor, tSCs, and composite images. In the composite image, AChRs are pseudocolored red, motor axons cyan, and tSCs green. Scale bar = 20 µm. "#" indicates examples of AChR fragments; arrowheads, examples of axon terminal branch points; asterisks cell bodies of tSCs. In P450 mdx, cells that cannot be positively identified as Schwann cells are evident. These cells are not labeled as tSCs in the panels nor included in measurements, and may be macrophages that express S100 and are plentiful in mdx tissue. (B) Junctional measurements in WT and mdx NMJs from P38 to P450 as described in "Image acquisition and analysis". Asterisks above solid bars denote significance between genotypes (t-test, * $P < 0.05$, ** $P < 0.01$, *** $P < 0.001$). 15 to 90 NMJs were compared for each measurement. Dashed lines denote significance between ages (2-Way ANOVA, Bonferroni post-hoc test, $P < 0.05$).

2.3.2. Mdx mice undergo progressive NMJ expansion and a dispersion of AChRs within the synaptic area

Fragmentation is one of the most striking postsynaptic changes in mdx NMJs, but other measurable differences were also evident. To approximate the size of the entire synaptic structure (i.e. the AChR aggregate, the motor axon terminal, and the tSCs), a polygon was drawn around the labeled receptor aggregate and its area was measured. This polygon included the totality of the receptors, but also included areas between the receptor aggregates that were not labeled with BTX. Thus, the polygon included areas containing tSC somata and processes, and the motor axon terminals ramifying above and between the synaptic contacts, even if these entities were not fluorescently labeled or imaged. I designate this measurement the junctional area. At all ages, the junctional area was larger in mdx than in WT (Figure 2.1B. P38 $t(36) = 6.581$, $P < 0.001$, P66 $t(84) = 2.319$, $P = 0.0228$, P450 $t(19) = 2.537$ $P = 0.0201$, t-tests). WT junctional area ranged from ~35% to ~80% of the mdx Junctional Area.

There was also an increase in junctional area in mdx from P38 to P450 (Figure 2.1B, $t(90) = 5.089$, $P < 0.001$, 2-Way ANOVA, Bonferroni post-hoc test), and P66 to P450 (Figure 2.1B, $t(90) = 5.380$, $P < 0.001$, 2-Way ANOVA, Bonferroni post-hoc test) that was not noted in WT animals. P450 mdx junctional area was about 2.5x that of P38 mdx.

An effort was made to measure just the area that AChRs occupied on the sarcolemma, not including the motor axon and tSCs. The receptor area was

defined as the area within the junctional area that fluoresced intensely when labeled with BTX conjugated to an AlexaFluor™ marker. Mdx NMJs displayed increased receptor area from WT only at P38 and P450 (Figure 2.1B. P38, $t(41) = 3.284$, $P = 0.0021$ and P450, $t(24) = 2.195$ $P = 0.0381$, t-tests). At P38, mdx receptor area was 1.3x as large as P38 WT, while at P450, mdx receptor area was 1.5x as large as P450 WT. In WT endplates, there were no significant changes in receptor area throughout life. The receptor area in mdx increased from ages P38 to P450 (Figure 2.1B. $t(90) = 4.277$, $P < 0.001$, 2-way ANOVA, Bonferroni post-hoc test). There was no increase in receptor area from P38 to P66 in NMJs of mdx mice. It should be noted that receptor area is not a receptor density measurement. While the space that these receptors occupy on the myofiber increases, the density may or may not change at the same time. I chose not to rely on fluorescence intensity measurements to estimate receptor density, as this measurement varies with junctional position in the muscle preparation thickness.

I also investigated the spread of receptors within the synaptic area. To quantify this spread, the receptor area was divided by the junctional area and termed the dispersion index (DI), a measure previously used by Pratt and colleagues (Pratt et al., 2015a). The lower this ratio the more spread there is of the receptor clusters within the junction. Junctions in the mdx animals were consistently more disperse, i.e. had a lower DI than age matched WT (Figure 2.1B. P38 $t(34) = 5.926$ $P < 0.001$, P66 $t(88) = 3.117$, $P = 0.0025$, P450 $t(38) = 5.034$, $P < 0.001$, t-tests). The DIs of mdx animals were ~70% - 90% of WT. The

spread of the receptors within the junction at P450 mdx is 1.2x that of P38 mdx animals ($t(90) = 2.264$, $P < 0.05$, 2-Way ANOVA, Bonferroni post-hoc test). As with fragmentation, this suggests that as mdx animals age, an increasing number of NMJs remodel from the healthy continuous state to the large, fragmented dystrophic state. These results also suggest that individual, dystrophic NMJs can become increasingly remodeled with time, a change not seen in older WT mice. By P66 nearly all the mdx NMJs are remodeled, but significant differences from P66 to P450 can be seen in all the postsynaptic characteristics measured in mdx. It is likely that ongoing degeneration and regeneration of the STM myofibers, not present in WT muscle, is driving these progressive alterations.

2.3.3. Mdx NMJs undergo a remodeling of the presynaptic apparatus

It has been established that mdx mice undergo bouts of myofiber necrosis and regeneration due to their high susceptibility to myofiber damage. This process along with concomitant motor terminal axon activity contributes to NMJ remodeling as noted in exogenous muscle damage (Li and Thompson, 2011). If the motor axon terminal is remodeled in a similar way in mdx to that of damage paradigms, it is possible that the same processes that remodel junctions following myofiber damage are the same that remodel in mdx and dystrophy. To investigate this possibility, measurements on the presynaptic apparatus of NMJs, namely the tSCs and motor axon terminal, were performed. Mdx animals were crossed to transgenic mice that express eGFP driven by the S100 promoter in Schwann cells (Zuo et al., 2004), and CFP in motor axons driven

by the Thy1 promoter (Feng et al., 2000). The number of motor axon branch points in proximity to the endplate was considered a measure of motor neuron terminal rearrangement. Branching pattern differences between mdx and WT animals were not significant except at P450 (Figure 2.1B. Branch Points, $t(21) = 4.816$ $P < 0.001$, t-test). It was noted, however, that the gross morphology of dystrophic terminal arbors was visually distinct from WT. As the motor neuron contacted the muscle fiber at the endplate of healthy WT animals, branches of the terminal tended to run smoothly along the tracks formed by the AChR gutters. Mdx axonal arbors were seen to have small, bulbous varicosities that made connections to the fragmented islands of AChRs (Figure 2.1A). These varicosities were not counted as branches because they were very short. The number of axonal branches did increase from 7.5 to 11.1 (Figure 2.1B. $t(52) = 4.010$, $P < 0.001$, 2-way ANOVA, Bonferroni post-hoc test) in mdx mice from P38 to P450. This trend was not apparent in WT mice, consistent with previous reports that normal junctions could grow and shrink without changing their branching pattern (Balice-Gordon and Lichtman, 1990), although slight changes in postsynaptic structure from P38 to P450 were noted in WT animals.

The number of tSCs was counted for both mdx and WT junctions based on GFP expressed in these cells and coincident nuclear DAPI label (Figure 2.2).

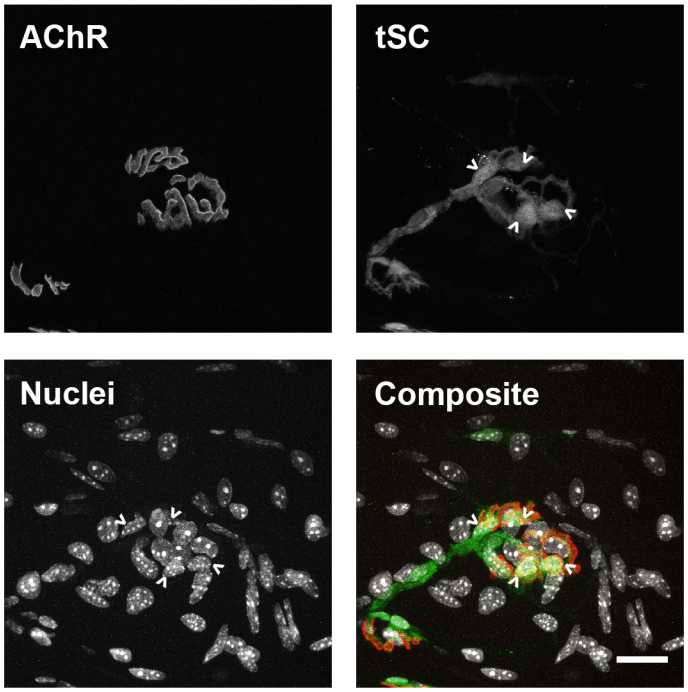

Figure 2.2. Terminal Schwann cell identification.
TSCs are identified by coincident DAPI and transgenic Schwann cells labelling. Arrowheads denote terminal Schwann cell somata identified in this manner. Scale bar = 20 μm.

Dystrophic endplates consistently had more tSCs than age matched WT endplates (Figure 2.1A, B. Terminal Schwann Cells, P38, $t(8) = 2.880$ $P = 0.0205$, P66 $t(33) = 3.655$, $P = 0.009$, P450 $t(21) = 6.711$, $P < 0.001$, t-tests). In mdx the number of tSCs increased with age, from P38 to P450 (Figure 2.1B. $t(45) = 3.441$, $P < 0.01$, 2-Way ANOVA, Bonferroni post-hoc test). The phenomenon was not apparent in WT mice. On average WT P38 animals had 2.8 tSCs per NMJ, while P450 had 3.1. In contrast, at the same ages, mdx NMJs had

on average 5.0 tSCs at P38 and 7.9 at P450. These findings fit well with observations that tSCs are added to the NMJ during the process of junction growth during development (Love and Thompson, 1998). During periods of little to no growth in healthy adult mice, no tSCs are added. However, during the expansion of the endplate from P38 to P450 in mdx mice, as suggested by increased junctional area, there is also an expected addition of tSCs.

2.3.4. GRMD dogs display similar changes in NMJ morphology to those in mdx mice

Mdx mice have a mild phenotype and near-normal lifespan compared to humans afflicted with DMD. Therapies that are effective in treating dystrophic mice have not translated well to humans in clinical settings (Gussoni et al., 1999; Fletcher et al., 2007). We, therefore, sought to determine whether the morphological changes seen in mdx mice also occur in GRMD, a canine model more clinically relevant to DMD (Kornegay et al., 2012). I harvested the midsection of cranial tibial muscles in the hind limb of adult GRMD, WT, and carrier dogs at necropsy performed for other non-related experiments. Carriers were not used as controls as they are female dogs, hemizygous for the GRMD mutation, and there are reports of carriers manifesting certain aspects of the disease state (Emery, 1965; Bostick et al., 2008; Soltanzadeh et al., 2010). A single example of a myostatin heterozygote, dystrophin null (MSTN/GRMD) animal was also included. These animals have a mixed pattern of muscle atrophy and hypertrophy (Kornegay et

al., 2016). Acetylcholine receptors, Schwann cells, and motor neurons were labeled via immunofluorescence and BTX labeling. When imaged using confocal microscopy, changes to the NMJ like those in mdx mice were found. The postsynaptic AChR aggregate was clearly abnormal (Fig 2.3A). The same NMJ measurements made on murine synapses were also made for canine preparations. The NMJs of GRMD dogs were 1.8x as large as their WT counterparts (Figure 2.4. Junctional Area, $q(484) = 9.723$, $P < 0.001$, 1-Way ANOVA, Tukey's post-hoc test). The spread of receptors in GRMD NMJs was 1.6x that of WT (Figure 2.4. Dispersion Index, $q(484) = 19.84$, $P < 0.001$, , 1-Way ANOVA, Tukey's post-hoc test). Finally, the number of fragments of AChRs was higher in dystrophic dogs than in WT (Figure 2.4. Fragmentation, $q(484) = 15.09$, $P < 0.001$, 1-Way ANOVA, Tukey's post-hoc test). WT animals had an average of 1.6 fragments per NMJ, and GRMD 5.8. Generally, no difference in the postsynaptic morphology was noted between WT and carrier groups, or GRMD and MSTN/GRMD groups (Figure 2.3). Trends that held for WT vs GRMD also held for WT vs MSTN/GRMD, Carrier vs GRMD, and Carrier vs MSTN/GRMD. For example, MSTN/GRMD junctional area was increased from WT and Carrier NMJs, and GRMD junctional area was also increased from WT and carrier. For full assessment see Figure 2.4. A significant increase in receptor area was only recorded between carrier and GRMD animals (Figure 2.4. Receptor Area, $q(484) = 5.030$, $P < 0.001$, 1-Way ANOVA, Tukey's post-hoc test), but receptor area for carriers was generally lower than all other groups. The

fact that differences between carriers and other groups were found at all, gives credence to the claims that carriers may have unrealized or mild phenotypes due to abnormal level of functional dystrophin (Soltanzadeh et al., 2010). While the distribution of dystrophin is uniform in carrier animals in adult hood, a mosaic pattern in the muscle fibers is observed earlier in life (Cooper et al., 1990). It is possible that the NMJ restructuring process in the carriers occurs when portions of the myofiber are more susceptible to damage due to lack of dystrophin expression. If this is the case it is unlikely that the morphology would revert back to that of a WT junction, as it is suggested that once an NMJ remodels it remains in its new morphology (see below).There was no statistically significant difference between WT and carrier, nor GRMD and GRMD/MSTN in any of the postsynaptic measurements.

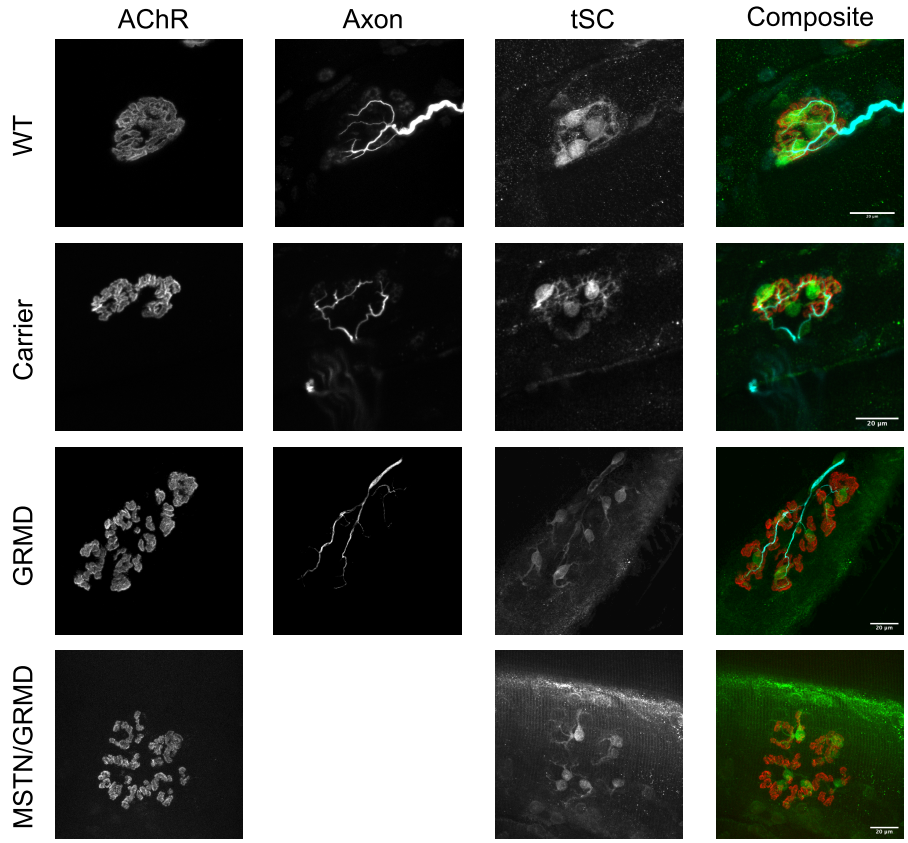

Figure 2.3. Canine NMJ morphology.
Confocal maximum intensity projection of adult WT, Carrier, GRMD, and MSTN/GRMD NMJs harvested from the cranial tibial muscle. Axon image from MSTN/GRMD missing due to lack of staining. Composite images pseudocolored red-AChR, cyan-motor axon, green-tSC. Scale bar = 20 μm. Note the difference in magnification between top two and bottom two rows.

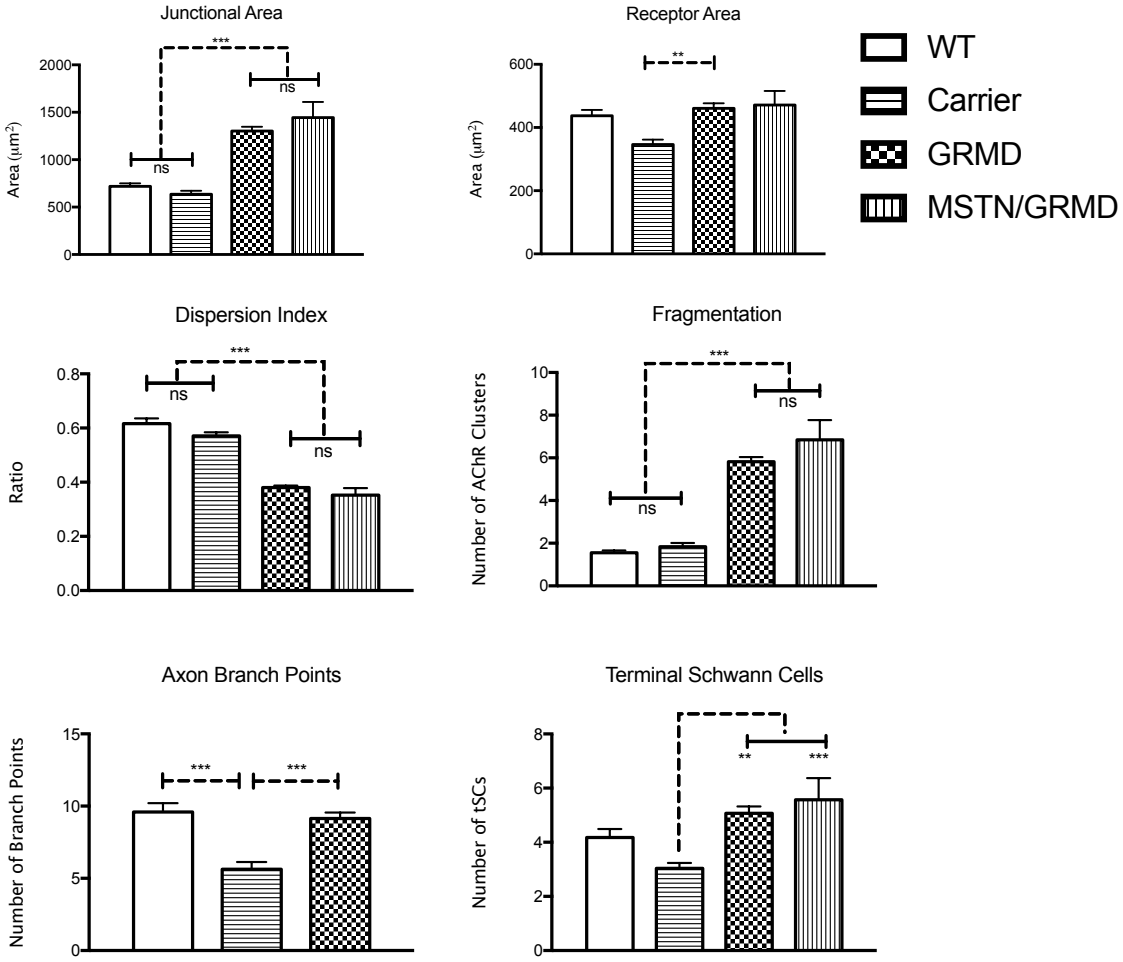

Figure 2.4. Canine NMJ measurements.
Junctional measurements in WT and GRMD NMJs as described in "Image acquisition and analysis". Solid lines between groups denotes no significant differences (ns). Dashed lines between groups denote significant differences. For example, there is no significant difference in Junctional Area between WT and Carrier, or GRMD and MSTN/GRMD. There is a significant difference between WT or Carrier and GRMD or MSTN/GRMD. Asterisks denote significant differences (** $P < 0.01$, *** $P < 0.001$). 1-Way ANOVA Tukey's post-hoc test.

When the presynaptic apparatus of the NMJ was investigated, no differences in the number of motor axon branches were noted between WT and GRMD (Figure 2.4. 1-Way ANOVA, Tukey's post-hoc test), similar to the case

of younger mdx reported above. However, the number of branch points in carriers was significantly lower than WT (Figure 2.4. $q(256) = 5.711$, $P < 0.001$, 1-Way ANOVA, Tukey's post-hoc test) and GRMD (Figure 2.4. $q(256) = 5.831$, $P < 0.001$). In some preparations, it was evident that GRMD axon terminals also synapsed on the myofiber in varicosities (Figure 2.5) similar to that of mdx. However, this was not apparent in all images, and is likely due to incomplete labeling using the antibodies to synaptic vesicles and neurofilament.

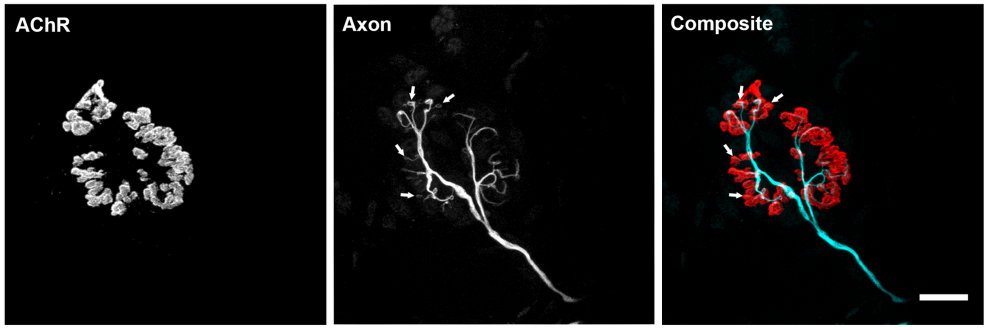

Figure 2.5. Motor axon varicosities in GRMD.
Maximum projection confocal images of a GRMD NMJ from the cranial tibial muscle. Arrows indicate bulbous varicosities in the nerve terminal. Not all varicosities are noted in the image. In composite image AChR are pseudocolored red and motor axons cyan. Scale bar = 20 μm.

Consistently weaker labeling was observed in the canine preparations than those obtained in mice. It is possible that older GRMD dogs would show increased changes like those in the P450 mdx mice, but this was not investigated.

Finally, there was no difference in the number of tSCs between GRMD and WT dogs, but again immunofluorescent labeling was the method used in dog preparations. In mouse investigations, the use of transgenic fluorescent proteins in the Schwann cells and the motor neurons allowed for more faithful labeling. Carriers, however, had less tSCs than GRMD (Figure 2.4. $q(142) = 6.174$, $P < 0.001$, 1-Way ANOVA, Tukey's post-hoc test) and GRMD/MSTN (Figure 2.4. $q(142) = 5.111$, $P < 0.01$, 1-Way ANOVA, Tukey's post-hoc test). Again, this indicates a potential subclinical phenotype in non-manifesting carriers of DMD. Alternatively, as all carriers are by necessity female, as GRMD is an X-linked genetic disease, there may be sex differences in the NMJ morphology. I attempted to control for this by including both male and female dogs in the WT group. Regardless, the similarities between mdx and GRMD NMJs suggest that remodeling occurs in all mammals that lack dystrophin. This includes boys with DMD. What exactly is causing these changes has not been satisfactorily investigated, however. In Section 3, I was able to investigate if myofiber degeneration and regeneration were indeed causative in remodeling in dystrophy.

2.3.5. Ghost junction observations

AChE is an enzyme tethered to the basal lamina within the synaptic cleft, and is critical to the function of the synapse. Because it is attached to the dense collagen matrix of the basal lamina, and not part of the muscle, nerve, or tSCs, following the removal of any of these cellular components of the NMJ, AChE will remain. Labeling with FasII, a toxin

like BTX that binds the AChE, allows researchers to identify areas on the muscle fiber that were previously NMJs even in the absence of other markers, like AChR. “Ghost” junctions, NMJs that retain AChE but have no indication of AChR, have been used to mark areas of myofiber degeneration at the endplate area. In both mdx and GRMD muscles, ghost junctions were found (Figure 2.6). In many cases, these had an abnormal appearance. The innervating axon remained and had bulbous varicosities presumably sitting on the myofiber where receptor had been previously. This observation substantiates the hypothesis that myofiber degeneration and regeneration does occur at the synaptic area and may somehow be linked to NMJ remodeling in muscular dystrophy.

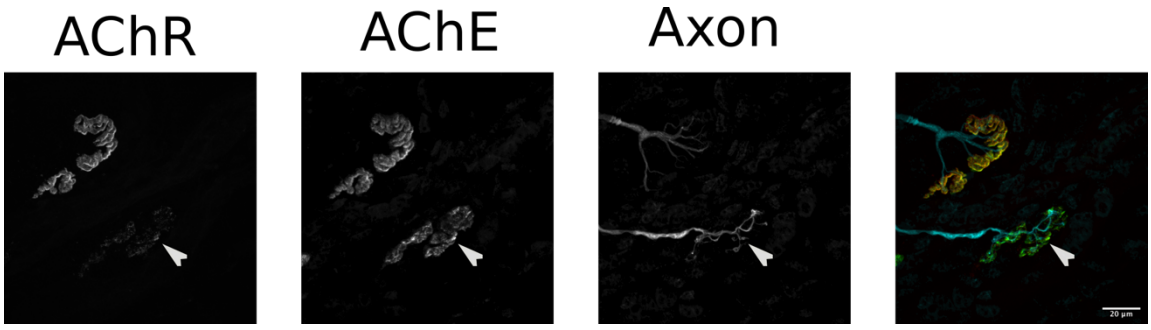

Figure 2.6. Canine ghost junction.
Maximum projection confocal micrographs of GRMD NMJ labeled with BTX, FasII. SMI-31 and SV2, for AChR, AChE, neurofilament, and synaptic vesicles respectively. Arrowheads denote ghost junctions. Right most panel is a composite image with AChR pseudocolored red, AChE green, and motor axon cyan. Yellow shows colocalization of AChR and AChE. Scale bar = 20 μm.

2.4. Discussion

The morphological abnormalities that are evident in mouse mdx NMJs also occur in the more clinically relevant canine GRMD model and the same processes that instruct remodeling mice likely also occur in GRMD. This suggests that NMJ remodeling is a common consequence of muscular dystrophy in all animals, including human DMD patients. It has been suggested that DMD NMJs are also fragmented, but this was assessed in cross sectional slices of myofibers, which does not give a fully realized assessment of the NMJ morphology (Theroux et al., 2008). Non-diseased human NMJs, however, display increased levels of fragmentation from WT mice (Jones et al., 2017), and the morphology does not change drastically throughout human life span, unlike mice. I provide evidence that the remodeling of mdx NMJs progresses with age, likely as a result of ongoing degenerative and regenerative events that occur in STM of mdx mice.

Muscle fiber damage has been shown to rearrange the NMJ. Based on observations in vivo of deliberate muscle fiber damage, this is thought to occur through the motor axon terminal, which is normally directly opposed to the receptor islands that appear after regeneration of each damaged fiber. The motor terminal was found to extend processes along the regenerating muscle fiber and it was proposed that the motor neuron directs the insertion of AChRs into new contact sites in the sarcolemma, resulting in a larger and fragmented endplate with a more complex motor axon terminal arbor (Li and Thompson, 2011). It is probable this phenomenon is occurring in dystrophic mice as well.

The tSCs of the dystrophic NMJ may also be contributing to the changes in morphology. When the activity of these glial cells is modified, NMJs are observed to be more fragmented in appearance without any indication of muscle fiber damage (il Lee et al., 2016). In dystrophic animals others and I noted changes to the tSCs, including increased number and the appearance of cellular processes (Personius and Sawyer, 2005). Sprouting of tSCs and axonal processes to nearby NMJs, however was not noted. When tSC number was plotted against fragmentation no significant correlation was noted, and thus not presented. I suggest that the main cause of NMJ remodeling is myofiber injury, but cannot totally discount that tSC activity also plays a role.

Fragmentation of the AChR aggregate is perhaps the most profound and progressive change seen in the mdx endplates. The vast increase in the number of fragments from the earlier time points (P38 and P66) to P450 is quite evident even without the use of descriptive statistics. An increase and then decrease in the number of fragments was noted in WT animals during the time course studies. However, this likely does not indicate the same remodeling process seen in mdx animals. While the maximum number of fragments in WT animals was recorded as 10 at P66, the maximum number of fragments in mdx was over 15 at all ages and in some cases reached over 20. The average number of fragments for WT animals was always under 5 for each age, which in some reports is used as the distinction between a non-fragmented and fragmented endplate (Valdez et al., 2010). Again, the change in the mdx animal seems to be permanent.

Observationally, past the P38 time point in STM no pretzel like endplates were seen. If fragmented junctions could return to a normal appearance, at least a small proportion of endplates would be pretzel-like. While some mdx are indeed more continuous in nature, they still look abnormal and resemble fragmented junctions whose receptor islands have collapsed into each other, not the normal AChR ribbons seen in WT.

I do not think that many of the changes seen in dystrophy, such as increase in junctional area, are due to increases in muscle fiber diameter. As muscle fibers grow, the receptor aggregate upon them also increases in size. One could postulate that the increase in junctional area of mdx junctions is a function of increased dystrophic muscle fiber size, possibly due to hypertrophy. This hypothesis does not hold under scrutiny for one decisive reason. While variation in muscle fiber cross sectional area is higher in mdx, the average myofiber cross sectional area is no different between WT and mdx animals (Coulton et al., 1988a; Briguet et al., 2004). This shows that the size of a dystrophic junction grows at a rate that is not mimicked by the myofiber cross sectional area. Observationally, much of the increase in dystrophic NMJ size occur along the length of the myofiber, though a direct measurement of the axis of growth was not made. An effort was made to sample a repertoire of NMJs in different lateral sections of the muscle filet to not skew our results towards a certain NMJ morphology. However, only superficial myofibers were assessed. If these myofibers on the outside of muscle are morphologically dissimilar to inner

fibers, our conclusions may be biased towards the larger fragmented NMJs of mdx animals. The same prep was used on WT muscles.

While many have postulated that the NMJ changes in mdx animals are due to myofiber damage, there has been little direct investigation of the link between these phenomena. Other investigators have correlated central chains of nuclei within a myofiber to fragmented junctions (Lyons and Slater, 1991), but it is unclear if central nuclei are a marker for recent myofiber regeneration. Historically, myofibers with nuclei in the center of the cytoplasm instead of the periphery have been used to identify regenerated muscles (Benoit and Belt, 1970). Unfortunately, this method of investigating regeneration has its drawbacks. For one, the time course over which myonuclei move from the center to the periphery of the fiber may be very long and not indicate truly recent regeneration (Wada et al., 2008). The incidence of encountering ghost junctions in dystrophic tissue, however, gave a further indication that myofiber degeneration was occurring at synaptic sites. This is worth noting as a homolog of dystrophin, utrophin is concentrated at the NMJ, and could have been providing a protective role against contraction induced damage. Upregulation of utrophin has in fact been shown to decrease the incidence of damage in mdx mice (Tinsley et al., 1998; Gilbert et al., 1999). The endplate area of the muscle, however, does not appear to be spared from degenerative and regenerative events. Ghost junctions, while not arranged in the classical fragmented appearance of dystrophic postsynaptic apparatus, did display changes to the presynaptic apparatus. Ghost junctions may indicate a step in the remodeling pathway, that occurs following myofiber degeneration. The nerve terminal

may then rearrange, and upon regeneration of the myofiber the AChR aggregate could also remodel as suggested by myofiber injury experiments (Li et al., 2011; Li and Thompson, 2011). In subsequent sections, I use a technique to identify recently regenerated myofibers at the synaptic site, and correlate this to the process of NMJ remodeling.

3. CAUSES OF NMJ REMODELING IN MDX[2]

3.1. Research impetus

Finding that two models of muscular dystrophy share a similar NMJ phenotype (Section 2), there was justification for investigating what causes these changes in mdx mice, as it is probably conserved in all mammals that lack the dystrophin protein. It has long been hypothesized that muscle degeneration and regeneration is the initial insult that results in NMJ remodeling. This is supported by experimentation showing fragmentation of the receptor endplate in deliberately damaged muscle fibers of healthy mice. It is well established that lack of dystrophin leaves muscle fibers more susceptible to contraction-induced damage (Moens et al., 1993). So, the linkage of two phenomena is well founded. Further indirect evidence that muscle fiber damage causes NMJ remodeling can be found when AChE is used as an indicator of muscle degeneration. AChE remains tethered to the basal lamina even after muscle fiber degradation; however, AChR is destroyed along with the muscle fiber membrane. NMJs with strong AChE label following damage, and weak or absent AChR, have been termed ghost

---

[2] The research presented below is adapted from Haddix SG, Lee Yi, Kornegay JN, Thompson WJ (2018) Cycles of myofiber degeneration and regeneration lead to remodeling of the neuromuscular junction in two mammalian models of Duchenne muscular dystrophy. PLoS ONE 13(10): e0205926

junctions. Ghost junction labeling has allowed researchers to determine the location of previous endplate areas, even in the absence of AChR labeling. Frequently, small puncta of AChR are detected directly under the strong AChE label, indicating receptor tethering to the basal lamina as well. In dystrophic muscle preparations, an increased incidence of ghost junctions suggests significant muscle fiber degeneration at the endplates of dystrophic muscles.

Neither a causal relationship, nor a direct correlation, between muscle fiber damage caused by dystrophy and NMJ remodeling have been adequately investigated. Using a methodology that detects changes in AChR loss and replacement from the sarcolemma over time, I have investigated whether NMJ remodeling is correlated with muscle fiber degeneration and regeneration in dystrophic mice. This method only allows us to make these correlations, but also examine whether myofiber degeneration and regeneration are ongoing phenomena in mdx mice. As mentioned before, the loss of dystrophin in mice is associated with early myofiber damage that stabilizes after about 12 weeks.

The research outlined here in Section 3 indicates that receptor replacement, due to muscle cell degeneration and regeneration, in mdx is associated with NMJ remodeling, and that in the STM myofiber injury is occurring at a constantly higher rate. Elevated myofiber degeneration is not confined to a crisis period in mdx STM. In muscle fiber injury paradigms, the motor axon terminal has a dominant role in remodeling (Li and Thompson, 2011), and the same is true in dystrophy as reported below. Myofiber

degeneration and regeneration triggers both presynaptic and postsynaptic apparatus rearrangement. While it has been suggested that a similar phenomenon takes place in mdx muscle fibers (Marques et al., 2007), this link needed further investigation. Here, I demonstrate that remodeling of the NMJ in mdx is initiated by myofiber injury, but that the motor axon terminal must be present for remodeling to occur.

3.2. Materials and methods

3.2.1. Mouse strains

Mice were generated as in Section 2.2.1. Three to seven male mice per genotype and age were used for each experiment, for a total of 111 mice in Sections 2, 3. Experimental procedures in the formation and maintenance of neuromuscular synapses (2016-0158 and 2019-0179) protocol were approved by Texas A&M University IACUC.

3.2.2. In vivo two-color α-bungarotoxin

Mice were anesthetized via isoflurane inhalation and placed in a supine position. To investigate the STM, neck hair was removed using a depilatory and the surgical site sterilized with povidone-iodine. An incision was made from chin to sternum and the skin retracted. The salivary glands were moved to the side to expose the STM. Surrounding connective tissue was gently removed and a non-saturating concentration (diluted 2 μg/mL in sterile lactated Ringers) of α-

bungarotoxin conjugated to Alexa Fluor™ 555 (ThermoFisher Scientific, Cat# 35451) applied to the surface of the muscles for 5 minutes (BTX-1). The neck cavity was then washed copiously with lactated Ringer's ten times. For muscle injury experiments, superficial muscle fibers at areas close to the site of entry of the accessory nerve into the muscle were cut with a sterile #15 surgical scalpel. The contralateral muscle was also labeled with BTX-1, but not injured and used as an internal control (IC). For denervation experiments both STM muscles were labeled with BTX-1 and the accessory nerve of one STM was severed near its insertion site into the muscle. The other muscle was spared and used as an IC. The salivary glands were moved back into place following labeling, washing, and injury. The skin was sutured with 8-0 silk and treated with 2% lidocaine hydrochloride jelly. Animals were allowed to convalesce for ten days post-surgery. Endpoints for the studies are labeled P38, P66, P160, and P450. P38 animals were 38 $\pm$ 3 days old, P66 animals were 66 $\pm$ 3 days old, P160 animals were P160 $\pm$ 3 days old, and P450 animals over 450 days old at the time of death. A similar protocol was used to investigate receptor replacement in the tibialis anterior (TA) of WT and mdx mice. An incision was made near the tarsal joint of mice that reached to above the knee. The skin was separated and the connective tissue surrounding the TA was gently removed. A 1:500 dilution of BTX-1 in Ringer's was continuously dripped onto the muscle for 5 minutes, and followed by a 5-minute Ringer's drip. The wound was closed using an 8-0 silk suture and the animal allowed to convalesce for 10 days. In order to match

previous research describing the cellular pathology of the mdx TA end points of P31, P45, and P100+ were used. Mice were killed via I.P. injection of 0.15 mL of Euthasol. The STM or TA was dissected, pinned at resting length to a sylgard dish and fixed using 4% PFA for 20 minutes. After fixation, the muscles were washed three times with PBS and labeled with α-bungarotoxin conjugated to Alexa Fluor™ 647 (ThermoFisher Scientific, Cat# 35450) for 5 minutes (BTX-2, diluted 2 μg/mL in PBS). DAPI (Thermo Fisher Scientific Cat# D3571, RRID:AB_2307445) was used to label nuclei (diluted 0.5 μg/mL in PBS). After three PBS washes, a longitudinal filet from across the surface of the muscle was dissected from distal to proximal tendon and mounted on a microscope slide in anti-fade fluorescence mounting medium.

3.2.3. Image acquisition, and NMJ characterization and analysis

Junctions were counted and categorized using a Leica DMRX epifluorescence microscope and a 40X Oil objective (NA 1.4). Junctions were considered fragmented if they had 5 or more non-connected clusters of AChRs in close proximity to each other on the same myofiber. Junctions were categorized based of the brightness of BTX-1 and BTX-2 labels, as well as if they were continuous (< 5 AChR clusters), or fragmented (> 5 AChR clusters). They were classified as stable if BTX-1 and BTX-2 labels were both bright, or as dynamic if BTX-1 label was totally or mostly absent and BTX-2 label bright. In many cases dynamic junctions did not completely lose BTX-1, and small puncta of fluorescence was seen. It is likely that these puncta are BTX-1 labeled

receptors tethered to the basal lamina and demarcate the initial synaptic site before myofiber degeneration. If both the BTX-1 and BTX-2 labels were faint, junctions were classified as lost, but this was rarely observed. In order to verify that dynamic junctions indeed lose their BTX-1 label, a subset of STMs were removed immediately following the initial exposure, at Day 0 without any convalescence. After dissection, the Day 0 muscles were labeled with BTX-2. In all junctions BTX-1 and BTX-2 labels were bright and junctions were all categorized as stable. Characterization and counts were performed by multiple researchers on the same muscle preparation, and similar results obtained. Fifty - 100 NMJs were characterized for each muscle preparation.

Confocal micrographs were collected on either a Leica TPS II SP5 or a Zeiss LSM780 microscope using a 40X Oil objective (NA 1.4). Step size was set between 300-500 nm. Laser lines 405 nm, 458 nm, 488 nm, 563 nm, and 633 nm were used as necessary. Images were analyzed in ImageJ (ImageJ, RRID:SCR_003070) by creating maximum intensity projection images from collected stacks. Junctional area was calculated by thresholding the BTX-2 labeled channel using the Auto Threshold tool provided by ImageJ. A polygon shaped region of interest was then circumscribed around the thresholded signal and the region of interest's area measured. Receptor Area was measured as the thresholded area of the BTX label within the circumscribed region of the AChR. Dispersion Index (Pratt et al., 2015a) was calculated as receptor area/junctional area. The number of AChR fragments (fragmentation) was measured using the objects counter in ImageJ by setting the minimum area for counts as 5 μm^2. This measurement does not consider fragments in separate z-planes, as they may be

superimposed in our maximum intensity projections, and it is a conservative estimate of fragmentation. The actual number of fragments for both WT and mdx is likely underestimated by this measurement. tSC counts were made by counting only fluorescently labeled Schwann cells in proximity to the endplate having coincident nuclear label via DAPI. Axon branch points were measured by creating 3D rotations of the confocal images of fluorescently labeled motor neurons, and then counting the number of times the axon splits. Small varicosities of the motor terminal were not counted as branches.

3.2.4. Statistics

For analyses of mouse confocal images, STMs from 3-5 individuals of each group were used. Animals were grouped by approximate age and genotype (P38 WT, P38 mdx, etc). 5-20 NMJs were imaged per muscle. NMJs were pooled for statistical analysis of confocal measurements. P38 animals were 38 $\pm$ 3 days old, P66 animals were 66 $\pm$ 3 days old, P160 animals were P160 $\pm$ 3 days old, and P450 animals over 450 days old at the time of death. P450+ mdx animals age average was 459.25 days, and WT 554.5 days. Measurements were averaged and a Student's t-test performed to assess for significant differences between genotypes. Within genotypes but among ages, 2-Way ANOVA with Bonferroni post-hoc tests were used. The degrees of freedom for each measurement is reported in text as t(df) = t-value, P-Value. For t-tests performed on these measurements the sample size n (number of pooled individual NMJs) can be calculated as df + 2.

For receptor replacement values and NMJ categorization (e.g. stable, continuous; dynamic, fragmented…), 4-7 animals per genotype and age were used. 50-100 junctions were categorized per muscle, based on the brightness of the BTX-1 label (e.g. stable, dynamic) and the morphology of the BTX-2 label (e.g. continuous, fragmented, or lost). Lost junctions are considered dynamic. Category counts were then transformed into percentages of total counted NMJs for each muscle prep. These percentages were averaged between groups (P38 WT, P66 mdx…). 2-Way ANOVA with Bonferroni post-hoc analyses were performed to assess significant differences both between genotypes and within genotypes. The degrees of freedom for each measurement is stated in text as t(df) = t-value, P-value. For statistical tests performed on these measurements, the sample size n (the number of mice compared) can be calculated as df + 2. Statistical analysis was performed using Prism GraphPad 5 software (GraphPad Prism, RRID:SCR_002798). Statistical significance was set at $P < 0.05$. In figures and text, results are presented as means with SEM unless otherwise noted.

3.3. Results

3.3.1. AChR replacement is elevated in mdx mice throughout life

I investigated whether the dynamics of the AChR expression and distribution could provide evidence of how the dystrophic NMJ becomes remodeled. The rationale behind the approach is that loss of receptors from the myofiber membrane, due to sarcolemma breakdown at the endplate area during necrosis,

should indicate recent degeneration of the myofiber (Li et al., 2011). Upon subsequent regeneration of the myofiber, new AChRs would be inserted into the membrane, allowing the resumption of neuromuscular transmission. A loss of receptors coincident with abnormal endplate morphology would suggest that necrosis and regeneration spurs morphological changes to the NMJ. Not only could the removal of receptors be correlated to changes in NMJ structure, this technique would allow us to determine if a crisis period of elevated myofiber degeneration is occurring in the labeled muscles, and if synaptic regions of the myofiber are spared from degenerative processes. If a crisis period is occurring, then receptor replacement in mdx muscles would initially be much elevated compared to WT, but then drop to lower levels.

To investigate this possibility, the AChRs of STMs and TAs were labeled with a sub-saturating dose of fluorescently tagged BTX (BTX-1) in live mdx and WT mice (Figure 3.1). The concentration and exposure time have previously been shown to not affect neuromuscular transmission or NMJ morphology (Akaaboune et al., 1999). Following a 10-day recovery period (endpoints of P38, P66, P160, and P450+) that allows for the occurrence of any ongoing myofiber degeneration and regeneration, the labeled muscle was dissected from the animal and labeled with a second spectral variant of fluorescently tagged BTX (BTX-2). This method is termed the in vivo two-color BTX method (Figure 3.1).

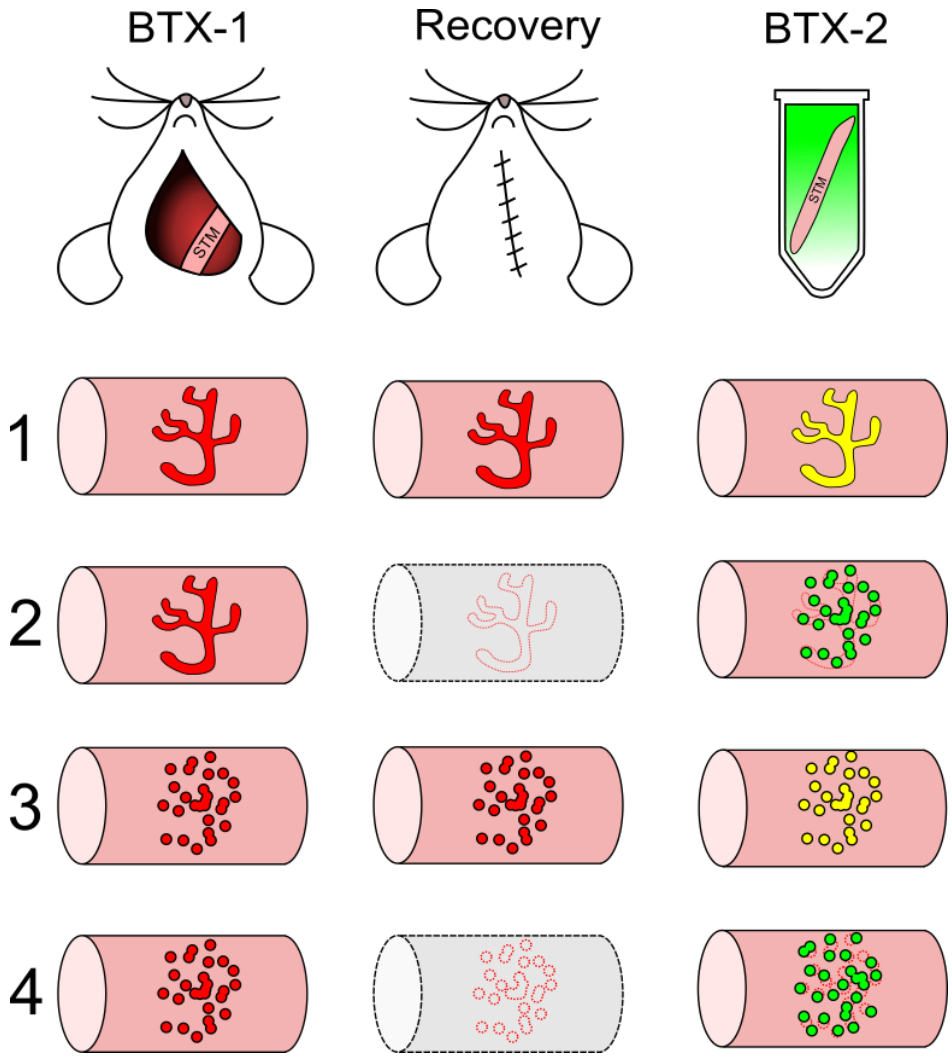

Figure 3.1. Two-color BTX experimental design and outcomes.
Two-color BTX experimental design. The STM or TA of mice was exposed and labeled with BTX-1 at Day 0 (BTX-1 column). The animal was allowed to recover from the surgery for 10 days (Recovery column) and then euthanized. The labeled muscle was dissected from the animal and labeled with BTX-2 (BTX-2 column). The lower portion illustrates four predicted outcomes of the experiment. In red is a possible morphology of BTX-1 labeled AChR aggregates at Day 0 of the experiment, in green BTX-2 label at Day 10. Colocalization of BTX-1 and BTX-2 is indicated with yellow. Intact myofibers are shown as pink tubes, and a degenerating myofiber is shown as a gray tube. Scenario 1 shows a stable, continuous junction. 2 a dynamic, fragmented junction. 3 a stable, fragmented junction, and 4 another dynamic, fragmented junction. Please note that because I do not image the junctions at Day 0, both scenario 2 and scenario 4 would be recorded as the same type of NMJ, a dynamic, fragmented junction.

Using epifluorescence microscopy, STM junctions were categorized based on both their morphology (fragmented or continuous) and the presence of each of the two spectral labels. If BTX-1 was lost and BTX-2 was bright, junctions were categorized as dynamic. If the brightness of the BTX-1 label was similar to BTX-2, junctions were categorized as stable (Figure 3.1 and 3.2A). If both BTX-1 and BTX-2 were weak, the junction was categorized as lost. It has been noted that there is rarely a complete removal of the BTX-1 label even after a bout of myofiber degeneration that follows deliberate damage to fibers. This residual label appears punctate and probably marks the initial synaptic site where, as mentioned earlier, some receptors remain tethered to the basal lamina after myofiber degradation (Slater, 1990; Li and Thompson, 2011).

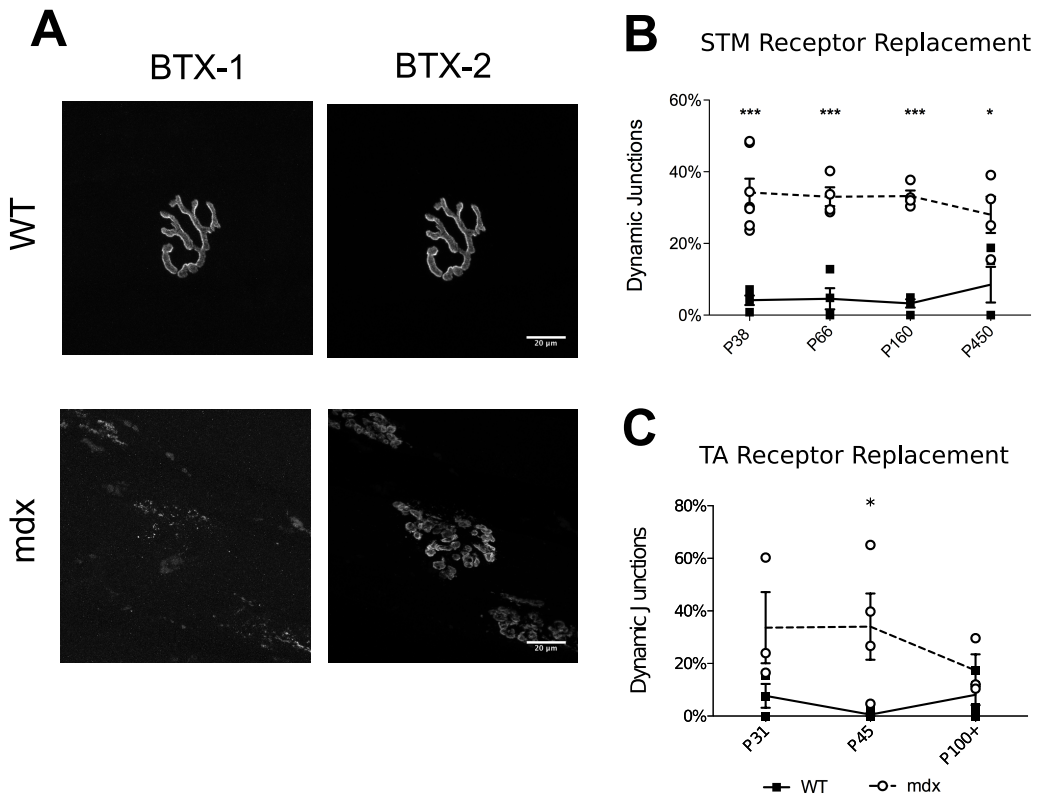

Figure 3.2. Two-color BTX results.
(A) Maximum intensity projection images of STM whole mounts that have undergone the two-color BTX procedure. Examples are from P66 mice. BTX-1 is the first receptor label. BTX-2 is the second applied 10 days later. The WT NMJ is stable continuous, and the mdx NMJ dynamic fragmented. Imaging follows muscle dissection. In mdx there is a loss of BTX-1 and frequently the BTX-2 label shows fragmentation. Scale bar = 20 µm (B) and (C) Receptor replacement in WT and mdx. Dots indicate individual data points. Receptor replacement, calculated as percentage of dynamic junctions, in mdx mice is constantly elevated compared to WT. Asterisks denote significance (* $P < 0.05$, *** $P < 0.001$, 2-Way ANOVA, Bonferroni post-hoc test). No effect of age was found on receptor replacement for either muscle, but there is a trend towards less replacement at P100+ in mdx TA.

In WT mice, receptor replacement, measured as the frequency of dynamic junctions, in STM is consistently low from P38 (Figure 3.2B), indicating no dramatic loss of receptors over the 10-day interval. However, when mdx animals

were investigated at P38, the proportion of dynamic junctions in the STM was 3.3x to 10x as large as WT controls (Figure 3.2B). Lost junctions were considered dynamic in these measurements, as they also indicate degeneration of the myofiber.

Surprisingly, there was no significant effect of age on the frequency of dynamic junctions in mdx muscles, indicating that receptor replacement in the STM is not confined to an early period during the lifetime of mdx mice, but occurs constantly from P38 to P450 (Figures 3.2B; P38 $t(9)= 6.468$, $P < 0.001$, P66 $t(6) = 5.433$, $P < 0.001$, P160 $t(6)= 5.712$, $P < 0.001$, P450 $(6) = 3.719$, $P < 0.01$, 2-Way ANOVA, Bonferroni post-hoc test). While dynamic junctions were used in this report to measure myofiber degeneration and regeneration, there was some evidence of central chains of nuclei directly under dynamic, fragmented junctions (A-1). It is possible that like the diaphragm of mdx mice, the STM does not undergo a crisis period and muscle fiber damage occurs constantly throughout the its life.

The TA had elevated receptor replacement in mdx as compared to WT at only P45 (Figure 3.2C; P45 $t(15) = 3.078$, $P < 0.05$, 2-Way ANOVA, Bonferroni post-hoc-test). While frequency of dynamic junctions was not affected by age in genotype, there was a trend in mdx TA of decreased receptor replacement at P100+. This could indicate that the TA, a hind limb muscle, may indeed be undergoing a crisis period, as has been suggested by previous researchers (Dangain and Vrbova, 1984).

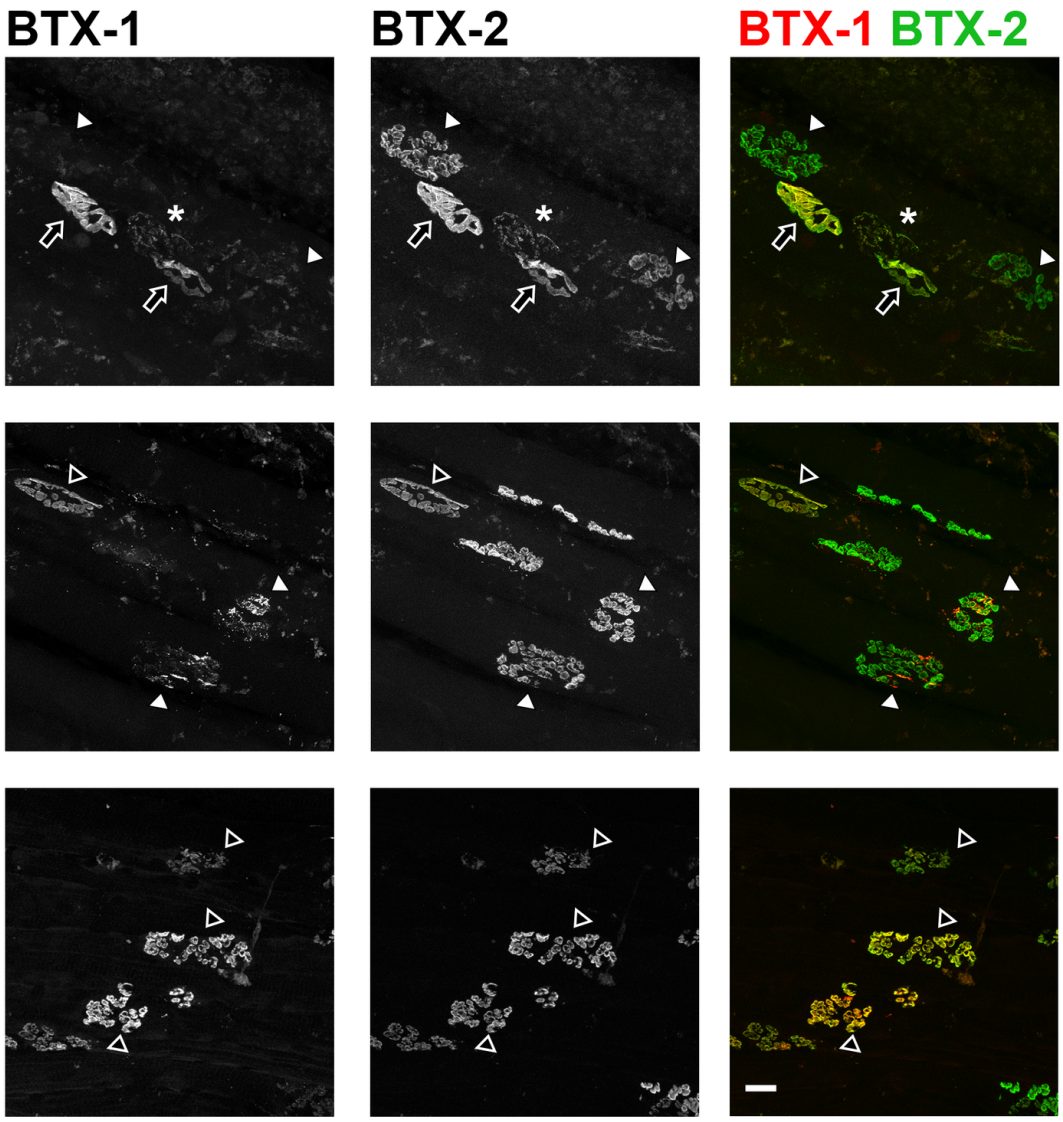

Figure 3.3. P38 mdx NMJ characterization and reproducibility (40X).
Maximum intensity projection images of P38 mdx NMJs following in vivo two-color BTX method. In composite BTX-1 is pseudocolored red and BTX-2 green. Yellow indicates strong colocalization. Black arrows denote stable, continuous junctions. Black arrow heads denote stable, fragmented junctions. White arrow heads denote dynamic, fragmented junctions. Asterisks denote lost junctions. Please note the presence of both dynamic and stable junctions in proximity to each other. This shows that receptor replacement occurs at individual junctions independent of neighboring endplates. This suggest that the absence of dystrophin does not simply shorten AChR half-life and that catastrophic receptor loss and replacement are likely due to myofiber degeneration and regeneration. Scale bar = 20 µm.

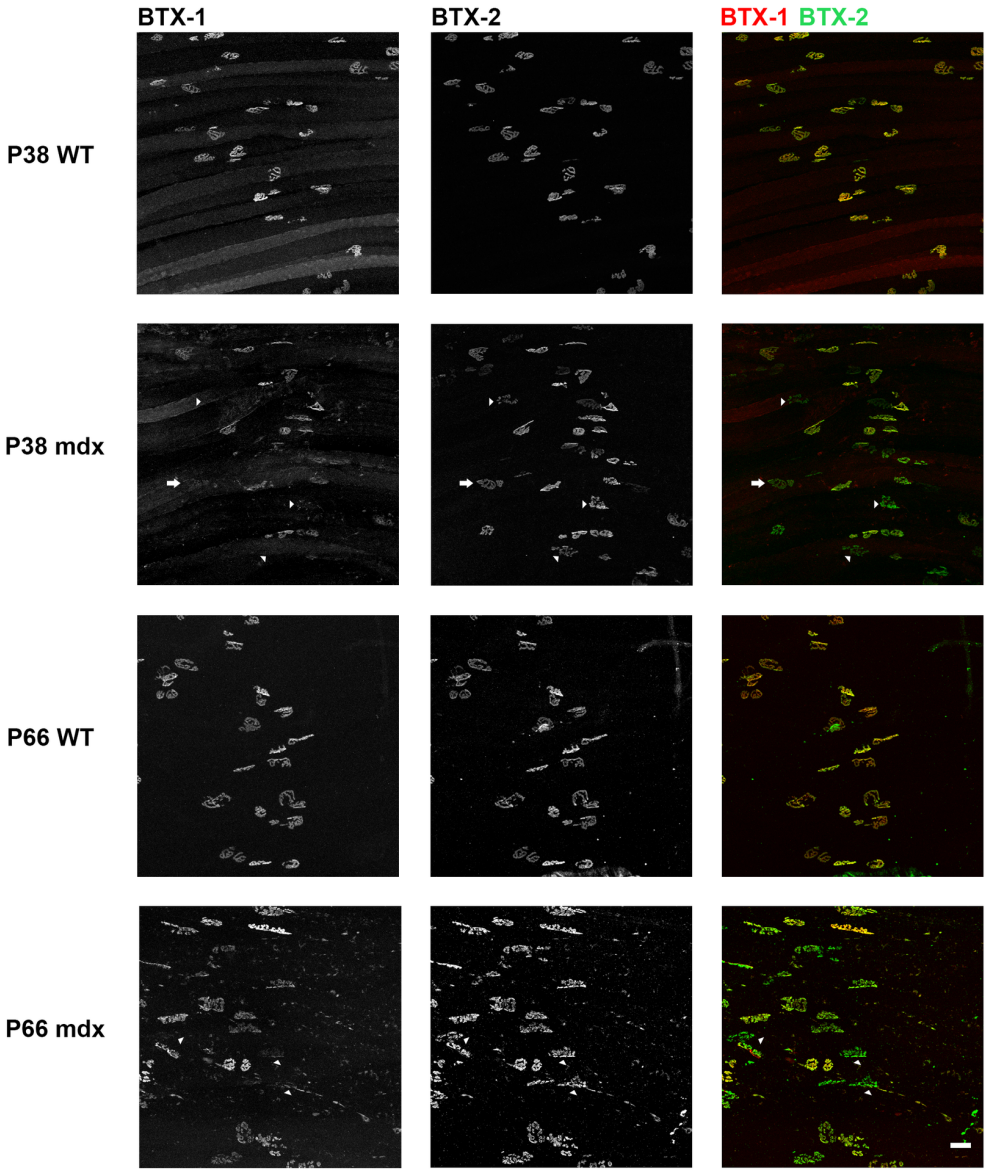

Figure 3.4. P38 and P66 NMJ characterization and reproducibility (20X).
Maximum intensity projection images of P38 and P66, mdx and WT NMJs following in vivo two-color BTX method. In composite BTX-1 is pseudocolored red and BTX-2 (continued)
green. White arrows show examples of dynamic, continuous junctions. White arrow heads denote dynamic, fragmented junctions. Scale bar = 50 μm.

When the morphology of junctions was assessed between mdx and WT animals, I noticed that the predicted decrease in the number of stable, continuous junctions in P38 mdx (Figures 3.3 and 3.5. $t(9) = 12.10$, $P < 0.001$, 2-Way ANOVA, Bonferroni post-hoc test) was accompanied by an increase in the number of dynamic, fragmented junctions (Figure 3.5. $t(9) = 5.763$, $P < 0.001$, 2-Way ANOVA, Bonferroni post-hoc test). This suggested that junctions shift from continuous to fragmented during muscle regeneration. Fragmentation and remodeling of the NMJ is a response to muscle fiber regeneration, that follows the degeneration of muscle cells. It is not that P38 muscles were used in this investigation (Figures 3.3 and 3.4), as after this time point a great majority of mdx endplates are fragmented, and once fragmented NMJs were not shown to revert back to a continuous morphology (Figure 3.4). This was also demonstrated by the constant characterization profile seen from P66 to P450 in mdx mice (Figure 3.5). That is to say stable, fragmented junctions were consistently more frequent than stable continuous, as well as an increased frequency of dynamic fragmented more frequent than dynamic continuous. Once lost stable, continuous junction frequency did not increase. The proportion of stable, fragmented junctions in mdx mice remained at about 60%, and the proportion of dynamic, fragmented junctions remains at about 30% from P66 to P450+. Stable, fragmented junctions indicate NMJs that were remodeling prior to the two-color BTX experiment, and these synapses did not undergo a degenerative process during the 10-day recovery period.

There was a shift in the characterization profile from P160 to P450+ when WT animals are observed. A noticeable increase in the amount of stable fragmented junctions in these older WT animals was seen. This is likely due to an increased amount of myofiber damage, as indicated by the receptor replacement elevation in Figure 3.2, which is simply a consequence of aging (Figure 3.2B). As the myofibers accumulate damage, one would expect to see an increase in frequency of the fragmented (or remodeled) junctions.

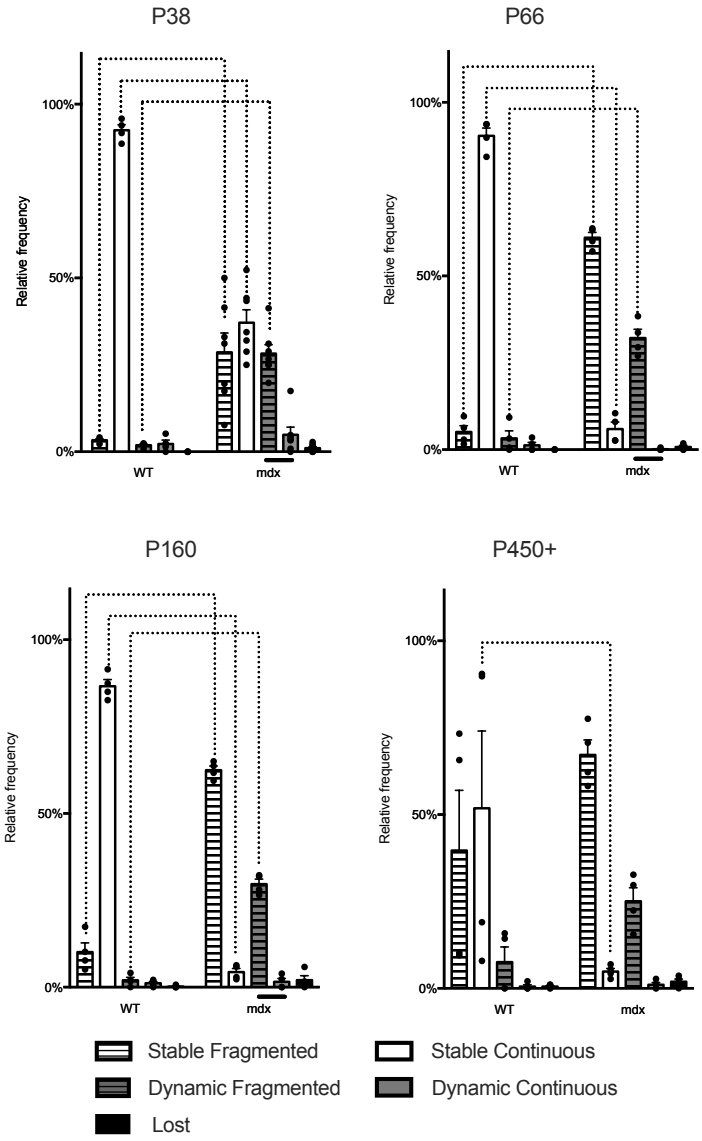

Figure 3.5. Two-color BTX NMJ categorization.
Categorization of WT and mdx junctions from P38 to P450+. Dots within the graph are individual data points. Dashed lines above graph denote significant differences between genotypes. Solid bars below graph indicate significant differences within genotypes (2-way ANOVA, Bonferroni post-hoc test, $P < 0.05$) A full account of statistical significance, including differences within genotypes can be found in A-2.

In P38 mdx animals, the two NMJ morphologies present allowed us to assess whether receptor replacement has any bearing on NMJ morphology. When the morphologies of dynamic junctions were compared within P38 mdx animals dynamic, fragmented junctions were seen at a higher frequency than dynamic, continuous (Figure 3.5. $t(30) = 5.992$, $P < 0.001$, 2-Way ANOVA, Bonferroni post-hoc test). Again, this suggests that in mdx animals, AChR replacement is associated with NMJ remodeling. This correlation was not apparent in P38 WT animals. In WT animals, I found a small fraction of dynamic junctions (both fragmented and continuous) with no significant difference between their morphologies (Figure 3.5). While I predicted that in both WT and mdx mice dynamic junctions would preferentially be fragmented, the WT observation that receptor replacement had no effect on junction morphology may be a result of the overall low levels of fiber damage even in normal muscles. Or alternatively, endplates may have to suffer from multiple bouts of injury in order to trigger the remodeling phenomenon. As such, any striking differences in the morphology of dynamic junctions might have been masked. While not indicated in Figure 3.5 for sake of brevity, a full account of NMJ categorization differences within genotypes (i.e. dynamic fragmented vs stable fragmented) is presented in A-2.

Overall, these results suggest that cycles of myofiber degeneration and regeneration lead to remodeling of their junctions in dystrophy. An alternative explanation is that more rapid receptor replacement is a characteristic of mdx junctions because dystrophin tethers receptors to the membrane, as suggested

from gamma counting of radio labeled AChRs in whole muscles (Xu and Salpeter, 1997). This is unlikely, however, given the presence of both dynamic and stable junctions in the same muscle (Figures 3.3 and 3.4). Elevated receptor replacement was encountered at only a subset of junctions. In fact, dynamic junctions were observed on fibers neighboring those with stable junctions. If dystrophin loss causes a decrease in AChR half-life as suggested in previous research (Xu and Salpeter, 1997)it would be expected that individual endplates would all lose similar amounts of receptors. Also, this rapid replacement is not a constant characteristic of all fragmented junctions. Many fragmented junctions still retain high levels of BTX-1 (i.e. were classified as stable), suggesting that they suffered damage before, rather than during, the 10-day experimental period. Thus, these experiments suggest that the increased receptor replacement is caused by myofiber necrosis resulting from mdx muscle's increased susceptibility to damage. I suggest the receptor replacement is not a primary effect of dystrophin loss, but a secondary effect resulting from dystrophic muscles increased incidence of degeneration and regeneration. I performed further experiments to address whether myofiber damage itself was indeed causing the observed changes in NMJs.

3.3.2. Mdx dynamic junctions show morphological differences compared to stable junctions

When morphological measurements of the NMJ were compared between dynamic and stable endplates of mdx mice, subtle but significant differences were observed. As described in Section 2, pre- and postsynaptic morphologies were analyzed. This included measurements of junctional area, receptor area, fragmentation, DI, number of motor axon branches, and number of tSCs. At P38, the DI of dynamic endplates showed greater spread of the AChR at dynamic junctions (stable = 0.3725 ± 0.02, dynamic = 0.3069 ± 0.016, $t(25) = 2.261$, $P = 0.0327$, t-test). The same trend was evident at P66 (stable = 0.3738 ± 0.013, dynamic = 0.3098 ± 0.028, $t(44) = 2.169$, $P = 0.0216$, t-test). Additionally, at P66, dynamic junctions had a lower receptor area than stable junctions (stable = 508.4 ± 34.21, dynamic = 304.4 ± 36.33, $t(44) = 3.246$, $P = 0.0009$, t-test). No other attributes measured were significantly different between dynamic and stable junctions. As mentioned before at P66, almost all endplates were fragmented. These results suggested that not only can myofiber degeneration and regeneration cause a morphological shift from continuous to fragmented, but also that an already fragmented endplate can rearrange further following additional rounds of myofiber degeneration and regeneration. Continued remodeling may explain the changes in DI, junctional area, and fragmentation in older mdx animals in Section 2. While not measured, there were no obvious receptor clusters in mdx that were not covered by axon terminals. This corresponds well

with our hypothesis and previous work showing that nerve terminal rearrangement following myofiber regeneration is responsible for endplate remodeling (Li and Thompson, 2011). In other words, the nerve likely grows and branches along the myofiber, and directs new sites of receptor accumulation, in non-continuous islands. The regenerating muscle does not first deposit AChRs, which the nerve then innervates.

3.3.3. Fiber damage at the endplate region of the muscle causes increased receptor replacement, in both mdx and WT animals

In order to test whether dynamic junctions are indeed a result of myofiber degeneration and regeneration, the same two-color BTX method was performed in conjunction with deliberate injury of the STM. Briefly, after the BTX-1 label was applied, a superficial cut was made across the muscle with a scalpel near the endplate region to spur myofiber necrosis. The contralateral muscle was also labeled, but not injured, and used as an IC. When this was performed in P38 WT animals, the proportion of dynamic junctions in damaged muscles was 19.1x that of the IC (Figure 3.6A. P38 $t(6) = 3.111$, $P = 0.0208$. t-test). In P66 WT animals, the proportion of dynamic junctions in damaged muscles was 31.6x as large as IC. (Figure 3.6A. P66, $t(6) = 3.963$, $P = 0.0074$, t-test). When deliberate injury was performed at the endplate area in P38 mdx, the proportion of dynamic junctions in damaged muscle was 1.7x as large as that of the IC, and at P66 the proportion of dynamic junctions in damaged muscle was 2.1x as large as the IC (Figure 3.6A. P38 $t(6) = 3.013$, $P = 0.0236$; P66 $t(6) = 3.772$, $P = 0.0093$, t-

test). This showed that myofiber damage near the endplate area was sufficient to induce increases in AChR replacement in both WT and mdx mice. A full accounting of significant differences in NMJ characterization can be found in A-3 and A-4.

Injury made near the sternum, as far as possible from the endplate band of the STM, did not result in significant increases in the amount of receptor replacement in either WT or mdx animals at either P38 or P66 (t-test, df = 6. n.s.). This suggests that damage to the muscle must be in the vicinity of the NMJ to elicit increases in receptor replacement associate with mdx. Myofiber damage in the mdx model likely does not propagate down the entire muscle fiber following a single insult. The long chains of central nuclei result not from a single catastrophic event, but the accumulation of many smaller events of segmental necrosis and regeneration in the myofiber. Our model of assessing myofiber damage and regeneration, however, was focused on the NMJ. Therefore, I could not assess the segmental nature of damage and can only suggest it does not travel down the myofiber.

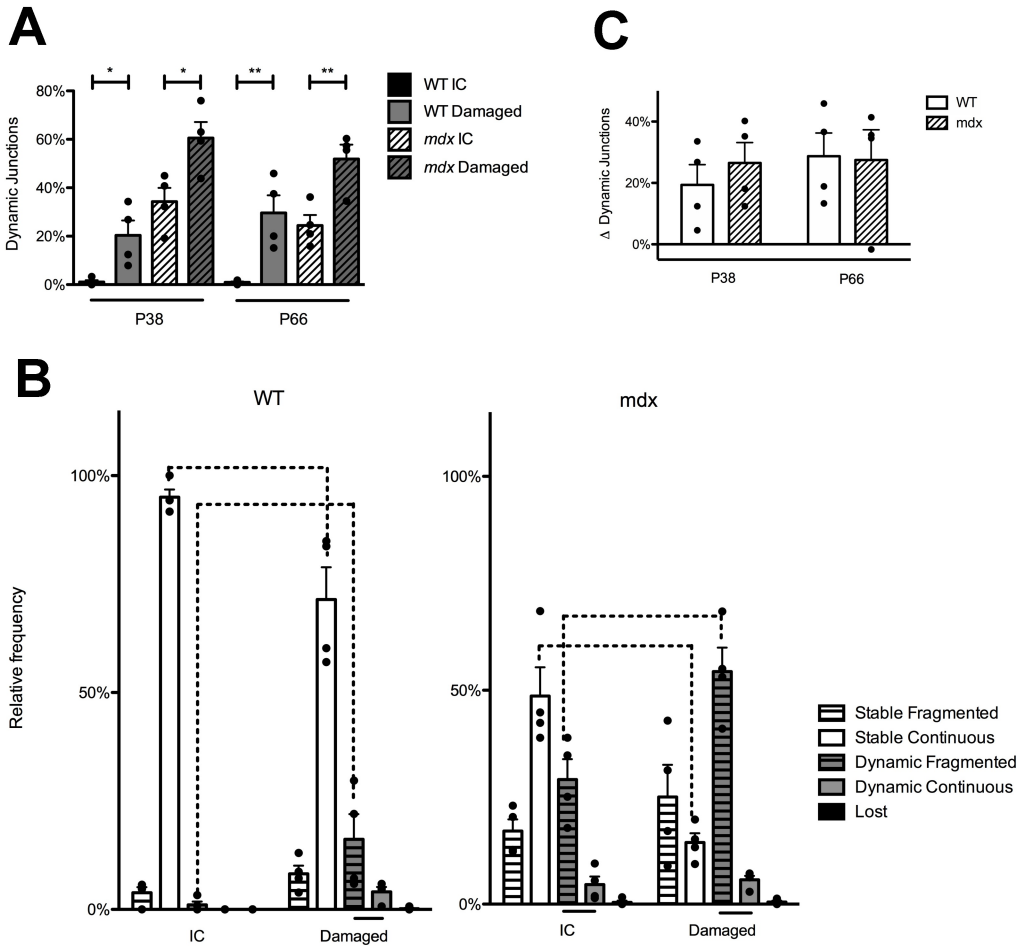

Figure 3.6. NMJ receptor replacement and categorization following myofiber cut.
(A) Receptor replacement following myofiber injury in WT and mdx STM. Both WT and mdx mice showed increases in receptor replacement following damage as assessed by percentage of dynamic junctions. Asterisks denoted significant differences (t-test, *
$P < 0.05$, ** $P < 0.001$). (B) NMJ categorization following myofiber injury in P38 WT and mdx. Following muscle injury, the proportion of dynamic, fragmented junctions was significantly increased and the proportion of stable, continuous junctions was decreased compared to ICs in both WT and mdx animals (2-Way ANOVA, Bonferroni post- hoc test, $P < 0.001$). Bars below the graphs indicate significant differences in the proportion of junctions within IC or damaged groups (2-Way ANOVA, Bonferroni post-hoc test, $P < 0.05$), while dashed lines above the graphs indicate significant differences between the two groups (2-Way ANOVA, Bonferroni post-hoc test, $P < 0.001$). Not all significant differences within genotypes are shown for sake of brevity. (C) Increases in receptor replacement following myofiber damage in WT and mdx. After damaging the STM, WT and mdx animals had similar increases in receptor replacement. This was true for both P38 and P66 animals (t-test, n.s.). This result was interpreted to mean that WT and mdx animals had similar degenerative and regenerative responses to cut damage near the endplate, and that the magnitude of our injury was constant. Exact n can be found in text as t(df) = t-value. n = df + 2. n is the number of mice compared. In all graphs, dots represent individual data points

In an effort to more closely mimic damage that would occur in the mouse, I also performed a similar experiment using a crush injury. In this paradigm the basal lamina surrounding the myofibers should be left generally intact. This is similar to how damage due to muscle contraction in dystrophy leaves the basal lamina intact, while macrophages phagocytize the myofiber. The regenerating myofiber then grows and matures within the basal lamina sheath. Similar results compared to the cut experiments were observed in crushed mdx muscle, but not WT muscle. Receptor replacement was not elevated in WT crushed muscles at P38 when compared to IC (Figure 3.7A), but was increased at P66 ($t(6) = 6.716$, $P = 0.0005$, t-test). On the other hand, mdx muscles at both ages displayed increases in receptor replacement in crushed muscles. Mdx muscle receptor replacement was 2x larger than IC at P38 ($t(6) = 3.089$, $P = 0.0214$, t-test) and P66 ($t(6) = 4.453$, $P = 0.0043$, t-test). When the magnitude of response to crush damage was compared between WT and mdx, P38 mdx animal's receptor replacement increase was 3.3x that of WT (Figure 3.7B, $t(6) = 2.668$, $P = 0.0371$, t-test).

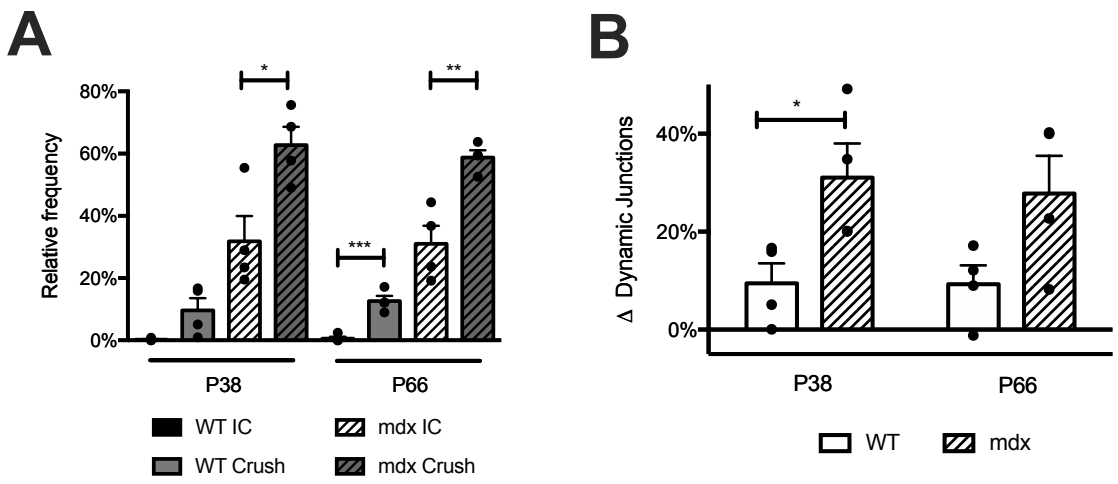

Figure 3.7. NMJ receptor replacement following myofiber crush.
(A) Receptor replacement following myofiber crush in WT and mdx STM. At P66 both WT and mdx mice showed increases in receptor replacement following damage, as assessed by percentage of dynamic junctions. Asterisks denote significant differences (t-test, *P < 0.05, ** P < 0.01, *** P < 0.001). (B) Increases in receptor replacement following myofiber damage in WT and mdx. After crushing the P38 STM, mdx animals responded to a greater degree than WT in terms of changes in receptor replacement (t-test, P < 0.05). This was not evident for both P66 animals. (t-test, n.s.). It is possible that due to the small size of the muscle at P38, the crush was closer to the endplate area at this age and mdx animals responded to a greater degree, as suggested by the relative frequency analysis in (A). Exact n can be found in text as t(df) = t-value. n = df + 2. n is the number of mice compared.

Taken together, I show here that muscular dystrophy in mdx mice causes increases in AChR replacement as NMJs remodel. This increased AChR replacement is due to myofiber degeneration and regeneration at the synaptic site and is correlated with abnormal endplate morphology. Still, the degeneration and regeneration causing NMJ remodeling is a byproduct of muscular dystrophy and the loss of dystrophin protein at those NMJs, as muscle damage away from the junction caused no significant increases in AChR replacement.

3.3.4. The innervating motor axon is necessary for remodeling to occur following receptor replacement

I next investigated the role that the innervating motor axon plays in receptor replacement and endplate remodeling in mdx mice. It has previously been suggested in mdx mice that the nerve is necessary to restructure the endplate upon muscle cell regeneration (Marques et al., 2007). However, in this experiment whether or not the endplate area of the muscle was injured could not be directly assessed. To investigate the role of innervation in remodeling specific to regenerated NMJs, the two-color BTX approach was again utilized, but the nerve that innervates a single STM (accessory nerve) was severed at the time of the first BTX exposure. After the 10-day convalescent period the nerve had not regrown to the endplate region and no NMJs were innervated (Figure 3.8A). The contralateral muscle was left innervated as an IC. The procedure was initiated in P28 mice. Again, at the endpoint of this experiment (P38) there are still a large number of junctions that were not fragmented in mdx mice, so I am able to record changes in the proportion of fragmented or continuous junctions with and without the nerve. Receptor replacement in denervated mdx muscles was elevated above those of ICs (Figure 3.8B. $t(6) = 3.227$, $P = 0.018$, t-test). This was somewhat surprising. Denervation and/or blocking muscle contractions is known to promote AChR replacement (Loring and Salpeter, 1980; Akaaboune et al., 1999), but it does not change the half-life of mdx AChRs (Xu and Salpeter, 1997). It is likely that increases in receptor replacement were due to both

myofiber damage at the endplate area, and denervation induced changes to receptor half-life. The total loss of receptors denoting dynamic junctions, however, is not a feature seen even in chronically denervated NMJs.

In comparison to innervated muscles, denervated P38 mdx STMs had an increase in the number of dynamic, continuous junctions (Figure 3.8C. $t(6) = 5.484$, $P < 0.001$, 2-Way ANOVA, Bonferroni post-hoc test) and a corresponding decrease in dynamic, fragmented junctions (Figure 3.8C. $t(6) = 3.684$, $P < 0.01$, 2-Way ANOVA, Bonferroni post-hoc test). This indicates that following receptor replacement—as denoted by dynamic junctions—the nerve must be in contact with the endplate area to cause NMJ remodeling.

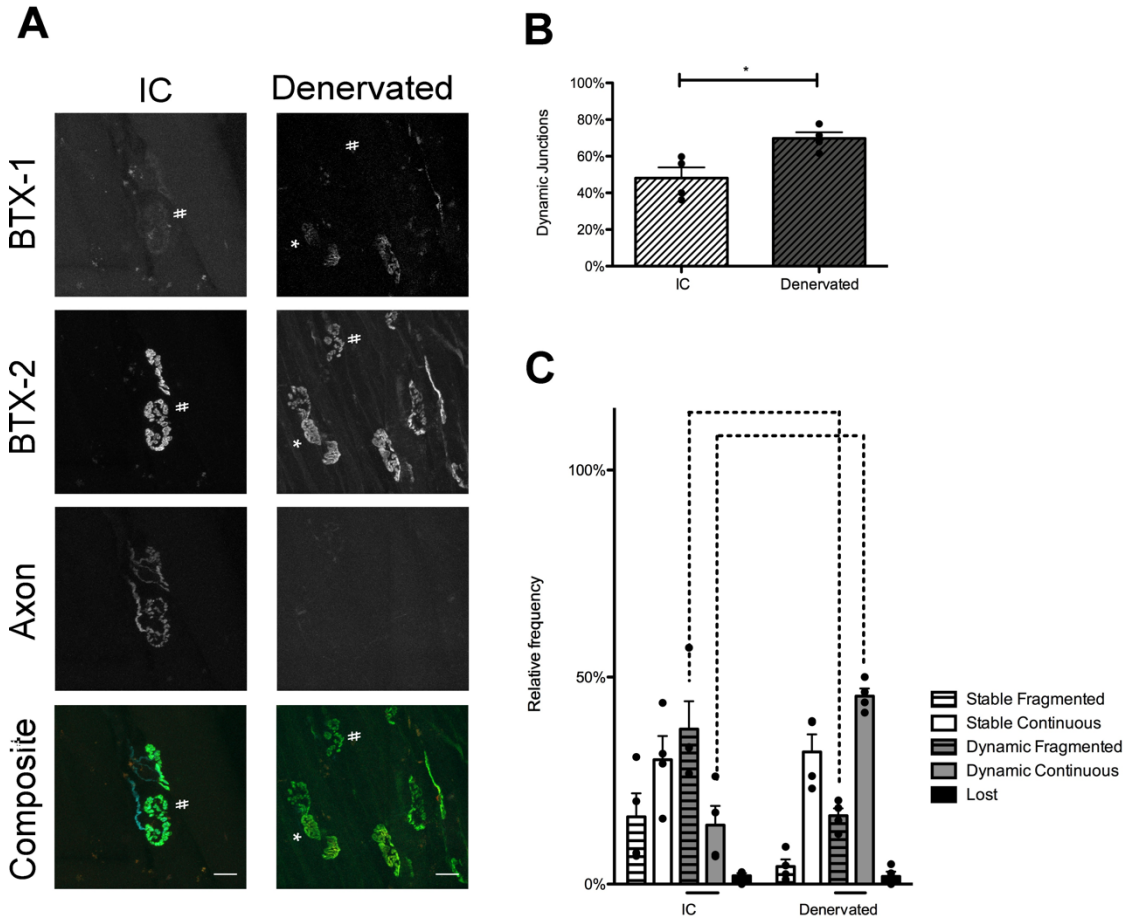

Figure 3.8. Innervation is required for NMJ remodeling in P38 mdx mice.
(A) Confocal maximum intensity projection of P38 mdx innervated (IC) and denervated STMs. "#" denotes dynamic, fragmented junctions. Asterisks denotes dynamic, continuous junctions. In the composite image BTX-1 has been pseudocolored red, BTX-2 green, and motor axon cyan. Note that in the denervated muscle there is no motor axon labeling in the maximum intensity projections. This indicates motor axon loss and no regeneration during the 10-day recovery period. Additionally, both the IC and denervated collections have NMJs with little or no BTX-1 label. This indicates AChR replacement attributed to myofiber degeneration/regeneration or increased in receptor half-life due to denervation in both NMJs with and without innervation. Scale bar = 20 μm. (B) Receptor replacement in P38 mdx following denervation. Receptor replacement, as assessed by dynamic junctions, is elevated in P38 mdx denervated muscles as compared to IC (t-test, $P < 0.05$). (C) NMJ categorization in P38 mdx mice after denervation. Following denervation, the proportion of dynamic, fragmented junctions is significantly decreased, and the proportion of dynamic, continuous junctions is decreased compared to non-denervated IC (2-Way ANOVA, Bonferroni post-hoc test, $P < 0.001$). Bars below the graphs indicate significant differences in the proportion of junctions within IC or denervated groups (2-Way AVOVA, Bonferroni post-hoc test, $P < 0.05$), while bars above the graphs indicate significant differences between the two groups (2-Way ANOVA, Bonferroni post-hoc test, $P < 0.001$). Not all significant differences within genotypes are shown for sake of brevity. This information can be found in A-5. Exact n can be found in text as t(df) = t-value. n = df + 2. n is number of mice compared.

3.4. Discussion

While many have postulated that the NMJ changes in mdx animals are due to myofiber damage, there has been little direct investigation of the link between these phenomena. Other investigators have correlated central chains of nuclei within a myofiber to fragmented junctions (Lyons and Slater, 1991), but it is unclear if central nuclei are a marker for recent myofiber regeneration. Historically, myofibers with nuclei in the center of the cytoplasm, instead of the periphery, have been used to identify regenerated muscles (Benoit and Belt, 1970). Unfortunately, this method of investigating regeneration has its drawbacks. For one, the time course over which myonuclei move from the center to the periphery of the fiber may be very long and not indicate truly recent regeneration (Wada et al., 2008). In vivo two-color BTX labeling made it possible here to identify recently regenerated muscle fibers and to categorize their NMJs by morphology. This approach has allowed the detection and quantification of dynamic junctions in normal, dystrophic and damaged muscle and our results indicate that recent myofiber degeneration and regeneration cycles leading to NMJ remodeling involves significant replacement of AChRs.

Two-color BTX experiments demonstrated that myofiber degeneration and regeneration is continuously elevated in mdx STM from P38 to P450. This finding contradicts previous reports that have described the pathology of mdx muscles as transitioning from an early necrotic stage at 3 weeks, to a regenerative state that closes at 12 weeks (DiMario et al., 1991). However, it must be mentioned that the STM was not investigated in these reports. Using tritiated thymidine and investigating satellite cell

nucleus incorporation into myofibers, an elevated level of myofiber regeneration in mdx was shown to be restricted to an acute period from P24 to P50. A chronic phase of myopathy follows with a much lower level of labeled nuclei (McGeachie et al., 1993). A similar observation of an early crisis period in mdx mice has been described by researchers via embryonic myosin expression and histological methods (DiMario et al., 1991; Pastoret and Sebille, 1995). However, other reports suggest that myofiber damage may still be vastly elevated past this crisis period (Coulton et al., 1988a; Pagel and Partridge, 1999). The results of the two-color BTX investigation hold with the latter conclusion. If the loss of the first BTX label is indeed due to myofiber necrosis at the synaptic site, then our results demonstrate that the degenerative and regenerative cycle of dystrophic muscle fibers extends well into the adult life of mdx STMs. I did, however, find evidence of an early life crisis period in mdx TA, as has been suggested by other researchers (Dangain and Vrbova, 1984). It is possible the differences in the incidence of receptor replacement, and therefore damage, in the different muscles is based on use. The STM is a neck muscle that is used in the feeding behavior of these mice. The TA is a hindlimb muscle used in movement, but these mice are housed in small cages and likely have a more sedentary lifestyle than would normally been seen, and mdx animals are also less active than WT (Hara et al., 2002). It is established the exercised mdx mice have higher rates of muscle damage and different pathological outcome than WT (Dupont-Versteegden and McCarter, 1992; Brussee et al., 1997).

Our results also show it is unlikely that the dystrophin loss itself causes increased receptor replacement, but such replacement is rather due to myofiber damage resulting

from the loss of the protein. Deliberate damage to muscle fibers in WT mice resulted in similar receptor replacement and NMJ remodeling as seen in mdx muscles. While there are reports of clustering abnormalities in myotubes in vitro lacking dystrophin (Kong and Anderson, 1999), AChRs clusters in mdx mice develop normally into a pretzel-shaped morphology early in life. It is only after the onset of myofiber necrosis at P21 that remodeling begins to occur. This suggests that myofiber damage is causative in NMJ remodeling in mdx mice. It has been shown that in other mouse models NMJ remodeling can occur without myofiber damage (Kong et al., 2012; il Lee et al., 2016). However, deliberate injury to the fibers near their endplates increased NMJ remodeling in mdx muscles.

The half-life of AChRs in healthy, innervated NMJs is about 14 days (Akaaboune et al., 1999). It has also been shown that there are different pools of AChR with distinct half-lives, the shortest being about 1-day (Strack et al., 2011). However, even when similar in vivo two-color BTX techniques are used in NMJs where metabolic receptor turnover was increased through long term denervation (Strack et al., 2011), the catastrophic loss of the first BTX label was not observed, as I see in dynamic junctions. This I believe shows the reliability of our measurements, and that dynamic junctions do indeed represent myofiber degeneration and regeneration. Again, while some loss of BTX-1 would be expected even in WT animals, the exaggerated, almost complete loss of receptors from dystrophic muscles over a 10-day period is abnormal. It must be noted that in the experimental procedure where fibers had been deliberately damaged, those injured fibers could not be relocated when imaged. I am, therefore, unable to definitely

link myofiber damage and dynamic junctions. Previous investigation, however, has shown that when deliberately damaged muscles are imaged over time NMJs become dynamic (Li and Thompson, 2011). It is possible that receptor replacement is not occurring on damaged myofibers, but on fibers subjected to disuse or inflammatory response. An effort, of course, was made to recover muscle fibers in the area of damage, but this cannot be guaranteed.

Increased AChR replacement has been observed at NMJs whose receptors have been blocked by a sufficiently high dose of BTX to cause neuromuscular transmission to fall below the threshold necessary for the generation of muscle action potentials. However, in these experiments, a sufficiently low concentration of BTX that does not accelerate the replacement of receptors was used to allow continued transmission, and to not perturb morphology (Akaaboune et al., 1999).

The STM and TA were chosen for examination in these experiments, largely because of their accessibility for BTX application and for in-vivo labeling. It is clear that different muscles in muscular dystrophy are affected to different degrees. For example, one of the muscles most affected in murine dystrophy is the diaphragm (Stedman et al., 1991; Petrof et al., 1993), while the extraocular muscles and small caliber muscle fibers might be spared (Karpati et al., 1988; Porter et al., 2003). The diaphragm exhibits signs of constant degeneration and subsequent fibrosis and adipose tissue deposition unlike many other muscles studied in the mouse. This likely is due to the amount of activation (and damage) to which the diaphragm is subjected via contractions during respiration. A similar phenomenon may be occurring in the STM of mdx mice. It is documented that

the trunk and neck muscles of neonatal GRMD dogs are more severely affected than appendicular muscle groups (Nguyen et al., 2002a), likely because they are postural muscles and they are used more constantly than muscles involved with movement, and therefore subjected to increased contraction induced damage. Atrophy of the truncal muscles has been noted in older animals as well (Valentine et al., 1988). The STM has not been typically investigated in dystrophy. While it would be interesting to use the two-color BTX approach in the diaphragm of mdx animals, such an experiment would be difficult, due to accessibility issues. As mentioned previously, however, experiments in the TA hinted that myofiber damage was restricted to a crisis period.

The innervating motor axon terminal plays a role in remodeling of the AChRs at the synapse after muscle injury (Li and Thompson, 2011) and has been implicated in dystrophy (Marques et al., 2007). Our investigation was able to examine individual myofibers and synaptic sites that have recently undergone replacement due to myofiber necrosis. In the absence of the nerve, the receptors are still lost from the membrane, but upon regeneration the morphology is continuous. It also suggests that mdx muscle damage can occur without transmission induced contraction, possibly due to preexisting fenestrations in the sarcolemma. Excepting denervation-induced fibrillation (Purves and Sakmann, 1974; Thesleff and Ward, 1975), it is unlikely that denervated muscles experience much contractile activity. Another explanation of BTX-1 loss in denervated STM is that immediately prior to denervation, or perhaps during the surgery, the muscle fiber was damaged and may have begun the process of necrosis. I hypothesize that in mdx mice, myofiber damage caused by lack of dystrophin leads to degeneration and

regeneration of the muscle fiber and this is the first step in the cascade of events that leads to NMJ rearrangement. Fragmentation and remodeling of the NMJ is a response to muscle fiber regeneration that follows the degeneration of muscle cells. It is not that the old NMJ is losing receptor sites due to patches of membrane degradation During regeneration, the innervating motor neuron axon, which remains on the basal lamina at the synaptic site of the damaged myofiber, sends out "sproutlets" and varicosities to search for the regenerating fiber (Li and Thompson, 2011). As the fiber regenerates, new AChRs are inserted into the sarcolemma at areas that are contacted by these varicosities and sproutlets. This causes a fragmented appearance on the postsynaptic AChR aggregate. If the motor axon is not present, when the myofiber regenerates, the AChR aggregate will remain in its original morphology. That is to say if the aggregate was previously continuous it will remain continuous upon myofiber regeneration. I show that the innervating motor axon is responsible for NMJ fragmentation, a hallmark of the dystrophic endplate. Without direction from the axon, NMJ remodeling does not occur. It is possible that factors like agrin released from the sproutlets result in the fragmented distribution of AChR.

A confounding attribute to the denervation experiments is that in the absence of innervation, myofibers undergo atrophy (Pellegrino and Franzini, 1963; Bodine et al., 2001). The increases in the number of continuous junctions may be a result of myofiber collapse. It is possible that the junctions do in fact restructure themselves morphologically even in the absence of neural input, but upon subsequent myofiber atrophy the fragments connect with each other. From the parameters this report and

others use to define fragmented (i.e. having 5 or more non-continuous clusters of AChR) versus continuous junctions, this remodeling might not have been realized. Whether the sparing of morphological change has any physiological consequence remains to be investigated.

Neuromuscular transmission properties of remodeled endplates in dystrophy should be closely investigated. There are a number of published studies that have researched the functionality and electrophysiology of dystrophic NMJs. However, the results are often contradictory, especially when miniature endplate potential (mEPP) amplitude and variability are investigated (Nagel et al., 1990; Lyons and Slater, 1991; Carlson and Roshek, 2001; van der Pijl et al., 2016). This could be due to the differences in experimental methods, or perhaps to the variability of the disease state and its progression, or even the muscles used. Researchers have shown that in aged NMJs, which have a similar morphology to dystrophic and damaged NMJs, there is little difference between normal and remodeled junction physiology (Willadt et al., 2016). In fact, the fragmented morphology may increase the efficiency of transmission. Whether or not this is the same for dystrophy remains to be clearly elucidated, but some experiments on the physiology of such junctions indicate an absence of major defects (Lyons and Slater, 1991), while others show obvious deficiencies in neuromuscular transmission (Personius and Sawyer, 2006). However, the current study shows the changes in junction morphology are progressive, in that remodeled junctions can likely further remodel. It is possible that significant changes in the physiology of neuromuscular transmission do appear in the later stages of the disease. Interestingly, in

DMD patients and clinically relevant animal models, such as GRMD, there is evidence of neuromuscular transmission deficiencies (Hilton-Brown et al., 1985; Sanders and Stålberg, 1996; Kornegay et al., 2012).

This study and others have shown that changes to the structure of the NMJ occur rapidly and irreversibly. Present treatments for DMD do not commonly begin until after the onset of the disease at which time changes to the morphology of the NMJ have already occurred. I believe it is important to study the remodeling of the NMJ as mitigation of this remodeling might alter the progression of the disease. This would especially be the case if remodeled junctions are physiologically deficient. Animal models are necessary for this sort of investigation, as the in vivo nature and invasiveness of the research prevent humans from being subjects. This study demonstrates that the sequence of events that lead to altered NMJs is dependent upon the motor neuron, but initiated by muscle damage. I suggest that an additional component to treatment of the disease besides sparing of muscle degeneration may be altering the changes that occur in muscle innervation.

4. FUNCTION OF DYSTROPHIC MUSCLE AND CARDIAC TISSUE THROUGH DISEASE PROGRESSION

4.1. Research impetus

While the force generation characteristics of mdx muscles have been characterized, there are only a handful of articles detailing neuromuscular performance of dystrophic NMJs (Nagel et al., 1990; Carlson and Roshek, 2001; Personius and Sawyer, 2006; van der Pijl et al., 2016; van der Pijl et al., 2018). These articles on the mdx model noted slight changes to neuromuscular transmission in the diaphragm, which includes variability in synaptic transmission (i.e., MEPP amplitude) and quantal content. While the diaphragm is characterized as the most affected muscle in mdx disease progression, I have shown (Sections 2 and 3) that the STM incurs a constantly elevated level of muscle degeneration and regeneration. It is possible then that this muscle, in comparison to limb muscles, also displays neuromuscular transmission deficits, perhaps to an even greater degree. These differential changes in disease impact may be due to NMJ remodeling and present a potential therapeutic target strategy to ameliorate dystrophic pathology. Additionally, as NMJ remodeling is progressive, it is possible that at later stages of the disease, NMJ dysfunction will be more evident.

As supportive treatments for DMD have advanced, specifically for respiratory issues, the main cause of mortality in patients shifted from respiratory failure to cardiac complications due to dilated cardiomyopathy (Eagle et al., 2002; McNally, 2007). This deadly heart compromise does not occur until later stages of the disease in most young

men, well past when skeletal muscle first weakens. A similar cardiomyopathy has been noted in mdx mice, but rigorous studies have not been performed in geriatric mdx mice. Echocardiography, a noninvasive technique used extensively in DMD patients, was adapted for use in both conscious and unconscious mdx mice near the end of their lives (16+ months). I investigated if cardiac function in geriatric dystrophic mice becomes significantly worse as compared the heart function in WT and younger mdx mice. I observed few significant changes in cardiac function between these groups.

4.2. Materials and methods

4.2.1. Geriatric skeletal muscle

4.2.1.1. Animals

Mice were generated as in Section 2.1.2.1. Animals were divided into four groups: WT mice (ages 3 – 7 months), mdx crisis (< 12 weeks old), mdx stable (12 weeks - 16 months old), and mdx geriatric (> 16 months). Muscles were collected from 3 – 7 mice for each group, for a total of 29 mice.

4.2.1.2. Mouse muscle preparation

Mice were euthanized via I.P. injection of 0.15 mL of Euthasol. The STM was dissected, pinned at resting length to a sylgard dish and fixed using 4% phosphate buffered PFA for 20 minutes. After fixation, the muscles were washed

three times with phosphate buffered saline (PBS) and labeled with α-bungarotoxin conjugated to Alexa Fluor™ 555 or Alexa Fluor™ 647 (ThermoFisher Scientific, Cat# 35450) for 5 minutes at a concentration of 2 μg/mL of PBS. DAPI (Thermo Fisher Scientific Cat# D3571, RRID:AB_2307445) was used to label nuclei (diluted 0.5 μg/mL in PBS). After three PBS washes, a longitudinal filet from across the surface of the muscle was dissected from distal tendon to proximal tendon and mounted on a microscope slide in anti-fade fluorescence mounting medium.

4.2.1.3. Image analysis

Confocal micrographs of labeled STM were collected on either a Leica TPS II SP5 or a Zeiss LSM780 microscope using a 40X Oil objective (NA 1.4). Step size was set between 300-500 nm. Laser lines 488 nm, 563 nm, and 633 nm were used as necessary. Images were analyzed in ImageJ (ImageJ, RRID:SCR_003070) by creating maximum intensity projection images from collected stacks. Junctional area was calculated by thresholding the BTX labeled channel using the Auto Threshold tool provided by ImageJ. A polygon shaped region of interest was then circumscribed around the thresholded signal and the region of interest's area measured. Receptor area was measured as the thresholded area of the BTX label within the circumscribed region of the AChR. Dispersion Index was calculated as receptor area/junctional area. The number of AChR fragments (fragmentation) was measured using the objects counter in ImageJ by setting the minimum area for counts as 5 μm^2. As this measurement does not consider

fragments in separate z-planes, it is a conservative estimate of fragmentation. The actual number of fragments for both WT and mdx is likely underestimated by this measurement.

4.2.1.4. Force recordings

Animals were weighed and the EDL, SOL, and STM were removed from animals from tendon to tendon with the associated peripheral nerve attached. Proximal tendons were attached to a piece of bone to provide an anchor for pinning. Due to fragility of EDL and STM distal tendons, an 8-0 surgical thread was tied around them. For the STM a loop was tied into the thread. Muscles were superfused with oxygenated Ringer's solution both during dissection and force recordings. Muscles were pinned to a sylgard dish via their proximal bone section, and to a hook force transducer (Harvard Apparatus, Massachusetts, USA) through their distal tendon. For STM, the hook was attached to the loop, while for EDL and SOL muscles, the attachments were made directly to the tendon. Optimum length of muscles was determined by delivering suprathreshold pulses to the nerve and stretching the muscle until no increases in force were noted. Isometric twitch forces were generated via a single suprathreshold (10-20 V) pulse (Grass Instruments). Direct stimulation (150 V) was delivered to the muscle through two titanium plates surrounding the muscle near its midsection. Indirect stimulation was delivered to the nerve via a suction electrode into which the attached nerve was inserted along with oxygenated Ringer's. Tetanic force was generated by 60 Hz stimulation for 2 s. Again, direct and indirect stimulation were applied to the muscle.

The twitch and tetanic force recordings were displayed on a Tektronics DPO 2024 oscilloscope (Oregon, USA) and maximal responses were measured from the traces following both direct and indirect stimulation. Fatigability of the muscles during tetanic stimulation was measured as the percent of maximum tetanic force retained from near the beginning of tetany to the force generated at the end of the 2 s train. To normalize measurements by body size, the force generated during stimulation was divided by the animal's body mass. NMJ performance was estimated as the ratio between indirect stimulation and direct stimulation for twitch and tetanic force, and the fatigability of muscle during indirect over direct tetanic stimulation. The SOL and/or EDL and/or STM were removed from the mouse and recorded from. Three to 7 of each muscles were recorded from in each genotype/age (WT, mdx crisis, mdx stable, mdx geriatric).

4.2.1.5. Statistics

NMJ morphology measurements were compared to those preceding them in age using a 1-Way ANOVA with a Sidak's post-hoc test (Graphpad, PRISM 7.0). Statistical significance was placed at P = 0.05. Significant or of interest P-values and degrees of freedom are recorded in text.

Muscle force recordings were compared to one another within groups using a 2-Way ANOVA with a Tukey's post-hoc test (Graphpad, PRISM 7.0). Statistical significance was placed at P = 0.05. Significant or of interest P-values and degrees of freedom are recorded in text.

4.2.2. Geriatric cardiac muscle

4.2.2.1. Animals

Mice were generated as in Section 2.1.2.1. Animals were divided into four groups. WT young (< 6 months), WT geriatric (> 16 months), mdx young (< 6 months old), and mdx geriatric (> 16 months). 3-5 mice per group were used for a total of 17 mice.

4.2.2.2. Echocardiography

The chest of the animals was depilated and covered in ultrasound jelly. For unconscious mice, the animals were incubated in a flow chamber delivering 4% isoflurane at a flow rate 1L/min. Following full anesthetization, mice were placed on a surgical platform and 1.5% isoflurane was delivered via a face mask for maintainence. B-Mode (which provides a 2D view of the heart), and M-Mode (which provides motion data across a single ultrasound beam in a wave form) echocardiograph images and videos of the left ventricle were collected using a Vevo 3100 (Visual Sonics, Ontario, Canada) with a 30 MHz probe. B-Mode parasternal long axis and M-mode parasternal short axis images were collected in unconscious mice. Myocardial strain was analyzed using B-mode videos. Following a 2-day recovery period, the same procedure was conducted in a conscious state. Conscious mice were restrained via scruffing, and care was taken to collect echocardiographs as quickly as possible to reduce stress to the animal.

4.2.2.3. Echocardiography analysis and statistics

Collected images and movies were analyzed in VevoLab or VevoStrain software (Visual Sonics, Ontario, Canada). VevoLab was used to analyze the M-mode collections and standard echocardiograph measurements of the left ventricle. These included morphological measurements, such as diastolic and systolic diameter and volume, and functional measurements such as ejection fraction (end systolic volume – end diastolic volume/end diastolic volume x 100), fractional shortening (end systolic diameter - end diastolic diameter/end diastolic diameter x 100), stroke volume (end diastolic volume – end systolic volume), cardiac output (stroke volume x heart rate), and heart rate. 1-Way ANOVA with Tukey's post-hoc test was used to compare groups to each other. Significance was set at $P < 0.05$.

Using VevoStrain software, B-mode long axis videos of the left ventricle were used to analyze strain and desynchrony of contraction. Strain was measured both radially and longitudinally using speckle tracking, a technique that uses the noise inherent in echocardiography images to analyze the elasticity of cardiac tissue. The endomyocardium was used as the reference for all strain analysis and the left ventricle segmented into 6 parts: posterior apical, posterior mid, posterior basal, anterior apical, anterior mid, and anterior basal. Peak global longitudinal strain and delay in peak global longitudinal strain between opposing walls were compared using a 1-Way ANOVA with a Tukey's post-hoc test. Segmental strain (both longitudinal and radial) were compared using a 2-Way ANOVA with a Tukey's post-hot test. Unless otherwise noted, graphs

display mean and standard error. Statistical analyses were performed in GraphPad Prism 7.0 (GraphPad Software, San Diego, USA).

4.3. Results

4.3.1. Geriatric mdx skeletal muscle

4.3.1.1. NMJs of geriatric mdx mice are further remodeled

When the morphology of geriatric mdx NMJs is compared to younger mdx mice, it is clear that remodeling of the synapse is an ongoing process that continues through the mdx crisis period, stable ages, and into near death, geriatric ages (Figure 4.1; P66, crisis; P450, stable; >16 months, geriatric). The postsynaptic apparatus was subjected to the same measurements previously outlined in Section 2. However, these measurements fail in some regards to describe the vast changes seen in the geriatric mdx NMJs. Observationally, the neuromuscular synapses of these very old animals can be divided into two distinct populations. One population takes on the fragmented appearance noted in all mdx animals past the onset of muscle damage at P21 (Figure 4.1; geriatric mdx). The other NMJ population has a vastly different appearance, where receptor clusters are neither continuous nor islands, but rather the endplate is granular and disintegrated (Figure 4.1; geriatric mdx). In fact, these geriatric NMJs resemble the BTX-1 label of dynamic junctions observed in younger mdx animals and those of experimentally-induced muscle damage at the synaptic site (Section 2). The geriatric fragmented and

granular junctions indicate that NMJs in mdx further remodel past the P450 time point, likely due to the accumulation of myofiber damage.

When the postsynaptic morphology of geriatric mdx NMJs are compared to those preceding them in age, a significant amount of remodeling can be appreciated (Figure 4.2). Junctional area, which increases 135% from in P66 mdx crisis NMJs to the P450 mdx stable NMJs ($P = 0.002$, $df = 119$, Sidak's multiple comparison test), actually decreases 43% in mdx geriatric NMJs from P450 junctions ($P = 0.0126$, $df = 119$, Sidak's multiple comparison test). Fragmentation was also found to exhibit an early increase of 64% followed by a decrease of 47% in mdx geriatric NMJs (P66 to P450: $P = 0.002$, $df = 119$; P450 to geriatric: $P < 0.001$, $df = 119$, Sidak's multiple comparison test). Although a similar trend existed for receptor area, only the increases P66 to P450 were statistically significant ($P = 0.0445$, $df = 119$, Sidak's multiple comparison test).

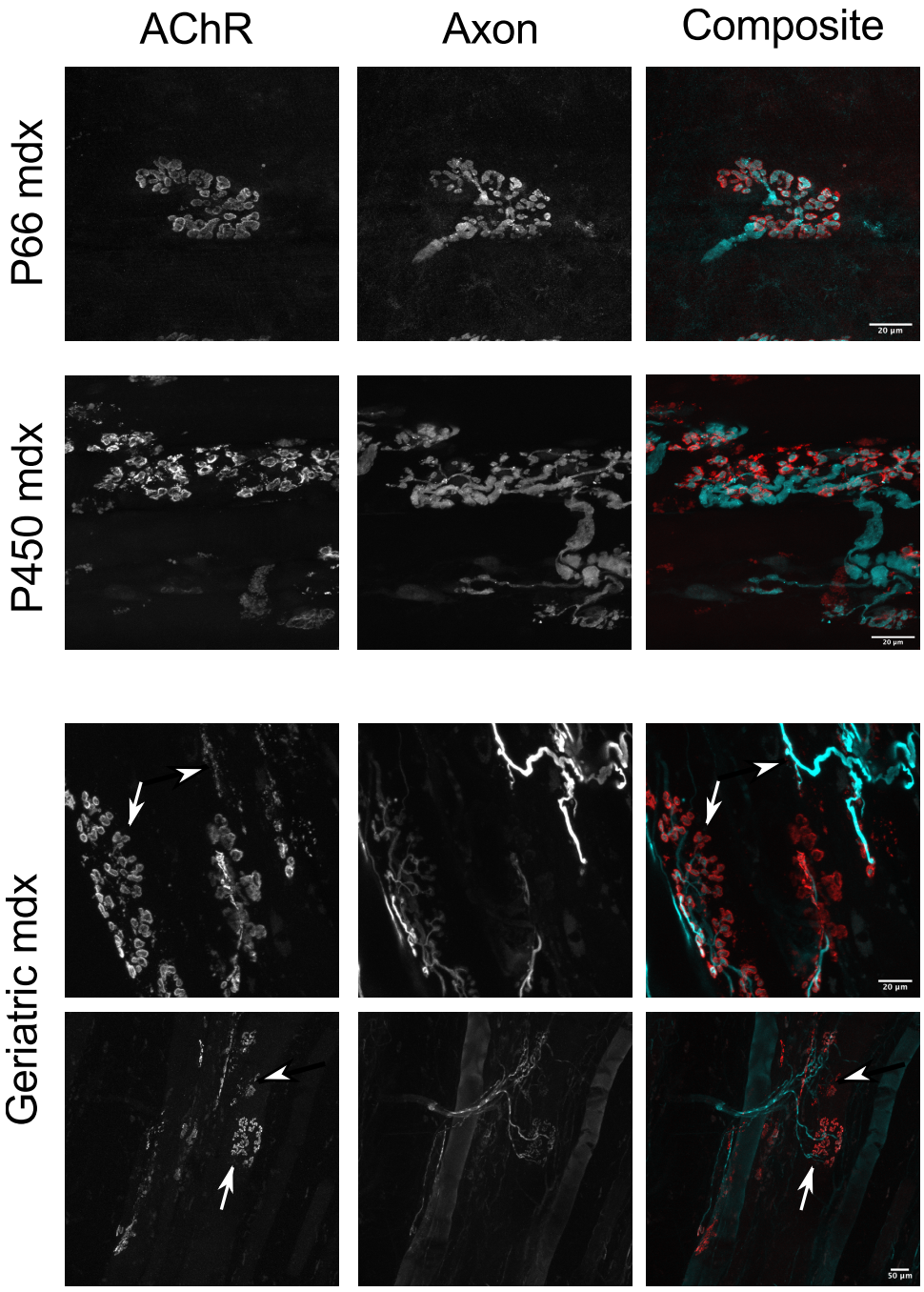

Figure 4.1. Geriatric mdx NMJs are further remodeled from those of adult mdx NMJs.
Confocal images of geriatric mdx NMJs in STM muscle. There are two populations of NMJs one that is fragmented in appearance (arrow) and one that is granular (arrowhead). P66 animals are within the time frame of the proposed crisis period, which does not occur in the STM, but does in the TA and likely other limb muscles. P450 animals and geriatric animals are well outside the proposed crisis period (3-12 weeks). Geriatric mdx images are from an animals over 19 months of age. Most junctions appear to be fully or partially innervated. In composite images AChR is pseudocolored red, and axons cyan. Scale for all images is 20 µm. Note the change is scale in the lowest row.

No differences were detected for DI. Again, these measurements indicate that NMJ remodeling continues to occur in the STM even at the end-stage of the disease and may result in decreased muscle function in diseased geriatric mice. In previous sections, I have described how the process of NMJ remodeling in younger animals is dictated by myofiber degeneration and regeneration, and is regulated, directly or indirectly through tSCs, by the motor axon. It is probable that the same phenomenon is occurring in the STM of geriatric STMs. However, this continued remodeling process involves disintegration of the NMJ's AChR cluster fragments and granularization of the remaining receptors. By and large, the granularized junctions appeared to be innervated, but this was not a measurement that was actively made. In some cases, faint axonal labeling was apparent and may have been a result of NMJ position in the tissue sample.

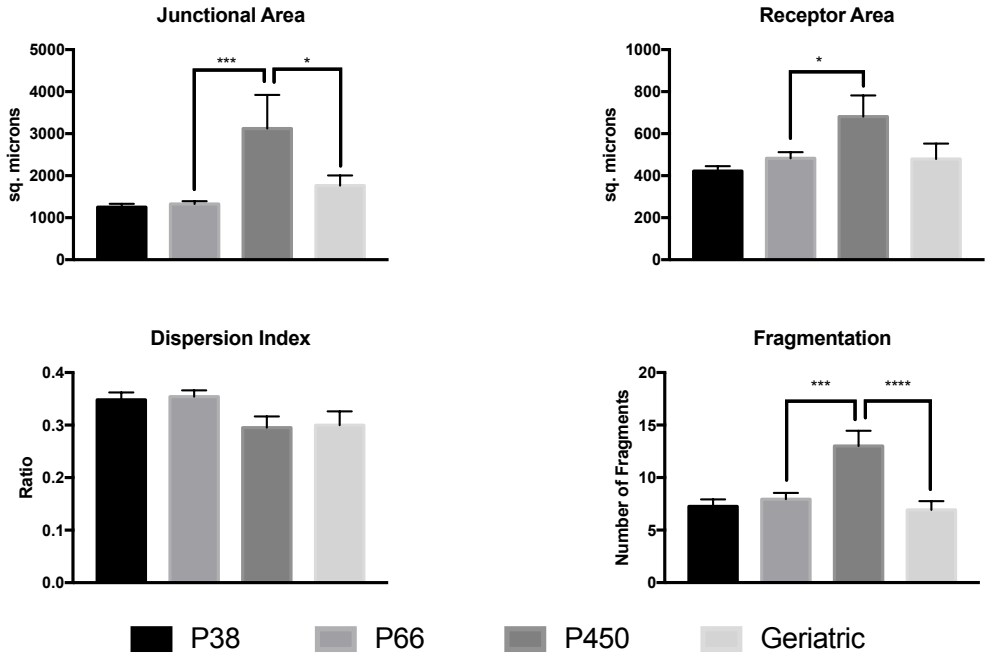

Figure 4.2. Mdx NMJs continue to remodel with into geriatric ages.
Postsynaptic measurements of mdx NMJs in STM from P38 to geriatric ages. 1-Way ANOVA with Sidak's post-hoc test. Groups were only compared to those that immediately preceded them in age (i.e. P66 to P38, P450 to P66, and geriatric to P450). Asterisks denote significant differences (* < 0.05, ** < 0.01, *** < 0.001, **** < 0.001)

4.3.1.2. Geriatric mdx muscle have decrements in force production

Geriatric mdx NMJs continue to remodel as they age (Figure 4.2). However, whether or not these further changes in synaptic structural organization impart functional consequences is unknown. To address this question, the force generation characteristics of EDL, SOL, and STM muscles were compared across ages to measure if evoked contraction properties of geriatric mdx muscles declined as they continued NMJ remodeling with age (Figure 4.3). Electrical current was delivered to both the muscle directly, and also indirectly to the motor nerve to elicit isometric muscle contractions.

For EDL and SOL muscle contractions few changes in direct twitch force or indirect twitch force were noted for any groups (WT, mdx crisis, mdx stable, mdx geriatric). Maximum tetanic force generated by SOL muscles of mdx crisis group were significantly smaller than those of mdx stable muscles ($P = 0.0213$, $df = 35$, 2-Way ANOVA, Tukey's post-hoc test). In mdx crisis STM muscles, where they produced less force during indirect tetanus than mdx stable muscles ($P = 0.0264$, $df = 37$, 2-Way ANOVA, Tukey's post-hoc test). More relevant to these aging studies, mdx geriatric STM in all cases produced less isometric force than mdx stable STMs for direct twitch ($P = 0.0077$, $df = 43$, 2-Way ANOVA, Tukey's post-hoc test), indirect twitch ($P = 0.0081$, $df = 44$, 2-Way ANOVA, Tukey's post-hoc test), direct tetanus ($P = 0.0213$, $df = 35$, 2-Way ANOVA, Tukey's post-hoc test), and indirect tetanus ($P = 0.0222$, $df = 37$, 2-Way ANOVA, Tukey's post-hoc test) stimulation groups (Figure 4.3).

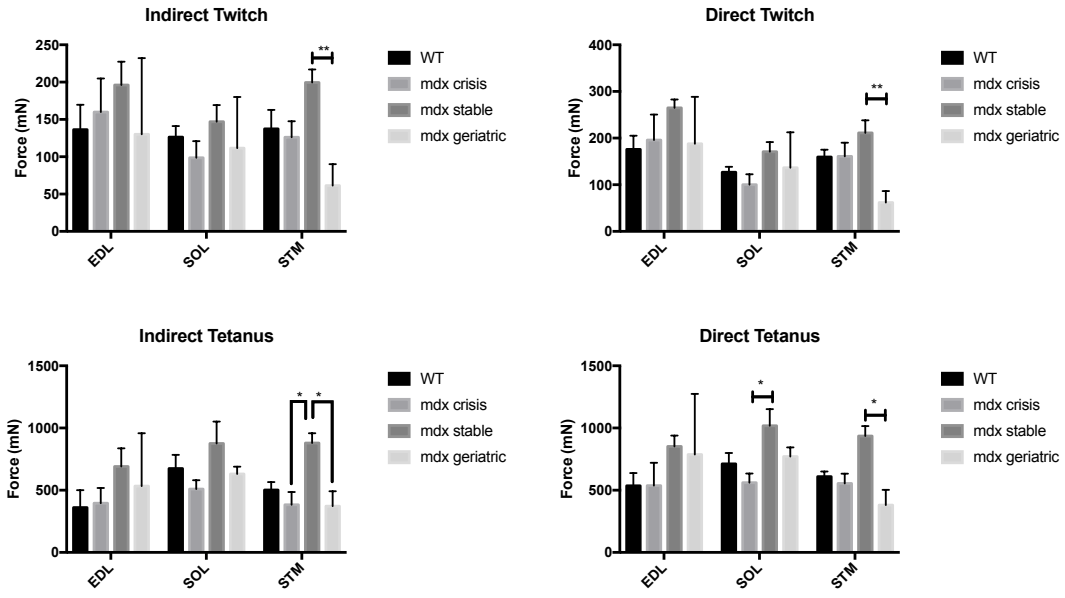

Figure 4.3. Force recordings from EDL, SOL, and STM muscles.
Direct (muscle evoked) and indirect (nerve evoked) isometric force from trunk and limb muscles. Twitch force was measured by delivering a single suprathreshold pulse to the nerve or muscle. Tetanic force was measure by delivering a 2 second train of stimuli at 60 Hz. 2-Way ANOVA, Tukey's post-hoc test. Asterisks denote significant differences (* $P < 0.05$, ** $P < 0.01$). Largely no changes in maximum isometric force were found between groups, except for geriatric mdx STM, which are significantly weaker than that of stable mdx.

When the isometric force was normalized by body weight, a similar trend was noted (Figure 4.4). Normalized data is presented because changes in muscle force could be a product of a natural developmental increase in overall muscle size and not due to changes in neuromuscular transmission or the contractile apparatus of myofibers. While muscle weights and cross sections were not collected in this report, animal body mass before death was used as a surrogate for normalization. It should be noted that an allometric technique of scaling the normalized data was not used, which has been

suggested when normalizing muscle strength measurements to body mass (Folland et al., 2008). Also, while increases in body mass as an approximation of increases in muscle mass could be accounted for, atrophy of muscles would be masked by the developmental increase in body size of mice. Decreases in normalized force could be overestimated in atrophied muscles.

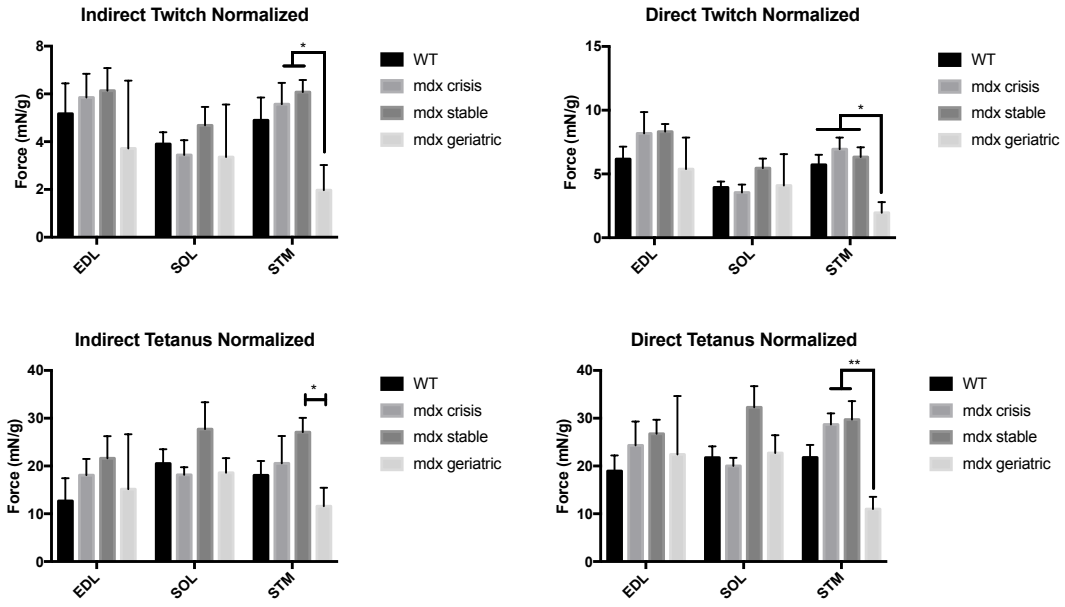

Figure 4.4. Normalized force recordings from EDL, SOL, and STM muscles. Direct (muscle evoked) and indirect (nerve evoked) isometric force from trunk and limb muscles. Twitch force was measured by delivering a single suprathreshold pulse to the nerve or muscle. Tetanic force was measure by delivering a 2 second train of stimuli at 60 Hz. Force recordings were normalized to body weight. 2-Way ANOVA, Tukey's post-hoc test. Asterisks denote significant differences (* $P < 0.05$, ** $P < 0.01$). Largely no changes in maximum isometric force were found between groups, except for geriatric mdx STM, which are significantly weaker than that of other groups.

In fact, the normalization process showed that for the younger ages, force production between WT, mdx crisis, and mdx stable muscles were more similar than when not normalized, but there was a trend of increasing strength in mdx stable muscles. The STMs of geriatric mdx mice, however, again produced significantly less force than mdx stable, but in some cases, less than WT and mdx crisis, as well. Significant changes are detailed in Table 4.1. Thus, coincident with remodeling involving AChR granularization in geriatric mdx NMJs in the STM, significant reductions in contractile force were observed. The pathology of the disease in terms of muscular force production remained largely stable until senescence, indicating an interaction between age and the dystrophic state. Loss of force was perhaps due to changes in NMJ structure.

Table 4-1. Normalized STM force recordings compared to mdx geriatric muscle.

	WT vs mdx geriatric	**mdx crisis vs mdx geriatric**	**mdx stable vs mdx geriatric**
Indirect Twitch	n.s.	P = 0.0383 df = 44	P = 0.0142 df = 44
Direct Twitch	P = 0.0369 df = 43	P = 0.0032 df = 43	P = 0.0158 df = 43
Indirect Tetanus	n.s.	n.s.	P = 0.0441 df = 37
Direct Tetanus	n.s.	P = 0.0084 df = 35	P = 0.0092 df = 35

Direct (muscle evoked) and indirect (nerve evoked) isometric force from STM muscles. Twitch force was measured by delivering a single suprathreshold pulse to the nerve or muscle. Tetanic force was measure by delivering a 2 second train of stimuli at 60 Hz. Force recordings were normalized to body weight. 2-Way ANOVA, Tukey's post-hoc test. n = df +2.

Seemingly, out of the muscles measured, the STM was the most affected during the progression of mdx muscular dystrophy in terms of muscle contractile properties and force production. It seems probable that this change in functionality was due to the ongoing myofiber degeneration and regeneration of the STM outlined in Section 3. The same constantly elevated degenerative process may not occur in the SOL and EDL, as it was not observed in the TA muscle. The TA underwent a true crisis period, of elevated myofiber damage followed by a mitigation period. Whether synaptic function is impacted by the ongoing degeneration and regeneration of the STM and/or the NMJ remodeling seen in geriatric mdx STM muscle remains unclear.

4.3.1.3. NMJ remodeling has no negative effect of neuromuscular transmission

Although direct electrophysiological recordings of neuromuscular synaptic transmission in mdx muscle were not conducted here, I assessed the NMJ performance by calculating an indirect-direct stimulation force ratio. For this calculation, indirect force measurements were divided by direct force measurements (Figure 4.4). Theoretically, if the synapse is functioning at 100% efficiency, the force elicited by direct and indirect methods should be roughly equivalent during supramaximal stimulation. A ratio of 1 indicates an perfectly efficient synapse. This however is usually not observed even in healthy NMJs and indirect force was in most cases less than that of direct.

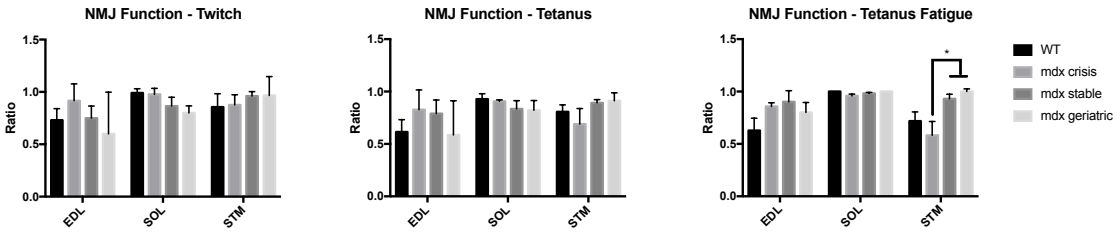

Figure 4.5. Functionality of mdx NMJs was not affected in geriatric mdx muscle. NMJ function in EDL, SOL, and STM muscles was determined by the ratio of indirect force/direct force. The closer the ratio was to 1, the higher the efficiency of neuromuscular transmission. Fatigue was measured as the decay in force following a 2-second tetanic train of 60Hz. 2 -Way ANOVA, Tukey's post-hoc test. Asterisks denote significant differences (* < 0.05). Largely no changes in maximum isometric force were found between groups, except for geriatric mdx STM, which were significantly weaker than that of stable mdx.

No differences were found in geriatric mdx NMJ functionality when compared to WT or stable mdx stable (12 – 16 weeks) junctions. When the synaptic function during tetanic fatigue (measured as the ratio of maximum tetanic force retained at the end of the 2 s train between direct and indirect stimulation) was used to assess the functionality of the STM synapse, the mdx stable and mdx geriatric muscles were more efficient than that of mdx crisis (mdx crisis vs stable: $P = 0.0287$, $df = 33$; mdx crisis vs mdx geriatric: $P = 0.0064$, $df = 33$. 2-Way ANOVA Tukey's post-hoc test). The remodeling process described in the STM NMJs of mdx mice may constitute a homeostatic response to spare the synapse from dysfunction. Synaptic functionality became more resistant to fatigue in geriatric and stable mdx NMJs, thus maintaining substantial reliability of muscle contraction as the dystrophic motor system aged.

4.3.2. Geriatric mdx cardiac function

4.3.2.1. M-Mode echocardiography

Since reduced life span in mdx mice is thought to involve declining heart physiology with age, I assessed if cardiac function decreased in geriatric mdx mice. Echocardiography was performed in both conscious and unconscious WT and mdx mice to determine cardiac characteristics in both young adult and geriatric mdx mice, noting that evaluating conscious mice was more clinically relevant to humans. Additionally, anesthetics have been shown to effect cardiac ultrasound measurements (Chaves et al., 2001; Roth et al., 2002). Unconscious M-Mode recordings from the parasternal, short axis window of the left ventricle indicated that several measures of geriatric mdx heart function were decreased, as compared to younger mdx animals (Figure 4.6). Fractional shortening (FS), a measurement of LV contractility, was decreased in geriatric mdx hearts compared to younger mdx hearts (Figure 4.6B). Furthermore, young mdx animals had larger FS measurements than young WT animals, suggesting that the LV of mdx animals had enhanced contractile function early in life that then declines significantly in old age. A similar event has been noted in GRMD animals and has been designated the hyperdynamic state (unpublished; Kornegay lab).

Ejection fraction (EF), an assessment of volume of blood ejected from the LV during a single heartbeat, was also significantly reduced in the hearts of geriatric mdx animals, as compared to younger mdx animals (Figure 4.6A). Although not significant, measurements of the size of the LV (EDV: end diastolic volume, ESV: end systolic

volume, EDD: end diastolic diameter, ESD: end systolic diameter) largely track with an incidence of dilated cardiomyopathy between young and geriatric mdx hearts. That is, the chamber and overall mass of the LV of the mdx heart becomes larger in comparison to the other age groups and WT animals (Figure 4.6C). These findings suggest that mdx mice can avoid debilitating cardiomyopathy for much of their life, as seen in the EF and FS of young mdx. However, combined with geriatric influences on cardiac function, significant deficits in mdx heart physiology emerge when compared to younger mdx animals, perhaps one of the causes of for mortality in these older mice.

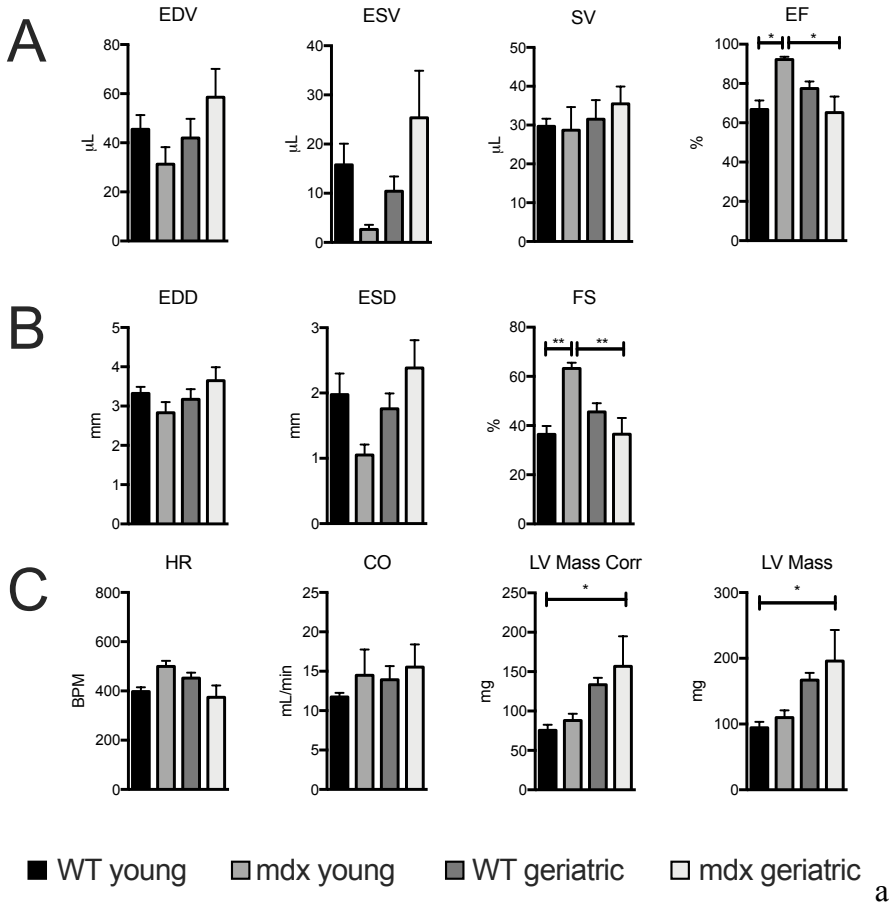

Figure 4.6. M-Mode Echocardiography Measurements.
A) Unconscious echocardiographic volumetric recordings. EDV - end diastolic volume; ESV - end systolic volume; SV - stroke volume; EF - ejection fraction. B) Unconscious echocardiographic diameter recordings. EDD - end diastolic diameter; ESV - end systolic diameter, FS – fractional shortening. C) Unconscious echocardiographic function and mass recordings. HR – heart rate; CO – cardiac output; LV Mass Corr – corrected left ventricular mass; LV Mass – left ventricular mass. One-Way ANOVA, Tukey's post-hoc test. * $P < 0.05$.

Conscious M-mode measurements did not reveal significance patterns of cardiomyopathy, as compared to those detected in unconscious animals. In fact, the trends noted in the unconscious animal recordings of heart function were completely

absent (A-6). This was most apparent in the cardiac function parameters, namely EF and FS. The single instance of difference in conscious mice was found in LV mass between young WT and mdx animals, importantly representing a morphological consequence with a physiological impact that is evident only in certain recording paradigms, namely in unconscious mice.

4.3.2.2. B-Mode echocardiography and strain analysis

Speckle tracking has been used in human and animal populations to predict the onset of dilated cardiomyopathy. However, this has not been compared between mice in conscious and unconscious states, nor has it been performed at all in very old mdx mice. I hypothesized that both longitudinal and radial strain, measures of heart elasticity, would be decreased in young mdx animals, and would become further decreased in geriatric mdx animals. Differences in global longitudinal strain (GLS), however, were not found, as no statistically significant disparities were detected across any groups in either conscious or unconscious animals (Figure 4.7A and E). There was an intriguing trend for geriatric animals to display less strain than their younger counter parts. However, geriatric WT and mdx unconscious global GLS measurements were virtually indistinguishable from each other (Figure 4.7E. One-Way ANOVA, Tukey's post-hot test, $P > 0.9999$).

A benefit of speckle tracking is that the LV can be divided into artificial sections and analysis performed on those specific sections. I artificially sectioned the ventricle into 6 parts (posterior base, posterior mid, posterior apex, anterior base, anterior mid,

anterior apex), and again analyzed the differences in peak strain between groups. Segmental strain was sub-divided into longitudinal and radial strain. Using this approach, segmental longitudinal strain assessment did indicate significant decreases in geriatric mdx animals. In unconscious geriatric mdx, longitudinal endocardial strain was significantly smaller than young WT animals in both basal segments (Figure 4.7C. 2-Way ANOVA, Tukey's post-hoc test, post base; $P = 0.0016$, ant base; $P = 0.0073$). In most segments, excluding posterior apex, geriatric mdx longitudinal strain trended lower than young mdx. Longitudinal strain measurements in conscious animals exhibited high variability and, therefore, the data was not of value for interpretation (A-7). Largely, though, geriatric mdx longitudinal strain was smaller than that detected in younger WT or mdx heart segments, supporting the general idea that very old age and dystrophy combine to compromise cardiac function in this dystrophic mouse model.

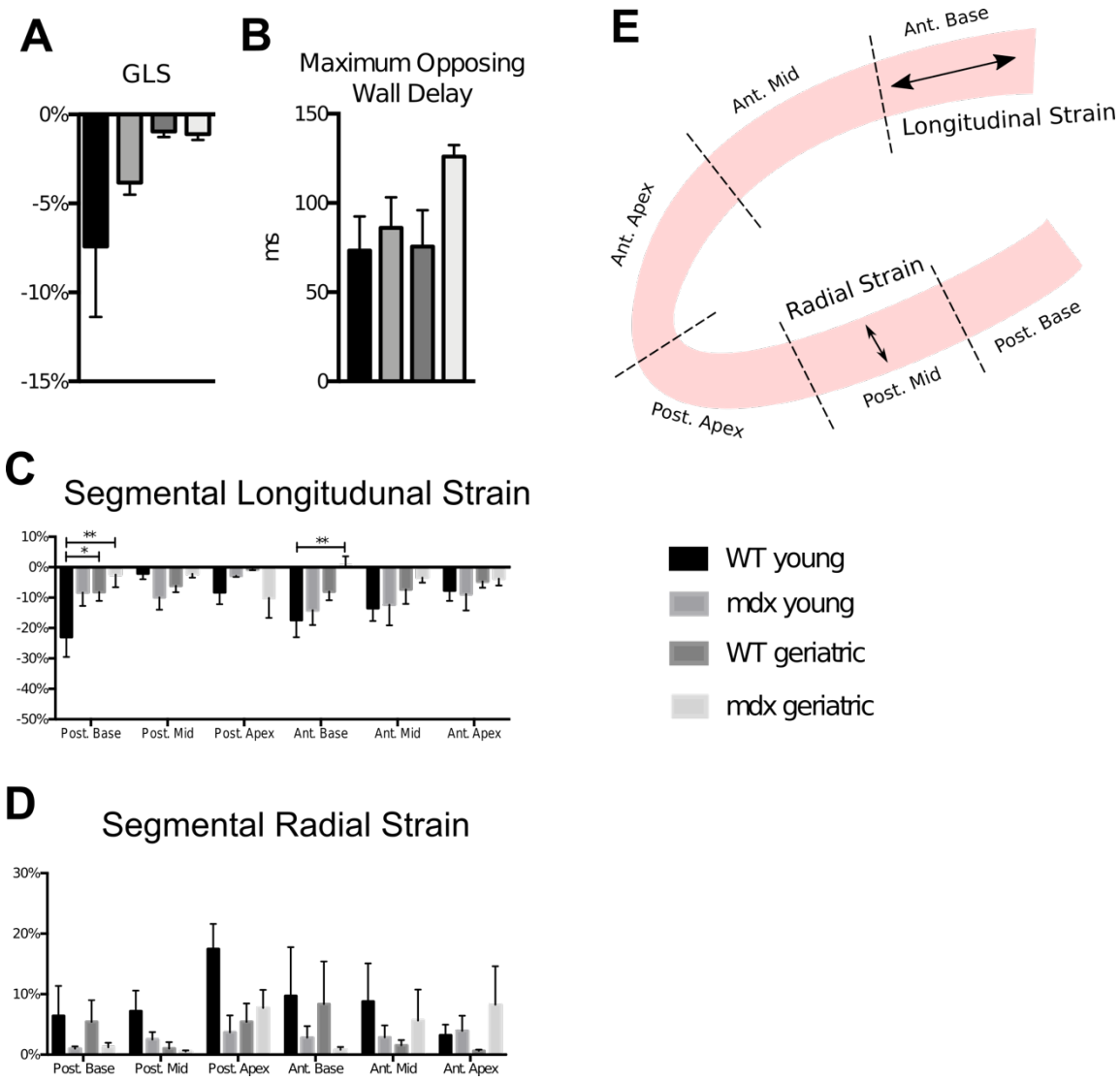

Figure 4.7. Echocardiograph Strain.
A) Global longitudinal strain. B) Desynchrony in left ventricular contraction in terms of peak strain. C) Peak longitudinal strain of the 6 segments. D) Peak radial strain of the 6 segments. E) Diagram of the segmental nature of the strain recordings of the left ventricle. A, B) 1-Way ANOVA. Tukey's post-hoc test. C, D) 2-Way ANOVA. Tukey's post-hoc test. Asterisk denote significance. * $P < 0.05$. ** < 0.01.

In both unconscious and conscious measures of radial strain, no significant differences were noted between any groups (Figure 4.7D and A-7), although trends similar to those seen in longitudinal strain were present. Strain was in most cases, however, less in geriatric mdx that young WT animals. Using longitudinal strain in unconscious animals seems to be a better indicator of heart dysfunction.

In an effort to measure desynchrony of the contracting LV, the maximum time delay of opposing walls in terms of time of peak longitudinal strain was measured. This is essentially a measure of whether sections of the LV are contracting in concert with each other. No significant differences in maximum opposing wall delay was noted between groups (Figure 4.7B, F and A-7).

4.4. Discussion

The data presented in Section 4 suggest that dystrophic contractile tissue is able to function quite normally until very advanced ages, and even then, only certain skeletal muscles are affected. Dystrophic EDL and SOL had few discernable differences from WT muscles at any age, while geriatric mdx STM muscles showed decreased contraction force production. As mentioned some muscle groups are ravaged by the disease while others are largely spared, such as the extraocular muscles (Porter et al., 2003). To our knowledge, this is the first force recording investigation of mdx STM. Moreover, I observed that the hind limb muscles, EDL and SOL, were not affected by the disease in terms of force production. This contradicts the results of others, which noted a age dependent reduction in normalized isometric force production in mdx compared to WT

(Lynch et al., 2001). The STM, however, displayed decreases in force at geriatric ages compared to young mdx animals, but was not significantly changed from WT. There is a possibility that in order to adapt to the changes in muscle that occur in dystrophy, homeostatic events take place to reestablish synaptic function and force characteristics in dystrophic muscle. The homeostatic event may be a consequence of the NMJ remodeling itself. Nonetheless, this mechanism is insufficient to overcome the combined impacts of dystrophic disease and advanced age, and certainly has little to no effect on cardiac function.

Changes to the mdx NMJ are progressive, at least in the STM muscle. The postsynaptic AChR aggregate became larger and more fragmented as the animal aged and muscle damage accumulated. Ultimately, at near the end of life stage in geriatric mice, the aggregate changed once again, becoming granular in appearance, possibly leading to dysfunctions in muscle contraction. I hypothesized that this would likely have a negative effect on the efficacy of the NMJ, but this was shown to be incorrect. Neuromuscular transmission (ratio of nerve evoked contractile force to direct muscle stimulation) in the STM of older mdx mice functioned equally compared to younger mdx and WT, and in some cases, was improved. This was evident when synaptic fatigability of the muscle during tetanus was investigated, where geriatric and stable mdx animals exhibited enhancements to neuromuscular transmission from those in the crisis period. NMJ remodeling has not fully taken place in all crisis mdx NMJs. It is not unlikely then that the remodeling process described in the STM of mdx mice, actually provides a means to increase the reliability of neuromuscular transmission. Ongoing

muscle fiber degeneration and regeneration eventually becomes pathological and the function of the muscle suffers as a result. In order to retain some functionality of the muscle, I suggest NMJ remodeling serves as a means to increase the response of the diseased tissue. This may only be during rigorous use, as twitch measurements of transmission efficacy in geriatric mice were not significantly changed from WT or younger animals. In terms of an animal's behavior, STM muscles of geriatric mice produced less force overall than younger mdx or WT animals, and therefore any amount of fatigue due to failures in neurotransmission could be catastrophic. Alternatively, however, it is possible that this increase in contraction reliability displayed in these muscles could result in increased damage to the already compromised muscle. The fragile myofibers contraction during intense use, such as tetanus, would further injure them resulting in sustained bouts of muscle fiber degeneration, inflammation, and muscle fiber replacement with connective tissue. In this scenario, enhancement of neuromuscular transmission would actually be maladaptive.

While the measurements above are categorized as measurements of reliability of neuromuscular transmission, the increased performance of the muscle during indirect stimulation could also be accounted for by myofiber type changes. This is a phenomenon that is known to occur in dystrophic muscle, as the proportion of type II fast twitch fibers decreases with an accompanying increase in the proportion of type I slow twitch fibers. In WT mice, the STM is made up of predominantly type II fast twitch muscle fibers. In 2 month old mdx animals, the relative ratios of myofiber types has not changed to a great degree (Guido et al., 2010). In mdx limb muscles, fiber type shifting does not begin until

later ages, which may also be the case for the STM (Carnwath and Shotton, 1987). The STM displays elevated signs of atrophy and immune cell infiltration at later stages of the disease in mdx. (Lefaucheur et al., 1995). It is possible that in the geriatric mdx STM, fiber type switching also occurs during this time which could affect the force characteristics of the muscle. Other researchers have noted that neurotransmission of remodeled junctions due to aging in WT animals is no different than younger counter parts, and also state that neurotransmission in fragmented junctions may be enhanced (Willadt et al., 2016). However, fiber type switching was not assessed in this report, either.

The other organ severely affected during the progression of DMD is the heart. This is unsurprising, as cardiac tissue is also made up of contracting cells, cardiomyocytes, with dystrophin tethered to the intracellular side of the membrane. Cardiac tissue, unlike skeletal muscle, does not have the ability to regenerate damaged myofibers. Therefore, any damage that the heart incurs due to the dystrophin loss is irreversible. In boys with DMD, this results in dilated cardiomyopathy. The same is true of mdx mice, which I demonstrate here becomes evident in older ages and may contribute to the early death in these dystrophic animals. In unconscious mice, geriatric mdx hearts were discovered to function poorly in comparison to younger mdx animals, and indicated the generation of a dilated cardiomyopathy. It is possible that, as in skeletal muscle, a compensatory mechanism actually strengthens mdx hearts through much of the animal's life, but ultimately begins to decline in dystrophic hearts at very old age. This has been termed the hyperdynamic state.

Conscious measurement of heart function detected no differences between any groups using M-mode echocardiography. The stress caused by conscious recordings likely served as a confounder during these experiments. During conscious recordings, the heart rate of all groups was elevated from that of unconscious, thus complicating systolic function analyses. Moreover, at systole, the LV would close almost fully for all mouse groups, regardless of age of disease. This resulted in similar cardiac function measurements across groups. To assess cardiac function in mdx mice, I suggest echocardiography in anesthetized states as opposed to conscious. While, this procedure does not closely match that for how echocardiographs are obtained in clinic, the stress induced during conscious measurements in mice is not ideal.

Speckle tracking analysis has previously been used to illustrate early changes in heart elasticity during mdx disease progression. Multiple groups have recorded changes to strain as early as 3 to 9 months in mdx animals when compared to WT (Spurney et al., 2011; Li et al., 2017; Zheng et al., 2017). Segmental analysis of the heart detected differences in region-specific strain between groups. The basal sections of the heart were the most affected, indicating that pathology is worse in these sections. This is corroborated by a recent report on GRMD cardiac function (Guo et al., 2019). Mdx LV have increased collagen and fibrotic tissue deposition beginning at early ages. It is possible that the loss of cardiomyocytes and replacement with non-contractile tissue occurs predominantly at these basal segments and result in less elasticity, indicated by changes to strain levels. No changes in radial strain nor desynchrony of development of peak longitudinal strain were noted here, in contradiction to other reports (Li et al.,

2017). What can be appreciated, however, is that radial strain measurements were very low in the posterior base and mid sections as well as the anterior base of the LV for geriatric mdx. The use of speckle tracking to investigate mdx animals is still relatively novel. As such, trouble shooting and the development of reproducible protocols must be established quickly, and agreements in what measurements are most meaningful should be analyzed. I conclude that segmental longitudinal speckle tracking in unconscious animals may be the most robust method for analyzing changes in the function of mdx cardiac tissue, and the development of cardiomyopathies.

5. CONCLUSIONS

5.1. The dystrophic neuromuscular junction

This investigation further describes the mdx mouse and GRMD dog models of Duchenne muscular dystrophy. I conclude that the abnormal appearance of NMJs, characterized for decades in mdx, is also apparent in the canine model of DMD as a consequence of continued myofiber degeneration and regeneration. Likely, the morphological change in NMJs described here are conserved among all mammalian models of the disease, including humans. The dystrophic NMJ is remodeled in such a way that the AChR-rich endplate becomes fragmented, and in the case of very old junctions, granularized. These rearrangements are initiated by myofiber injury, and the innervating motor neuron must be present for remodeling to occur. This work has largely focused on the STM muscle, which may be an excellent muscular tissue for investigation of mdx dystrophic pathology. This neck muscle does not undergo a crisis period of increased muscle damage, as seen in limb muscles such as the TA, and muscle fiber degeneration and regeneration is elevated throughout the animal's life span. The constant restructuring of the NMJ in dystrophic STMs may in fact protect the muscle from synaptic rundown during strenuous use.

The conservation of NMJ remodeling in the mammalian models of DMD suggest this phenomena also occurs in humans, but no satisfactory investigation of a human DMD NMJ has been made. Therefore, it is possible that human DMD NMJs are distinct from mdx or GRMD. Human NMJs in healthy muscle already have a fragmented

appearance when compared to that of rodents or dogs (Jones et al., 2017), so the remodeling process, if it occurs, may not parallel that noted in mdx or GRMD. Human tissue is especially difficult to obtain, especially in children and young adults, to our knowledge, a single investigation imaged DMD NMJs, albeit in cross section (Theroux et al., 2008). Thus, no information exists to assess in the detail presented above for the dystrophic mouse the morphology of these human junctions, especially in terms of fragmentation. In mdx and GRMD animals, I noted that not only did fragmentation of the postsynaptic AChR aggregate occur, but the area that synapse occupied was expanded during disease progression. These sorts of changes may also be occurring in the human NMJs and would not be appreciated in cross section as a large amount of the growth occurs along the length of the myofibers as opposed to its width.

Both the murine and canine models of dystrophy studied here involve the loss of the protein dystrophin in the muscle membrane. Therefore, it is reasonable to conclude that much of the NMJ remodeling that occur in these animals is due to disruption of DGC, and the resulting sarcolemmal instability. Even so, I cannot rule out the possibility that the remodeling process displayed in models of DMD is due to activity changes in other proteins, such as rapsyn or agrin, that are instrumental in regulating the developmental maturation of the NMJ. There is a reported decrease in the amount of MuSK (Pratt et al., 2015b) and a decrease in non-synaptic agrin expression in dystrophic mice (Eusebio et al., 2003). Mdx receptor endplates mature normally, from plaque to pretzel, until the onset of muscle damage in the mouse model, so developmental clustering must be taking place (Minatel et al., 2003). As the mdx animal never

expresses dystrophin during development, utrophin and the UGC provide the cues necessary for the initial maturation and remodeling process. In fact, the UGC is normally located at the synaptic area, while dystrophin is expressed throughout the muscle. The decreases in MuSK and agrin may prime the NMJ for remodeling in some fashion, as they are considered to be proteins integral to the aggregation and maintenance of receptor clusters at the NMJ. When agrin is removed from already mature NMJs, postsynaptic apparatus is disassembled, including the AChR aggregate (Samuel et al., 2012). Perhaps the changes in mdx DI are an indicator of the lower levels of agrin which maintains this structure. Observationally, the changes seen in damaged muscles, which express dystrophin and normal levels of the clustering proteins, are not nearly as drastic as those of the mdx. So, deficiencies in the activities of these AChR clustering proteins may indeed play a role in the restructuring process of dystrophy, although minor as compared to the degeneration of muscle fibers during dystrophic disease advancement.

Alternatively, the retention of agrin in the basal lamina, and not its decreased expression, may dictate the remodeling process after myofiber injury. Following myofiber degeneration, agrin remains even as the basement membrane collapses. During regeneration, as the muscle expands, it will contact agrin and the membrane bound MuSK and LRP4 associated with the UGC will begin the receptor clustering process. Another theory is that new agrin may be released from neural varicosities of the newly rearranged motor axon as it grows in contact with the regenerated myofiber. The varicose nature of the regenerated nerve terminal and the location of new agrin in the

basal lamina would mediate AChR clustering into the fragmented morphology seen in dystrophy.

The extent to which neuron-to-muscle signaling or muscle-to-neuron signaling contribute to the remodeling of the NMJ during development has garnered significant study and debate for decades (McMahan, 1990; Kim and Burden, 2008; Yumoto et al., 2012). Similarly, whether or not dystrophic remodeling of the NMJ has detrimental effects on neuromuscular transmission or the physiology of the dystrophic muscle is a contested subject. In mdx, indicators are present suggesting that synaptic function is perturbed (Nagel et al., 1990; Carlson and Roshek, 2001). The overall behavior of the mdx model does seem to be affected, but not much in terms of non-normalized isometric muscular force production (Lynch et al., 2001). It is not until the very last stages of the disease in mdx that any overt neuromuscular transmission deficits become appreciable, at least in our preparations, and then particularly in the STM, as compared to the other muscles studied. The aging process even in WT mice involves changes in NMJ morphology, again due to ongoing degeneration and regeneration of myofibers. These changes with aging, however, are mostly an increase in the number of AChR fragments (Willadt et al., 2016), and possibly junctional and receptor area (Cardasis and LaFontaine, 1987; Deschenes et al., 2011). In aged and remodeled junctions, there are no indications of failed neuromuscular transmission, and aged fragmented junctions may in fact be more reliable than younger synapses (Willadt et al., 2016). This agrees with studies that conclude that efficiencies of neuromuscular transmission is influenced by NMJ morphology. NMJs of different muscles have variable morphologies, which

correlate with the muscle on which they reside. Some NMJs are larger, some are smaller, and some are more fragmented than others (Jones et al., 2016). Although the morphological aspects of NMJs may be variable, their ultimate function is consistent. Evoked EPPs from populations of NMJs on different muscles, with distinct morphological attributes, were on average indistinguishable from each other. However, when quantal release was investigated, it was noted that the morphology of the NMJ dictated synaptic release characteristics. Smaller NMJs had larger MEPPs that were less frequent, and evoked release events had a lower quantal content.

5.2. Functional properties of the dystrophic neuromuscular junction

Variation in NMJ morphology is striking across animal species, but these differences in form do not dramatically dictate synaptic function. Still, at the vertebrate NMJ, some aspects of its structure assure that excitation of the muscle is much greater than that needed for repeated, forceful contraction. This ability to remain effective under broad physiological conditions due to over excitation of the muscle fiber is termed the NMJ's safety factor, and postsynaptic folding associated with the muscle endplate is thought to be central to this phenomenon (Martin, 1994; Wood and Slater, 1997). Species-specific attributes of the NMJ correspond well to changes seen in the morphology of the dystrophic junction. Others and I report on the fragmentation of the receptor aggregate and describe an expansion of the endplate as well (Lyons and Slater, 1991; Pratt et al., 2013; Haddix et al., 2018). Mdx mice also display a reduction in the length of postsynaptic membrane invaginations, but no decreases in the amount of AChR sites per

NMJ (Lyons and Slater, 1991). This suggests that while the NMJ structure drastically changes during the dystrophic disease advancement, homeostatic changes are perhaps being made to the NMJ to preserve neuromuscular function. These linked changes in NMJ morphology and function would be highly adaptive. The loss of junctional folds following the regeneration of the NMJ might decrease the safety factor of synaptic transmission and excitation-contraction coupling. To compensate, it is plausible that the synapse expands in order to release more, and more effective, quanta of transmitter upon terminal excitation. However, some previous investigations indicate quantal content is not increased in young mdx animals (Nagel et al., 1990; Lyons and Slater, 1991), while other demonstrate decreases in MEPP amplitude and increases in quantal content (Carlson and Roshek, 2001). Our data also suggests that endplate size and receptor area does not significantly grow until later in life, which may explain the discrepancies in mdx synaptic function between ours and others interpretations suggested previously. Indeed quantal content does increase at 37 weeks of age (Nagel et al., 1990), but these researchers also noted an increase in endplate size at early time points without corresponding neuromuscular transmission changes.

There does seem to be some amount of conflict and variance in the data generated from different labs on the neuromuscular transmission properties in mdx mice. Although there is general agreement that the morphology of the junction is rearranged in dystrophy, it remains poorly understood if, or how, these changes result in quantal acetylcholine release changes. Some of these discrepancies likely arise from the different muscles studied (diaphragm versus ETA, for example) and the different time points in

disease progression analyzed. Here, I demonstrate that the remodeling process of the NMJ in dystrophy in both dogs and mice is progressive, following the advancement of the disease. I suggest that a certain amount of remodeling must take place before significant changes to quantal release might be observed. As evidence to this point, I show that neuromuscular efficiency, as the ratio between muscle evoked and motor neuron evoked fatigue during tetanic stimulation, was increased in older mdx STMs, as compared to the normal efficiency at crisis period NMJs of young mdx mice (Section 4). Increased safety factors are not necessary for non-taxing contractions such as twitch, but they are for highly rigorous, high frequency behaviors. During tetanic stimulation, muscle fatigability was equal between both direct and indirectly stimulated highly remodeled NMJs. While not significant, there is a 50% increase in the density of synaptic vesicles at mdx terminals (Nagel et al., 1990), which could account for the protection against tetanic fatigue seen in geriatric mdx STM NMJs, even with highly fragmented, sometimes disintegrating, endplate structure. As such, the pool of vesicles available to respond to a nerve impulse may not run down, as there are simply more than enough in a releasable state or in reserve. This would absolutely be necessary if the receptor response to acetychloline was diminished (smaller MEPP) and the junctional folds were lost. Therefore, a homeostatic increase in quantal content (i.e., the number of vesicles involved per motor neuron action potential) would likely be needed to illicit the same, efficacious response in a geriatric mdx muscle. To elucidate what exactly protects geriatric mdx junctions from dysfunction in the STM, future single fiber

electrophysiology, with corresponding ultrastructural analysis of the NMJ, would be very beneficial.

It should be noted that the investigations here of progressive remodeling were limited to the STM muscle, and it is entirely possible that muscles that experience the crisis period, or even those that do not, during disease progression may not remodel the NMJ in quite the same way, as suggested by the decrease in receptor replacement noted in mdx TA after 5 weeks. Although the force generation characteristics of STM, SOL, and EDL were studied, no effort was made to correlate synaptic structure to electrophysiological properties of the NMJ. It should also be noted that no similar neuromuscular physiology had been conducted on GRMD dog muscles, and very little is known in DMD boys. Therefore, a complete picture of the functional properties of the dystrophic neuromuscular junction remains to be elucidated.

As mentioned earlier, the normal human NMJ, while relatively smaller than that of a rodent, has a fragmented appearance. While not to the degree of an mdx mouse or GRMD dog, the receptor clusters are arranged in discrete islands, with terminal varicosities juxtaposed to the receptor aggregates (Oda, 1984; Slater et al., 1992). Furthermore, the vesicle release machinery is organized in a distinctly different fashion from that of rodent terminal boutons (Jones et al., 2017). The total area of active zone puncta, as determined by SNAP25 labeling, a presynaptic protein involved in transmitter secretion, is similar between mice and humans, but the density and spatial organization of those puncta are different between the two. As the human NMJs are smaller, the density of the labeled puncta is higher, but also located at the periphery of the synaptic

boutons in a ring like manner, rather than the seemingly random arrangement within the ribbons of the mouse junction. Whether this is the same for the mdx puncta is not known.

There seem to be two possibilities for how the mdx active zones are organized over the islands of AChR aggregation. 1) The synaptic vesicle machinery is rearranged in the mdx boutons to that similar to humans or 2) the mdx presynaptic apparatus remains dispersed, similar to that of WT mice. The latter would require a different structure from the peripheral ring architecture observed in human terminals. The first possibility is supported by our observational data from both dystrophic mice and dogs. When labeled for neurofilament and SV2, a protein found on synaptic vesicles, a ring of fluorescence is seen within the terminal boutons, similar to SNAP25 labeling seen at human junctions. This ring is likely SV2, as neurofilament does not in normal circumstances extend into the terminal area (observational). The high density of synaptic vesicles in the ring formation is indicative of active zone locational changes and support a homeostatic rearrangement of the secretory machinery at remodeled dystrophic junctions. The second possibility is supported by two pieces of evidence, one morphological and one based on electrophysiology. Human NMJs have a much more complex secondary folding of the postsynaptic membrane, in contrast to mice. This greater complexity of the endplate corresponds to changes on the presynaptic side of the human junction, where the density of active zones is increased, and their distribution changed compared to mouse junction, as mentioned above (Jones et al., 2017). Even more different are the junctional folds of mdx synapses, which are not nearly as

numerous or deep as WT NMJs, suggesting again through correlation that active zones might also differ between dystrophic and healthy synapses, although this has not been reported in the limited mdx NMJ ultrastructure investigations, which tend to focus only on junctional folds. Additionally, human quantal content is much lower than that of mice, and mdx quantal content is even higher than that of WT mice. Again, the much greater transmitter release in mdx may be explained by the increased size of the endplate and possible relocalization of active zones. However, as indicated by our force recordings, the extensive structural changes that occur during the remodeling of the mdx NMJ do not result in result in significant decreases in synaptic function. I conclude that as yet unknown changes in synaptic physiology are homeostatic in nature and compensate for lost of NMJ structural integrity, while maintaining efficiency of neuromuscular transmission and ensuring the reliability of skeletal muscle contractile function.

To fully appreciate potential changes to presynaptic machinery and vesicle fusion sites, labeling experiment of active zone proteins would be instructive. Investigating the distribution of SNAP25, piccolo, bassoon, or other vesicle proteins involved in vesicle fusion with super resolution microscopy, combined with new tissue clearing approaches (Williams et al., 2019), will allow researchers to determine the extent of active zone and release apparatus rearrangement at mdx NMJs. Such an approach would reveal hot spots of transmitter release and any unequal distribution of the same across NMJ fragments. It has been demonstrated using synaptoPHlorin (an optical indicator of neurotransmitter release), that in WT murine NMJs not all areas of the endplate have equal amounts of

synaptic vesicle fusion (Wyatt and Balice-Gordon, 2008). Variability in presynaptic-postsynaptic transmission machinery matching, I predict, would not only exist, but be greater in the highly fragmented NMJs of older and geriatric mdx mice and restricted to only certain "islands". Although not addressed here, the presynaptic function of the mdx model would be of special interest for future studies, particularly in the older dystrophic animals as our indirect measures of synaptic reliability was increased in highly remodeled junctions.

As mentioned above, changes in neuromuscular transmission efficiency and force generation were only observed at older ages in mdx mice, and only in the STM muscle. In these muscles, a resiliency against fatigue during tetanic stimulation was seen. This resiliency in function was surprising, especially in geriatric mdx NMJs which were have two distinct morphologies: a highly fragmented form, and an even less structured form that I termed granular or disintegrated, and was unlikely to be physiologically active. Initial time course studies of NMJ remodeling in mdx mice suggested that dystrophic junctions continue to grow larger with disease progression, but here I report that this did not hold true. However, it should be noted that junctional size measurements from granular junctions were included in the analysis, which may have skewed the data toward smaller junction sizes. Frequently, small granular junctions were observed adjacent to fragmented ones. Granular junctions were usually innervated, but whether that innervation was full or partial was difficult to assess and therefore not measured.

Regardless, I believe that remodeled junctions (either fragmented to granular) may be responsible for the increase efficiency in the geriatric mdx STM. In order to increase synaptic strength and reliability at junctions on the verge of disintegration, there would likely need to be a concomitant reorganization of active zones and the corresponding postsynaptic junctional sarcolemma. Since the reappearance of junctional folds in geriatric mdx animals is unlikely, I conclude that the presynaptic apparatus or properties of receptors themselves are the likely culprits contributing to surprising function of remodeled NMJs. Ultimately, direct assessments of neuromuscular transmission and the synaptic machinery will reveal the nature of NMJ strengthening of the granular and fragmented remodeled synapse in mdx muscle.

Another possibility there is significant myofiber loss in the geriatric mdx animals. The NMJs investigated above may reside on myofibers that were resistant to damage or had characteristics that increased their regenerative capacity. Synapses that were on inefficient myofibers could be selectively lost. The incidence of myofiber loss in these end-stage mdx animals is currently being investigated by the Thompson Lab (Ryan Massopust, unpublished data).

5.3. Dystrophic cardiomyopathy

The other majorly affected body system in DMD, apart from the skeletal muscle, is the cardiovascular system. It is well documented that afflicted men develop cardiomyopathies in the later stages of this dystrophic disease. Echo- and electrocardiography reveal that the pathology progresses from pre-clinical (or non-

symptomatic), to hypertrophic cardiomyopathy, and finally to dilated cardiomyopathy (Nigro et al., 1990). Hypertrophic cardiomyopathy is ultimately defined as a change in the ratio between the septum width and the LV free wall width. Dilated cardiomyopathy is characterized as an increase in the size of the LV, and changes to the contractility of the chamber usually present as decreases in EF).

Dystrophic canines also develop a cardiomyopathy associated with the loss of dystrophin from cardiomyocytes (Valentine et al., 1989; Moise et al., 1991; Yugeta et al., 2006). The GRMD cardiomyopathy proceeds much like that of DMD boys, at least in terms of microscopic pathology changes. A pre-pathological stage advances to an intermediate stage at about 1 year. At this point, the GRMD hearts display fibrotic deposition and signs of cardiomyocyte necrosis, predominantly in the epimyocardium of the LV. At 6 years, the cardiomyopathy becomes pathological, in that decreases in LV movement are noted via echocardiography. This corresponds to increased fibrotic deposition, fatty tissue disposition, and more of the heart being subjected to contractile tissue removal. Additionally, as seen in myofibers, there is an increase in the variation in the myocardial cell size (Valentine et al., 1989). This suggests that an event similar to that in muscles is occurring in GRMD cardiac tissue. Specifically, there is significant cellular damage due to contraction forces generated in the absence of cardiac dystrophin. As mentioned before, cardiac tissue does not have resident stem cells like skeletal muscle to respond to cellular necrosis. Tissue lost due to damage in the heart is irreplaceable.

Echocardiography and more advanced imaging techniques of GRMD corroborate both previous investigations of dystrophic canine hearts, and our data in mdx hearts (Guo et al., 2019). Circumferential strain, measured with speckle tracking, was shown to be a sensitive measure for the development of cardiomyopathy in dogs. This is similar to our finding that segmental longitudinal strain could discover cardiac dysfunction in geriatric mdx left ventricles as compared to young WT. Additionally, late gadolinium enhancement in cardiac magnetic resonance indicated that the basal segments of left ventricle were the most majorly affected areas in GRMD. This again agrees with our data in mdx that shows that anterior and posterior basal segments of the LV are affected in geriatric mdx hearts.

Like dystrophic dogs, the mdx mouse undergoes similar cardiomyopathic events to DMD (Bridges, 1986). The development of the murine cardiomyopathy seems restricted mostly to the LV as seen in DMD, and the canine model. A similar progression from a mild to more severe dilated cardiomyopathy is also noted. Fibrosis due to cellular damage is evident in the later stages, and this leads to dilated cardiomyopathy, in which heart contractility is compromised (Quinlan et al., 2004; van Putten et al., 2014). As opposed to the canine model, there is always an increased macrophagic infiltration in mdx hearts (Van Erp et al., 2010). Perhaps the pathological advancement of the two diseases is dissimilar. Evan's blue dye uptake, however, is constantly elevated in the murine model, indicating a continuous level of membrane damage occurs, much like that observed in the mdx STM.

The systolic function of mdx hearts as assessed by traditional echocardiography, largely does not show functional deficits until the later stages of the disease, and are not distinguishable from WT before 6 months of age (Quinlan et al., 2004; Au et al., 2011). Some researchers, however, have noted a very different pattern of cardiac involvement. In fact, it has been noted that early in life (2 months) the mdx heart contracts more than that of WT (van Putten et al., 2014). This is similar to our echocardiographic data in the young mdx mice. Where our results begin to differ from the reports of others is in the geriatric ages of mdx mice. Although I did record a decrease in the function of the geriatric versus younger mdx hearts, EF and SV were indistinguishable from that of WT animals. It is possible that just as with the NMJ, mdx cardiac physiology may involve a homeostatic regulation. The increased contractility of the heart may be in response to an overall instability of the cardiomyocytes, and an early functional hypertrophic event of the myocardium. Although few studies have investigated the heart functionality at geriatric ages, those that have noted a significant decreases in heart function compared to WT (Bostick et al., 2009; Bostick et al., 2010). In our geriatric mdx analyses, significant decrease in cardiac function (EF and FS) were found only when comparing geriatric mdx hearts to young mdx hearts. These patterns did not exist in the conscious mice, likely due to the stress caused by the recording procedures.

It is possible that the mdx heart must contract at a greater intensity to function the same as the WT heart, perhaps due to metabolic or vascular changes in the mdx mouse. In this case, the decrease in EF and FS in the geriatric mdx animals as compared to young mdx, may indicate a true pathological event and a dilated cardiomyopathy as

noted by increased in LV mass. While I did not investigate the actual morphology or fibrotic deposition within dystrophic hearts, contractile heart tissue begins to be replaced by connective and fibrotic tissue early in life (Van Erp et al., 2010).

It should be noted that the ages of the geriatric mdx studied here are all above 19 months. It was not recorded, but there was a noticeable dropout of animals within our colony, as has been seen in natural life history assessments of mdx populations (Chamberlain et al., 2007). It is entirely possible that the small geriatric sample from our colony represents dystrophic individuals who are not as affected by the disease state or are especially capable of mounting homeostatic mechanisms to compensate for disease progression. Here, our younger sample would be more representative of the total population, while the geriatric animals might not display the same progression of heart involvement. As echocardiography is a completely non-invasive technique, it would be beneficial to perform a longitudinal study from 3 months to the end stage of the disease, rather than the typical study endpoint at 12 months of age, which is only about midlife for mdx animals.

5.4. Summary

Overall, our results give a refined view of neuromuscular and cardiac changes caused by dystrophy in dog and mouse models. In summary, I found:

1) The morphology of mdx NMJs is vastly different than WT and changes to the dystrophic NMJ are progressive and advance with the disease state in the STM.

2) GRMD NMJs display similar changes to those of mdx, and these aberrations are likely conserved in all mammalian dystrophic states, including DMD.

3) The dystrophic STM does not undergo an early life crisis period of muscle fiber injury, like that seen in the TA of mdx mice. Myofiber degeneration and regeneration are constantly elevated in the dystrophic STM.

4) NMJ remodeling in mdx is initiated by myofiber damage near the endplate region of the muscle, and the motor axon terminal must be present for remodeling to occur in murine dystrophy.

5) Remodeled junctions in mdx are not deficient in neuromuscular transmission, and at geriatric ages may actually serve to increase response to synaptic stimuli.

6) The NMJ is not a good target for treatment to ameliorate DMD pathology and disease progression.

7) On the other hand, morphological changes to the NMJ are excellent biomarkers for disease severity and progression, and the STM, like the diaphragm offers a model muscle for investigation of the disease.

8) The cardiac function of mdx mice is best assessed in unconscious mice.

9) Geriatric mdx cardiac function is not changed from that of WT, although young mdx mice display increased cardiac contractility. Geriatric mdx heart function is decreased as compared to young mdx.

10) Strain analysis, via speckle tracking, indicates that the basal segments of the left ventricle are the most affected regions of the heart of geriatric mdx mice, but defects are only appreciable at geriatric ages.

REFERENCES

Akaaboune M, Culican SM, Turney SG, Lichtman JW (1999) Rapid and reversible effects of activity on acetylcholine receptor density at the neuromuscular junction in vivo. Science 286:503-507.

Amoasii L, Hildyard JC, Li H, Sanchez-Ortiz E, Mireault A, Caballero D, Harron R, Stathopoulou T-R, Massey C, Shelton JM (2018) Gene editing restores dystrophin expression in a canine model of Duchenne muscular dystrophy. Science 362:86-91.

Apel ED, Glass DJ, Moscoso LM, Yancopoulos GD, Sanes JR (1997) Rapsyn is required for MuSK signaling and recruits synaptic components to a MuSK-containing scaffold. Neuron 18:623-635.

Arthur-Farraj PJ, Latouche M, Wilton DK, Quintes S, Chabrol E, Banerjee A, Woodhoo A, Jenkins B, Rahman M, Turmaine M (2012) c-Jun reprograms Schwann cells of injured nerves to generate a repair cell essential for regeneration. Neuron 75:633-647.

Au CG, Butler TL, Sherwood MC, Egan JR, North KN, Winlaw DS (2011) Increased connective tissue growth factor associated with cardiac fibrosis in the mdx mouse model of dystrophic cardiomyopathy. International Journal of Experimental Pathology 92:57-65.

Babiuk RP, Zhang W, Clugston R, Allan DW, Greer JJ (2003) Embryological origins and development of the rat diaphragm. Journal of Comparative Neurology 455:477-487.

Balice-Gordon R, Lichtman J (1990) In vivo visualization of the growth of pre-and postsynaptic elements of neuromuscular junctions in the mouse. Journal of Neuroscience 10:894-908.

Balice-Gordon RJ, Lichtman JW (1994) Long-term synapse loss induced by focal blockade of postsynaptic receptors. Nature 372:519-524.

Bengtsson NE, Hall JK, Odom GL, Phelps MP, Andrus CR, Hawkins RD, Hauschka SD, Chamberlain JR, Chamberlain JS (2017) Muscle-specific CRISPR/Cas9 dystrophin gene editing ameliorates pathophysiology in a mouse model for Duchenne muscular dystrophy. Nature Communications 8.

Benoit PW, Belt WD (1970) Destruction and regeneration of skeletal muscle after treatment with a local anaesthetic, bupivacaine (Marcaine). Journal of Anatomy 107:547.

Betz W, Sakmann B (1973) Effects of proteolytic enzymes on function and structure of frog neuromuscular junctions. The Journal of Physiology 230:673-688.

Bodine SC, Stitt TN, Gonzalez M, Kline WO, Stover GL, Bauerlein R, Zlotchenko E, Scrimgeour A, Lawrence JC, Glass DJ (2001) Akt/mTOR pathway is a crucial regulator of skeletal muscle hypertrophy and can prevent muscle atrophy in vivo. Nature Cell Biology 3:1014.

Boldrin L, Zammit PS, Morgan JE (2015) Satellite cells from dystrophic muscle retain regenerative capacity. Stem Cell Research 14:20-29.

Bonilla E, Samitt CE, Miranda AF, Hays AP, Salviati G, DiMauro S, Kunkel LM, Hoffman EP, Rowland LP (1988) Duchenne muscular dystrophy: deficiency of dystrophin at the muscle cell surface. Cell 54:447-452.

Bostick B, Yue Y, Duan D (2010) Gender influences cardiac function in the mdx model of Duchenne cardiomyopathy. Muscle & Nerve 42:600-603.

Bostick B, Yue Y, Long C, Duan D (2008) Prevention of dystrophin-deficient cardiomyopathy in twenty-one-month-old carrier mice by mosaic dystrophin expression or complementary dystrophin/utrophin expression. Circulation Research 102:121-130.

Bostick B, Yue Y, Long C, Marschalk N, Fine DM, Chen J, Duan D (2009) Cardiac Expression of a Mini-dystrophin That Normalizes Skeletal Muscle Force Only Partially Restores Heart Function in Aged Mdx Mice. Molecular Therapy 17:253-261.

Bridges L (1986) The association of cardiac muscle necrosis and inflammation with the degenerative and persistent myopathy of MDX mice. Journal of the Neurological Sciences 72:147-157.

Briguet A, Courdier-Fruh I, Foster M, Meier T, Magyar JP (2004) Histological parameters for the quantitative assessment of muscular dystrophy in the mdx-mouse. Neuromuscular Disorders 14:675-682.

Brimijoin S (1983) Molecular forms of acetylcholinesterase in brain, nerve and muscle: nature, localization and dynamics. Progress in Neurobiology 21:291-322.

Brussee V, Tardif F, Tremblay JP (1997) Muscle fibers of mdx mice are more vulnerable to exercise than those of normal mice. Neuromuscular Disorders 7:487-492.

Bruusgaard J, Liestøl K, Ekmark M, Kollstad K, Gundersen K (2003) Number and spatial distribution of nuclei in the muscle fibres of normal mice studied in vivo. The Journal of Physiology 551:467-478.

Buddhe S, Lewin M, Olson A, Ferguson M, Soriano BD (2016) Comparison of left ventricular function assessment between echocardiography and MRI in Duchenne muscular dystrophy. Pediatric Radiology 46:1399-1408.

Buller A, Eccles JC, Eccles RM (1960) Interactions between motoneurones and muscles in respect of the characteristic speeds of their responses. The Journal of Physiology 150:417-439.

Burden SJ, Sargent PB, McMahan U (1979) Acetylcholine receptors in regenerating muscle accumulate at original synaptic sites in the absence of the nerve. The Journal of Cell Biology 82:412-425.

Busetto G, Buffelli M, Tognana E, Bellico F, Cangiano A (2000) Hebbian mechanisms revealed by electrical stimulation at developing rat neuromuscular junctions. Journal of Neuroscience 20:685-695.

Campagna JA, Rüegg MA, Bixby JL (1995) Agrin is a differentiation-inducing “stop signal” for motoneurons in vitro. Neuron 15:1365-1374.

Campbell M, Ganetzky B (2012) Extensive morphological divergence and rapid evolution of the larval neuromuscular junction in Drosophila. Proceedings of the National Academy of Sciences 109:E648-E655.

Cardasis CA, LaFontaine DM (1987) Aging rat neuromuscular junnctions: A morphometric study of cholinesterase-stained whole mounts and ultrastructure. Muscle & Nerve: Official Journal of the American Association of Electrodiagnostic Medicine 10:200-213.

Carlson GC, Roshek DM (2001) Adult dystrophic (mdx) endplates exhibit reduced quantal size and enhanced quantal variation. Pflügers Archiv 442:369-375.

Carnwath JW, Shotton DM (1987) Muscular dystrophy in the mdx mouse: histopathology of the soleus and extensor digitorum longus muscles. Journal of the Neurological Sciences 80:39-54.

Catterall WA (1991) Excitation-contraction coupling in vertebrate skeletal muscle: A tale of two calcium channels. Cell 64:871-874.

Chamberlain JS, Metzger J, Reyes M, Townsend D, Faulkner JA (2007) Dystrophin-deficient mdx mice display a reduced life span and are susceptible to spontaneous rhabdomyosarcoma. The FASEB Journal 21:2195-2204.

Chan S, Head S, Morley J (2007) Branched fibers in dystrophic mdx muscle are associated with a loss of force following lengthening contractions. American Journal of Physiology-Cell Physiology 293:C985-C992.

Chaves AA, Weinstein DM, Bauer JA (2001) Non-invasive echocardiographic studies in mice: influence of anesthetic regimen. Life Sciences 69:213-222.

Chazaud B, Brigitte M, Yacoub-Youssef H, Arnold L, Gherardi R, Sonnet C, Lafuste P, Chretien F (2009) Dual and Beneficial Roles of Macrophages During Skeletal Muscle Regeneration. Exercise and Sport Sciences Reviews 37:18-22.

Chipman PH, Franz CK, Nelson A, Schachner M, Rafuse VF (2010) Neural cell adhesion molecule is required for stability of reinnervated neuromuscular junctions. European Journal of Neuroscience 31:238-249.

Ciciliot S, Schiaffino S (2010) Regeneration of mammalian skeletal muscle: basic mechanisms and clinical implications. Current Pharmaceutical Design 16:906-914.

Coley WD, Bogdanik L, Vila MC, Yu Q, Van Der Meulen JH, Rayavarapu S, Novak JS, Nearing M, Quinn JL, Saunders A (2015) Effect of genetic background on the dystrophic phenotype in mdx mice. Human Molecular Genetics 25:130-145.

Connor NP, Suzuki T, Sewall GK, Lee K, Heisey DM (2002) Neuromuscular junction changes in aged rat thyroarytenoid muscle. Annals of Otology, Rhinology & Laryngology 111:579-586.

Cooper B, Gallagher E, Smith C, Valentine B, Winand N (1990) Mosaic expression of dystrophin in carriers of canine X-linked muscular dystrophy. Laboratory Investigation; a Journal of Technical Methods and Pathology 62:171-178.

Coulton G, Morgan J, Partridge T, Sloper J (1988a) The mdx mouse skeletal muscle myopathy: I. A histological, morphometric and biochemical investigation. Neuropathology and Applied Neurobiology 14:53-70.

Coulton G, Curtin N, Morgan J, Partridge T (1988b) The mdx mouse skeletal muscle myopathy: II. Contractile properties. Neuropathology and Applied Neurobiology 14:299-314.

Dangain J, Vrbova G (1984) Muscle development in mdx mutant mice. Muscle & Nerve 7:700-704.

Danialou G, Comtois AS, Dudley R, Karpati G, Vincent G, Des Rosiers C, Petrof BJ (2001) Dystrophin-deficient cardiomyocytes are abnormally vulnerable to mechanical stress-induced contractile failure and injury. The FASEB Journal 15:1655-1657.

Dellorusso C, Crawford RW, Chamberlain JS, Brooks SV (2001) Tibialis anterior muscles in mdx mice are highly susceptible to contraction-induced injury. Journal of Muscle Research & Cell Motility 22:467-475.

Deschenes MR, Roby MA, Glass EK (2011) Aging influences adaptations of the neuromuscular junction to endurance training. Neuroscience 190:56-66.

Deschenes MR, Brewer RE, Bush JA, McCoy RW, Volek JS, Kraemer WJ (2000) Neuromuscular disturbance outlasts other symptoms of exercise-induced muscle damage. Journal of the Neurological Sciences 174:92-99.

DiMario JX, Uzman A, Strohman R (1991) Fiber regeneration is not persistent in dystrophic (MDX) mouse skeletal muscle. Developmental Biology 148:314-321.

Dunaevsky A, Connor EA (1995) Long-term maintenance of presynaptic function in the absence of target muscle fibers. Journal of Neuroscience 15:6137-6144.

Dunaevsky A, Connor EA (1998) Stability of frog motor nerve terminals in the absence of target muscle fibers. Developmental Biology 194:61-71.

Dupont-Versteegden EE, McCarter RJ (1992) Differential expression of muscular dystrophy in diaphragm versus hindlimb muscles of mdx mice. Muscle & Nerve: Official Journal of the American Association of Electrodiagnostic Medicine 15:1105-1110.

Dutton EK, Simon AM, Burden SJ (1993) Electrical activity-dependent regulation of the acetylcholine receptor delta-subunit gene, MyoD, and myogenin in primary myotubes. Proceedings of the National Academy of Sciences 90:2040-2044.

Eagle M, Baudouin SV, Chandler C, Giddings DR, Bullock R, Bushby K (2002) Survival in Duchenne muscular dystrophy: improvements in life expectancy since 1967 and the impact of home nocturnal ventilation. Neuromuscular Disorders 12:926-929.

Edwards R, Jones D, Newham D, Chapman S (1984) Role of mechanical damage in pathogenesis of proximal myopathy in man. The Lancet 323:548-552.

Emery AE (1965) Muscle histology in carriers of Duchenne muscular dystrophy. Journal of Medical Genetics 2:1.

Emery AEH, Muntoni F (2003) Duchenne muscular dystrophy : by Alan E. H. Emery, Francesco Muntoni: Oxford : New York : Oxford University Press, 2003. Third edition.

Eusebio A, Oliveri F, Barzaghi P, Ruegg MA (2003) Expression of mouse agrin in normal, denervated and dystrophic muscle. Neuromuscular Disorders 13:408-415.

Feng G, Mellor RH, Bernstein M, Keller-Peck C, Nguyen QT, Wallace M, Nerbonne JM, Lichtman JW, Sanes JR (2000) Imaging neuronal subsets in transgenic mice expressing multiple spectral variants of GFP. Neuron 28:41-51.

Feng Z, Ko CP (2008a) The role of glial cells in the formation and maintenance of the neuromuscular junction. Annals of the New York Academy of Sciences 1132:19-28.

Feng Z, Ko C-P (2008b) Schwann cells promote synaptogenesis at the neuromuscular junction via transforming growth factor-β1. Journal of Neuroscience 28:9599-9609.

Ferns MJ, Campanelli JT, Hoch W, Scheller RH, Hall Z (1993) The ability of agrin to cluster AChRs depends on alternative splicing and on cell surface proteoglycans. Neuron 11:491-502.

Fine DM, Shin J-H, Yue Y, Volkmann D, Leach SB, Smith BF, McIntosh M, Duan D (2011) Age-matched comparison reveals early electrocardiography and echocardiography changes in dystrophin-deficient dogs. Neuromuscular Disorders 21:453-461.

Fletcher S, Honeyman K, Fall AM, Harding PL, Johnsen RD, Steinhaus JP, Moulton HM, Iversen PL, Wilton SD (2007) Morpholino oligomer–mediated exon skipping averts the onset of dystrophic pathology in the mdx mouse. Molecular Therapy 15:1587-1592.

Folland JP, Mc Cauley TM, Williams AG (2008) Allometric scaling of strength measurements to body size. European Journal of Applied Physiology 102:739-745.

Frankel KA, Rosser RJ (1976) The pathology of the heart in progressive muscular dystrophy: epimyocardial fibrosis. Human Pathology 7:375-386.

Gautam M, Noakes PG, Mudd J, Nichol M, Chu GC, Sanes JR, Merlie JP (1995) Failure of postsynaptic specialization to develop at neuromuscular junctions of rapsyn-deficient mice. Nature 377:232.

Gautam M, Noakes PG, Moscoso L, Rupp F, Scheller RH, Merlie JP, Sanes JR (1996) Defective neuromuscular synaptogenesis in agrin-deficient mutant mice. Cell 85:525-535.

Georgiou J, Robitaille R, Charlton MP (1999) Muscarinic control of cytoskeleton in perisynaptic glia. The Journal of Neuroscience 19:3836-3846.

Gilbert R, Nalbantoglu J, Petrof BJ, Ebihara S, Guibinga G-H, Tinsley JM, Kamen A, Massie B, Davies KE, Karpati G (1999) Adenovirus-mediated utrophin gene transfer mitigates the dystrophic phenotype of mdx mouse muscles. Human Gene Therapy 10:1299-1310.

Guido AN, Campos GER, Neto HS, Marques MJ, Minatel E (2010) Fiber Type Composition of the Sternomastoid and Diaphragm Muscles of Dystrophin-Deficient mdx Mice. The Anatomical Record: Advances in Integrative Anatomy and Evolutionary Biology 293:1722-1728.

Gulati AK, Reddi AH, Zalewski A (1983) Changes in the basement membrane zone components during skeletal muscle fiber degeneration and regeneration. The Journal of Cell Biology 97:957-962.

Guo LJ, Soslow JH, Bettis AK, Nghiem PP, Cummings KJ, Lenox MW, Miller MW, Kornegay JN, Spurney CF (2019) Natural History of Cardiomyopathy in Adult Dogs With Golden Retriever Muscular Dystrophy. Journal of the American Heart Association 8:e012443.

Gussoni E, Soneoka Y, Strickland CD, Buzney EA, Khan MK, Flint AF, Kunkel LM, Mulligan RC (1999) Dystrophin expression in the mdx mouse restored by stem cell transplantation. Nature 401:390.

Haddix S, Lee Y, Kornegay J, Thompson W (2018) Cycles of myofiber degeneration and regeneration lead to remodeling of the neuromuscular junction in two mammalian models of Duchenne muscular dystrophy. PloS One 13:e0205926-e0205926.

Hamer P, McGeachie J, Davies M, Grounds M (2002) Evans Blue Dye as an in vivo marker of myofibre damage: optimising parameters for detecting initial myofibre membrane permeability. Journal of Anatomy 200:69-79.

Hara H, Nolan PM, Scott MO, Bucan M, Wakayama Y, Fischbeck KH (2002) Running endurance abnormality in mdx mice. Muscle & Nerve 25:207-211.

Harper SQ, Hauser MA, DelloRusso C, Duan D, Crawford RW, Phelps SF, Harper HA, Robinson AS, Engelhardt JF, Brooks SV, Chamberlain JS (2002) Modular flexibility of dystrophin: Implications for gene therapy of Duchenne muscular dystrophy. Nature Medicine 8:253-261.

Hilton-Brown P, Stålberg E, Trontelj J, Mihelin M (1985) Causes of the increased fiber density in muscular dystrophies studied with single fiber EMG during electrical stimulation. Muscle & Nerve 8:383-388.

Hoffman EP, Brown RH, Kunkel LM (1987) Dystrophin: the protein product of the Duchenne muscular dystrophy locus. Cell 51:919-928.

il Lee Y, Li Y, Mikesh M, Smith I, Nave K-A, Schwab MH, Thompson WJ (2016) Neuregulin1 displayed on motor axons regulates terminal Schwann cell-mediated synapse elimination at developing neuromuscular junctions. Proceedings of the National Academy of Sciences 113:E479-E487.

Jones G, Moore C, Hashemolhosseini S, Brenner HR (1999) Constitutively active MuSK is clustered in the absence of agrin and induces ectopic postsynaptic-like membranes in skeletal muscle fibers. Journal of Neuroscience 19:3376-3383.

Jones RA, Reich CD, Dissanayake KN, Kristmundsdottir F, Findlater GS, Ribchester RR, Simmen MW, Gillingwater TH (2016) NMJ-morph reveals principal components of synaptic morphology influencing structure–function relationships at the neuromuscular junction. Open Biology 6:160240.

Jones RA, Harrison C, Eaton SL, Hurtado ML, Graham LC, Alkhammash L, Oladiran OA, Gale A, Lamont DJ, Simpson H (2017) Cellular and Molecular Anatomy of the Human Neuromuscular Junction. Cell Reports 21:2348-2356.

Kang H, Lichtman JW (2013) Motor axon regeneration and muscle reinnervation in young adult and aged animals. Journal of Neuroscience 33:19480-19491.

Karpati G, Carpenter S, Prescott S (1988) Small-caliber skeletal muscle fibers do not suffer necrosis in mdx mouse dystrophy. Muscle & Nerve 11:795-803.

Khurana TS, Watkins SC, Chafey P, Chelly J, Tomé FM, Fardeau M, Kaplan J-C, Kunkel LM (1991) Immunolocalization and developmental expression of dystrophin related protein in skeletal muscle. Neuromuscular Disorders 1:185-194.

Kim N, Burden SJ (2008) MuSK controls where motor axons grow and form synapses. Nature Neuroscience 11:19.

Kim N, Stiegler AL, Cameron TO, Hallock PT, Gomez AM, Huang JH, Hubbard SR, Dustin ML, Burden SJ (2008) Lrp4 is a receptor for Agrin and forms a complex with MuSK. Cell 135:334-342.

Kong J, Anderson JE (1999) Dystrophin is required for organizing large acetylcholine receptor aggregates. Brain Research 839:298-304.

Kong J, Yang L, Li Q, Cao J, Yang J, Chen F, Wang Y, Zhang C (2012) The absence of dystrophin rather than muscle degeneration causes acetylcholine receptor cluster defects in dystrophic muscle. Neuroreport 23:82-87.

Kornegay JN, Cundiff DD, Bogan DJ, Bogan JR, Okamura CS (2003) The cranial sartorius muscle undergoes true hypertrophy in dogs with golden retriever muscular dystrophy. Neuromuscular Disorders 13:493-500.

Kornegay JN, Bogan DJ, Bogan JR, Childers MK, Cundiff DD, Petroski GF, Schueler RO (1999) Contraction force generated by tarsal joint flexion and extension in dogs with golden retriever muscular dystrophy. Journal of the Neurological Sciences 166:115-121.

Kornegay JN, Bogan JR, Bogan DJ, Childers MK, Li J, Nghiem P, Detwiler DA, Larsen CA, Grange RW, Bhavaraju-Sanka RK (2012) Canine models of Duchenne muscular dystrophy and their use in therapeutic strategies. Mammalian Genome 23:85-108.

Kornegay JN, Bogan DJ, Bogan JR, Dow JL, Wang J, Fan Z, Liu N, Warsing LC, Grange RW, Ahn M (2016) Dystrophin-deficient dogs with reduced myostatin have unequal muscle growth and greater joint contractures. Skeletal Muscle 6:14.

Law PK, Saito A, Fleischer S (1983) Ultrastructural changes in muscle and motor end-plate of the dystrophic mouse. Experimental Neurology 80:361-382.

Lefaucheur JP, Pastoret C, Sebille A (1995) Phenotype of dystrophinopathy in old mdx mice. The Anatomical Record 242:70-76.

Li Y, Thompson WJ (2011) Nerve terminal growth remodels neuromuscular synapses in mice following regeneration of the postsynaptic muscle fiber. Journal of Neuroscience 31:13191-13203.

Li Y, il Lee Y, Thompson WJ (2011) Changes in aging mouse neuromuscular junctions are explained by degeneration and regeneration of muscle fiber segments at the synapse. The Journal of Neuroscience 31:14910-14919.

Li Z, Li Y, Zhang L, Zhang X, Sullivan R, Ai X, Szeto C, Cai A, Liu L, Xiao W (2017) Reduced myocardial reserve in young X-linked muscular dystrophy mice diagnosed by two-dimensional strain analysis combined with stress echocardiography. Journal of the American Society of Echocardiography 30:815-827. e819.

Loring RH, Salpeter MM (1980) Denervation increases turnover rate of junctional acetylcholine receptors. Proceedings of the National Academy of Sciences 77:2293-2297.

Love FM, Thompson WJ (1998) Schwann cells proliferate at rat neuromuscular junctions during development and regeneration. Journal of Neuroscience 18:9376-9385.

Lu QL, Mann CJ, Lou F, Bou-Gharios G, Morris GE, Xue S-a, Fletcher S, Partridge TA, Wilton SD (2003) Functional amounts of dystrophin produced by skipping the mutated exon in the mdx dystrophic mouse. Nature Medicine 9:1009.

Lynch GS, Hinkle RT, Chamberlain JS, Brooks SV, Faulkner JA (2001) Force and power output of fast and slow skeletal muscles from mdx mice 6-28 months old. The Journal of Physiology 535:591-600.

Lyons P, Slater C (1991) Structure and function of the neuromuscular junction in young adultmdx mice. Journal of Neurocytology 20:969-981.

Mann CJ, Honeyman K, Cheng AJ, Ly T, Lloyd F, Fletcher S, Morgan JE, Partridge TA, Wilton SD (2001) Antisense-induced exon skipping and synthesis of dystrophin in the mdx mouse. Proceedings of the National Academy of Sciences 98:42-47.

Marques MJ, Conchello J-A, Lichtman JW (2000) From plaque to pretzel: fold formation and acetylcholine receptor loss at the developing neuromuscular junction. Journal of Neuroscience 20:3663-3675.

Marques MJ, Taniguti APT, Minatel E, Neto HS (2007) Nerve terminal contributes to acetylcholine receptor organization at the dystrophic neuromuscular junction of mdx mice. The Anatomical Record 290:181-187.

Marshall LM, Sanes JR, McMahan U (1977) Reinnervation of original synaptic sites on muscle fiber basement membrane after disruption of the muscle cells. Proceedings of the National Academy of Sciences 74:3073-3077.

Martin A (1994) Amplification of neuromuscular transmission by postjunctional folds. Proceedings of the Royal Society of London Series B: Biological Sciences 258:321-326.

Mavrogeni S, Papavasiliou A, Spargias K, Constandoulakis P, Papadopoulos G, Karanasios E, Georgakopoulos D, Kolovou G, Demerouti E, Polymeros S (2010) Myocardial inflammation in Duchenne Muscular Dystrophy as a precipitating factor for heart failure: a prospective study. BMC Neurology 10:33.

McGeachie JK, Grounds MD, Partridge TA, Morgan JE (1993) Age-related changes in replication of myogenic cells in mdx mice: quantitative autoradiographic studies. Journal of the Neurological Sciences 119:169-179.

McMahan U (1990) The agrin hypothesis. In: Cold Spring Harbor symposia on quantitative biology, pp 407-418: Cold Spring Harbor Laboratory Press.

McNally EM (2007) New approaches in the therapy of cardiomyopathy in muscular dystrophy. Annu Rev Med 58:75-88.

Minatel E, Neto HS, Marques MJ (2003) Acetylcholine receptor distribution and synapse elimination at the developing neuromuscular junction of mdx mice. Muscle & Nerve 28:561-569.

Misgeld T, Kummer TT, Lichtman JW, Sanes JR (2005) Agrin promotes synaptic differentiation by counteracting an inhibitory effect of neurotransmitter. Proceedings of the National Academy of Sciences 102:11088-11093.

Moens P, Baatsen P, Maréchal G (1993) Increased susceptibility of EDL muscles from mdx mice to damage induced by contractions with stretch. Journal of Muscle Research & Cell Motility 14:446-451.

Moise NS, Valentine BA, Brown CA, Erb HN, Beck KA, Cooper BJ, Gilmour RF (1991) Duchenne's cardiomyopathy in a canine model: electrocardiographic and echocardiographic studies. Journal of the American College of Cardiology 17:812-820.

Moransard M, Borges LS, Willmann R, Marangi PA, Brenner HR, Ferns MJ, Fuhrer C (2003) Agrin regulates rapsyn interaction with surface acetylcholine receptors, and this underlies cytoskeletal anchoring and clustering. Journal of Biological Chemistry 278:7350-7359.

Nagel A, Lehmann-Horn F, Engel AG (1990) Neuromuscular transmission in the mdx mouse. Muscle & Nerve 13:742-749.

Nguyen F, Cherel Y, Guigand L, Goubault-Leroux I, Wyers M (2002a) Muscle lesions associated with dystrophin deficiency in neonatal golden retriever puppies. Journal of Comparative Pathology 126:100-108.

Nguyen QT, Sanes JR, Lichtman JW (2002b) Pre-existing pathways promote precise projection patterns. Nature Neuroscience 5:861.

Nigro G, Comi L, Politano L, Bain R (1990) The incidence and evolution of cardiomyopathy in Duchenne muscular dystrophy. International Journal of Cardiology 26:271-277.

Oda K (1984) Age changes of motor innervation and acetylcholine receptor distribution on human skeletal muscle fibres. Journal of the Neurological Sciences 66:327-338.

Ogata H, Nakatani S, Ishikawa Y, Negishi A, Kobayashi M, Ishikawa Y, Minami R (2007) Myocardial strain changes in Duchenne muscular dystrophy without overt cardiomyopathy. International Journal of Cardiology 115:190-195.

Okada K, Inoue A, Okada M, Murata Y, Kakuta S, Jigami T, Kubo S, Shiraishi H, Eguchi K, Motomura M (2006) The muscle protein Dok-7 is essential for neuromuscular synaptogenesis. Science 312:1802-1805.

Pagel C, Partridge T (1999) Covert persistence of mdx mouse myopathy is revealed by acute and chronic effects of irradiation. Journal of the Neurological Sciences 164:103-116.

Passamano L, Taglia A, Palladino A, Viggiano E, D'AMBROSIO P, Scutifero M, Cecio MR, Torre V, De Luca F, Picillo E (2012) Improvement of survival in Duchenne Muscular Dystrophy: retrospective analysis of 835 patients. Acta Myologica 31:121.

Pastoret C, Sebille A (1995) Mdx mice show progressive weakness and muscle deterioration with age. Journal of the Neurological Sciences 129:97-105.

Patton BL, Connolly AM, Martin PT, Cunningham JM, Mehta S, Pestronk A, Miner JH, Sanes JR (1999) Distribution of ten laminin chains in dystrophic and regenerating muscles. Neuromuscular Disorders 9:423-433.

Pellegrino C, Franzini C (1963) An electron microscope study of denervation atrophy in red and white skeletal muscle fibers. The Journal of Cell Biology 17:327-349.

Personius KE, Sawyer RP (2005) Terminal Schwann cell structure is altered in diaphragm of mdx mice. Muscle & Nerve 32:656-663.

Personius KE, Sawyer RP (2006) Variability and failure of neurotransmission in the diaphragm of mdx mice. Neuromuscular Disorders 16:168-177.

Petrof BJ, Shrager JB, Stedman HH, Kelly AM, Sweeney HL (1993) Dystrophin protects the sarcolemma from stresses developed during muscle contraction. Proceedings of the National Academy of Sciences 90:3710-3714.

Popot J-L, Changeux J-P (1984) Nicotinic receptor of acetylcholine: structure of an oligomeric integral membrane protein. Physiological Reviews 64:1162-1239.

Porter JD, Merriam AP, Khanna S, Andrade FH, Richmonds CR, Leahy P, Cheng G, Karathanasis P, Zhou X, Kusner LL (2003) Constitutive properties, not molecular adaptations, mediate extraocular muscle sparing in dystrophic mdx mice. The FASEB Journal 17:893-895.

Pratt SJ, Valencia AP, Le GK, Shah SB, Lovering RM (2015a) Pre-and postsynaptic changes in the neuromuscular junction in dystrophic mice. Frontiers in Physiology 6.

Pratt SJ, Shah SB, Ward CW, Inacio MP, Stains JP, Lovering RM (2013) Effects of in vivo injury on the neuromuscular junction in healthy and dystrophic muscles. The Journal of Physiology 591:559-570.

Pratt SJ, Shah SB, Ward CW, Kerr JP, Stains JP, Lovering RM (2015b) Recovery of altered neuromuscular junction morphology and muscle function in mdx mice after injury. Cellular and Molecular Life Sciences 72:153-164.

Purves D, Sakmann B (1974) Membrane properties underlying spontaneous activity of denervated muscle fibres. The Journal of Physiology 239:125-153.

Quinlan JG, Hahn HS, Wong BL, Lorenz JN, Wenisch AS, Levin LS (2004) Evolution of the mdx mouse cardiomyopathy: physiological and morphological findings. Neuromuscular Disorders 14:491-496.

Rando TA (2001) The dystrophin–glycoprotein complex, cellular signaling, and the regulation of cell survival in the muscular dystrophies. Muscle & Nerve 24:1575-1594.

Reddy LV, Koirala S, Sugiura Y, Herrera AA, Ko C-P (2003) Glial cells maintain synaptic structure and function and promote development of the neuromuscular junction in vivo. Neuron 40:563-580.

Rich M, Lichtman JW (1989a) Motor nerve terminal loss from degenerating muscle fibers. Neuron 3:677-688.

Rich MM, Lichtman JW (1989b) In vivo visualization of pre-and postsynaptic changes during synapse elimination in reinnervated mouse muscle. Journal of Neuroscience 9:1781-1805.

Roth DM, Swaney JS, Dalton ND, Gilpin EA, Ross Jr J (2002) Impact of anesthesia on cardiac function during echocardiography in mice. American Journal of Physiology-Heart and Circulatory Physiology 282:H2134-H2140.

Rousse I, Robitaille R (2006) Calcium signaling in Schwann cells at synaptic and extra-synaptic sites: Active glial modulation of neuronal activity. Glia 54:691-699.

Ruegg MA, Tsim KW, Horton SE, Kröger S, Escher G, Gensch EM, McMahan U (1992) The agrin gene codes for a family of basal lamina proteins that differ in function and distribution. Neuron 8:691-699.

Sacco A, Mourkioti F, Tran R, Choi J, Llewellyn M, Kraft P, Shkreli M, Delp S, Pomerantz JH, Artandi SE (2010) Short telomeres and stem cell exhaustion model Duchenne muscular dystrophy in mdx/mTR mice. Cell 143:1059-1071.

Salpeter MM, Harris R (1983) Distribution and turnover rate of acetylcholine receptors throughout the junction folds at a vertebrate neuromuscular junction. The Journal of Cell Biology 96:1781-1785.

Samuel MA, Valdez G, Tapia JC, Lichtman JW, Sanes JR (2012) Agrin and synaptic laminin are required to maintain adult neuromuscular junctions.

Sanders DB, Stålberg EV (1996) AAEM minimonograph# 25: Single-fiber electromyography. Muscle & Nerve 19:1069-1083.

Sanes JR, Lichtman JW (1999) Development of the vertebrate neuromuscular junction. Annual Review of Neuroscience 22:389-442.

Sanes JR, Schachner M, Covault J (1986) Expression of several adhesive macromolecules (N-CAM, L1, J1, NILE, uvomorulin, laminin, fibronectin, and a heparan sulfate proteoglycan) in embryonic, adult, and denervated adult skeletal muscle. The Journal of Cell Biology 102:420-431.

Selvan VA (2011) Single-fiber EMG: A review. Annals of Indian Academy of Neurology 14:64.

Sharp N, Kornegay J, Van Camp S, Herbstreith M, Secore S, Kettle Sa, Hung W-Y, Constantinou C, Dykstra M, Roses A (1992) An error in dystrophin mRNA processing in golden retriever muscular dystrophy, an animal homologue of Duchenne muscular dystrophy. Genomics 13:115-121.

Sicinski P, Geng Y, Ryder-Cook AS, Barnard EA, Darlison MG, Barnard PJ (1989) The molecular basis of muscular dystrophy in the mdx mouse: a point mutation. Science 244:1578-1581.

Slater C, Lyons P, Walls T, Fawcett P, Young C (1992) Structure and function of neuromuscular junctions in the vastus lateralis of man. Brain 115:451-478.

Slater CR (1990) The basal lamina and stability of the mammalian neuromuscular junction. Prog Brain Res 84:73-81.

Slater CR (2008) Structural factors influencing the efficacy of neuromuscular transmission. Annals of the New York Academy of Sciences 1132:1-12.

Smith IW, Mikesh M, Il Lee Y, Thompson WJ (2013) Terminal Schwann cells participate in the competition underlying neuromuscular synapse elimination. Journal of Neuroscience 33:17724-17736.

Soltanzadeh P, Friez MJ, Dunn D, von Niederhausern A, Gurvich OL, Swoboda KJ, Sampson JB, Pestronk A, Connolly AM, Florence JM (2010) Clinical and genetic characterization of manifesting carriers of DMD mutations. Neuromuscular Disorders 20:499-504.

Son Y-J, Thompson WJ (1995) Schwann cell processes guide regeneration of peripheral axons. Neuron 14:125-132.

Spurney C, Yu Q, Nagaraju K (2011) Speckle tracking analysis of the left ventricular anterior wall shows significantly decreased relative radial strain patterns in dystrophin deficient mice after 9 months of age. PLoS Currents 3.

Stålberg E (2004) Clinical Neurophysiology of disorders of muscle and neuromuscular junction, including fatigue.

Stedman H, Sweeney H, Shrager J, Maguire H, Panettieri R, Petrof Ba, Narusawa M, Leferovich J, Sladky J, Kelly A (1991) The mdx mouse diaphragm reproduces the degenerative changes of Duchenne muscular dystrophy. Nature 352:536.

Strack S, Petersen Y, Wagner A, Röder IV, Albrizio M, Reischl M, Wacker IU, Wilhelm C, Rudolf R (2011) A novel labeling approach identifies three stability levels of acetylcholine receptors in the mouse neuromuscular junction in vivo. PLoS One 6:e20524.

Tanabe Y, Esaki K, Nomura T (1986) Skeletal muscle pathology in X chromosome-linked muscular dystrophy (mdx) mouse. Acta Neuropathologica 69:91-95.

Tegeler CJ, Grange RW, Bogan DJ, Markert CD, Case D, Kornegay JN, Childers MK (2010) Eccentric contractions induce rapid isometric torque drop in dystrophin-deficient dogs. Muscle & Nerve 42:130-132.

Terada M, Lan YB, Kawano F, Ohira T, Higo Y, Nakai N, Imaizumi K, Ogura A, Nishimoto N, Adachi Y (2010) Myonucleus-related properties in soleus muscle fibers of mdx mice. Cells Tissues Organs 191:248-259.

Theroux MC, Olivant A, Akins RE (2008) C Histomorphology of neuromuscular junction in Duchenne muscular dystrophy. Pediatric Anesthesia 18:256-259.

Thesleff S, Ward M (1975) Studies on the mechanism of fibrillation potentials in denervated muscle. The Journal of Physiology 244:313-323.

Tinsley J, Deconinck N, Fisher R, Kahn D, Phelps S, Gillis J-M, Davies K (1998) Expression of full-length utrophin prevents muscular dystrophy in mdx mice. Nature Medicine 4:1441.

Valdez G, Tapia JC, Kang H, Clemenson GD, Gage F, Lichtman JW, Sanes JR (2010) Attenuation of age-related changes in mouse neuromuscular synapses by caloric restriction and exercise. Proceedings of the National Academy of Sciences 107:14863-14868.

Valentine B, Cummings J, Cooper B (1989) Development of Duchenne-type cardiomyopathy. Morphologic studies in a canine model. The American Journal of Pathology 135:671.

Valentine BA, Cooper BJ, Cummings JF, deLahunta A (1986) Progressive muscular dystrophy in a golden retriever dog: light microscope and ultrastructural features at 4 and 8 months. Acta Neuropathologica 71:301-310.

Valentine BA, Cooper BJ, de Lahunta A, O'Quinn R, Blue JT (1988) Canine X-linked muscular dystrophy: an animal model of Duchenne muscular dystrophy: clinical studies. Journal of the Neurological Sciences 88:69-81.

van der Pijl EM, van Putten M, Niks EH, Verschuuren JJ, Aartsma-Rus A, Plomp JJ (2016) Characterization of neuromuscular synapse function abnormalities in multiple Duchenne muscular dystrophy mouse models. European Journal of Neuroscience 43:1623-1635.

van der Pijl EM, van Putten M, Niks EH, Verschuuren JJ, Aartsma-Rus A, Plomp JJ (2018) Low dystrophin levels are insufficient to normalize the neuromuscular synaptic abnormalities of mdx mice. Neuromuscular Disorders 28:427-442.

Van Erp C, Loch D, Laws N, Trebbin A, Hoey AJ (2010) Timeline of cardiac dystrophy in 3–18-month-old MDX mice. Muscle & Nerve 42:504-513.

van Putten M, van der Pijl EM, Hulsker M, Verhaart IE, Nadarajah VD, van der Weerd L, Aartsma-Rus A (2014) Low dystrophin levels in heart can delay heart failure in mdx mice. Journal of Molecular and Cellular Cardiology 69:17-23.

Wada KI, Katsuta S, Soya H (2008) Formation process and fate of the nuclear chain after injury in regenerated myofiber. The Anatomical Record 291:122-128.

Warren GL, Ingalls CP, Shah SJ, Armstrong R (1999) Uncoupling of in vivo torque production from EMG in mouse muscles injured by eccentric contractions. The Journal of Physiology 515:609-619.

Willadt S, Nash M, Slater CR (2016) Age-related fragmentation of the motor endplate is not associated with impaired neuromuscular transmission in the mouse diaphragm. Scientific Reports 6.

Williams MPI, Rigon M, Straka T, Hörner SJ, Gretz N, Hafner M, Reischl M, Rudolf R (2019) A Novel Optical Tissue Clearing Protocol for Mouse Skeletal Muscle to Visualize Endplates in Their Tissue Context. Frontiers in Cellular Neuroscience 13:49.

Wood S, Slater C (1997) The contribution of postsynaptic folds to the safety factor for neuromuscular transmission in rat fast-and slow-twitch muscles. The Journal of Physiology 500:165-176.

Wood SJ, Slater CR (2001) Safety factor at the neuromuscular junction. Progress in Neurobiology 64:393-429.

Wyatt RM, Balice-Gordon RJ (2008) Heterogeneity in Synaptic Vesicle Release at Neuromuscular Synapses of Mice Expressing SynaptopHluorin. The Journal of Neuroscience 28:325-335.

Xu L, Park KH, Zhao L, Xu J, El Refaey M, Gao Y, Zhu H, Ma J, Han R (2016) CRISPR-mediated genome editing restores dystrophin expression and function in mdx mice. Molecular Therapy 24:564-569.

Xu R, Salpeter MM (1997) Acetylcholine Receptors in Innervated Muscles of Dystrophicmdx Mice Degrade as after Denervation. The Journal of Neuroscience 17:8194-8200.

Yang X, Arber S, William C, Li L, Tanabe Y, Jessell TM, Birchmeier C, Burden SJ (2001) Patterning of muscle acetylcholine receptor gene expression in the absence of motor innervation. Neuron 30:399-410.

Yao Y (1988) Maintenance of axon terminals at synaptic sites in the absence of muscle fibers. Current Issues in Neural Regeneration Research:167-178.

Yugeta N, Urasawa N, Fujii Y, Yoshimura M, Yuasa K, Wada MR, Nakura M, Shimatsu Y, Tomohiro M, Takahashi A, Machida N, Wakao Y, Nakamura A, Takeda Si (2006) Cardiac involvement in Beagle-based canine X-linked muscular dystrophy in Japan (CXMDJ): electrocardiographic, echocardiographic, and morphologic studies. BMC Cardiovascular Disorders 6:47.

Yumoto N, Kim N, Burden SJ (2012) Lrp4 is a retrograde signal for presynaptic differentiation at neuromuscular synapses. Nature 489:438.

Zheng M, Pan F, Liu Y, Li Z, Zhou X, Meng X, Liu L, Ge S (2017) Echocardiographic strain analysis for the early detection of myocardial structural abnormality and initiation of drug therapy in a mouse model of dilated cardiomyopathy. Ultrasound in Medicine & Biology 43:2914-2924.

Zong Y, Zhang B, Gu S, Lee K, Zhou J, Yao G, Figueiredo D, Perry K, Mei L, Jin R (2012) Structural basis of agrin–LRP4–MuSK signaling. Genes & Development 26:247-258.

Zuo Y, Lubischer JL, Kang H, Tian L, Mikesh M, Marks A, Scofield VL, Maika S, Newman C, Krieg P (2004) Fluorescent proteins expressed in mouse transgenic lines mark subsets of glia, neurons, macrophages, and dendritic cells for vital examination. Journal of Neuroscience 24:10999-11009.

APPENDIX A

A-1. 3D rotation of P66 mdx NMJ.

https://www.dropbox.com/sh/0qwmxx48u6kxbsn/AABtEe-sNjBvzc6ZdKKTEXo4a?dl=0

URL link above to 3D maximum intensity projection of confocal stack. 0.5 µm gap between collection slices interpolated via ImageJ 3D Projection tool. BTX-1 pseudocolored red. BTX-2 pseudo colored green. DAPI nuclear label pseudocolored gray. Note the occurrence of a central chain of nuclei running within the myofiber directly under the dynamic, fragmented junction

A-2. Significant differences in NMJ categorization following in vivo two- color BTX experiments (P38 WT and mdx).

		Stable		Dynamic		
WT		Continuous	Fragmented	Continuous	Fragmented	Lost
Stable	Continuous		***	***	***	***
	Fragmented			ns	ns	ns
Dynamic	Continuous				ns	ns
	Fragmented					ns

		Stable		Dynamic		
mdx		Continuous	Fragmented	Continuous	Fragmented	Lost
Stable	Continuous		ns	***	ns	***
	Fragmented			***	ns	***
Dynamic	Continuous				***	ns
	Fragmented					***

Comparisons within genotypes. 2-Way ANOVA with Bonferroni post-hoc test. Red boxes indicate redundancy. Black boxes indicate comparisons of the same categories. * $P < 0.05$. ** $P < 0.01$. *** $P < 0.001$.

A-3. Significant differences in NMJ categorization following in vivo two- color BTX experiments (P38 WT myofiber cut damage at the endplate and IC).

WT Internal Control		Stable		Dynamic		
		Continuous	Fragmented	Continuous	Fragmented	Lost
Stable	Continuous		***	***	***	***
	Fragmented			ns	ns	ns
Dynamic	Continuous				ns	ns
	Fragmented					ns

WT Endplate Damage		Stable		Dynamic		
		Continuous	Fragmented	Continuous	Fragmented	Lost
Stable	Continuous		***	***	***	***
	Fragmented			ns	ns	ns
Dynamic	Continuous				*	ns
	Fragmented					***

Comparisons within groups. 2-Way ANOVA with Bonferroni post-hoc test. Red boxes indicate redundancy. Black boxes indicate comparisons of the same categories. * $P < 0.05$. ** $P < 0.01$. *** $P < 0.001$.

A-4. Significant differences in NMJ categorization following in vivo two- color BTX experiments (P38 mdx myofiber crush damage and IC).

mdx Internal Control		Stable		Dynamic		
		Continuous	Fragmented	Continuous	Fragmented	Lost
Stable	Continuous		***	***	**	***
	Fragmented			ns	ns	*
Dynamic	Continuous				***	ns
	Fragmented					***

mdx Endplate Damage		Stable		Dynamic		
		Continuous	Fragmented	Continuous	Fragmented	Lost
Stable	Continuous		ns	ns	***	*
	Fragmented			**	***	***
Dynamic	Continuous				***	ns
	Fragmented					***

Comparisons within groups. 2-Way ANOVA with Bonferroni post-hoc test. Red boxes indicate redundancy. Black boxes indicate comparisons of the same categories. * $P < 0.05$. ** $P < 0.01$. *** $P < 0.001$.

A-5. Significant differences in NMJ categorization following in vivo two-color BTX experiments (P38 mdx denervation and IC).

mdx Internal Control		Stable		Dynamic		
		Continuous	Fragmented	Continuous	Fragmented	Lost
Stable	Continuous		*	*	ns	***
	Fragmented			ns	**	*
Dynamic	Continuous				***	ns
	Fragmented					***

mdx Denervation		Stable		Dynamic		
		Continuous	Fragmented	Continuous	Fragmented	Lost
Stable	Continuous		***	*	*	***
	Fragmented			***	ns	ns
Dynamic	Continuous				***	***
	Fragmented					*

Comparisons within groups. 2-Way ANOVA with Bonferroni post-hoc test. Red boxes indicate redundancy. Black boxes indicate comparisons of the same categories. * $P < 0.05$. ** $P < 0.01$. *** $P < 0.001$.

A-6. M-Mode Echocardiography Measurements.

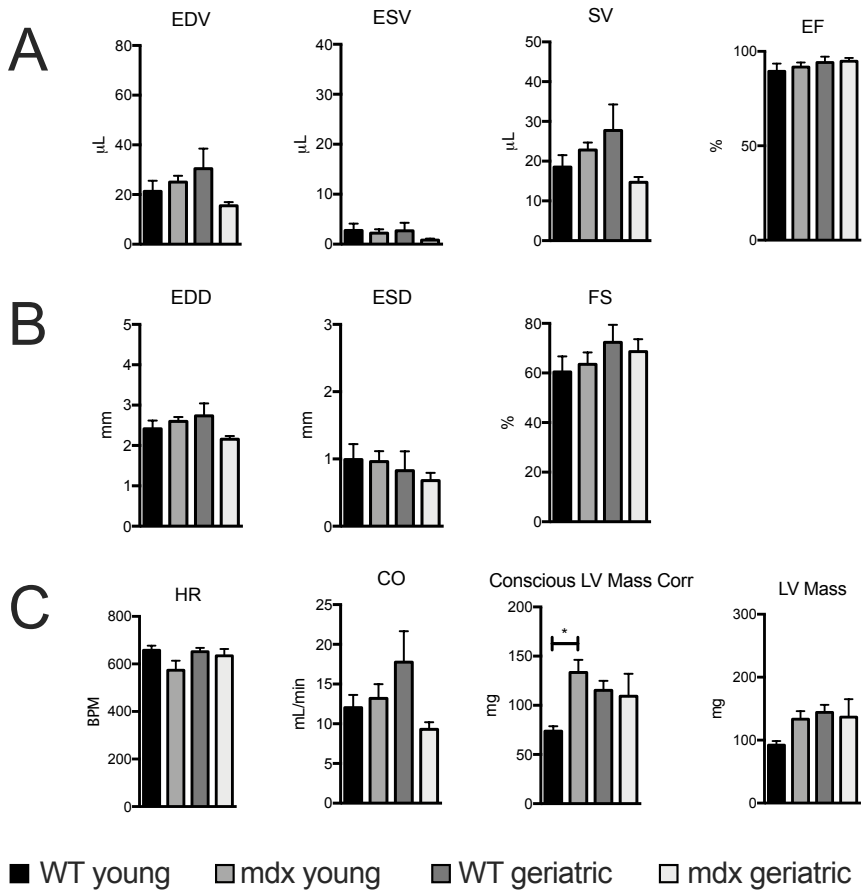

A) Conscious echocardiographic volumetric recordings. EDV - end diastolic volume; ESV - end systolic volume; SV - stroke volume; EF - ejection fraction. B) Conscious echocardiographic diameter recordings. EDD - end diastolic diameter; ESV - end systolic diameter, FS – fractional shortening. C) Conscious echocardiographic function and mass recordings. HR – heart rate; CO – cardiac output; LV Mass Corr – corrected left ventricular mass; LV Mass – left ventricular mass. 1-Way ANOVA, Tukey's post-hoc test. * $P < 0.05$.

A-7. Conscious cardiac strain analysis.

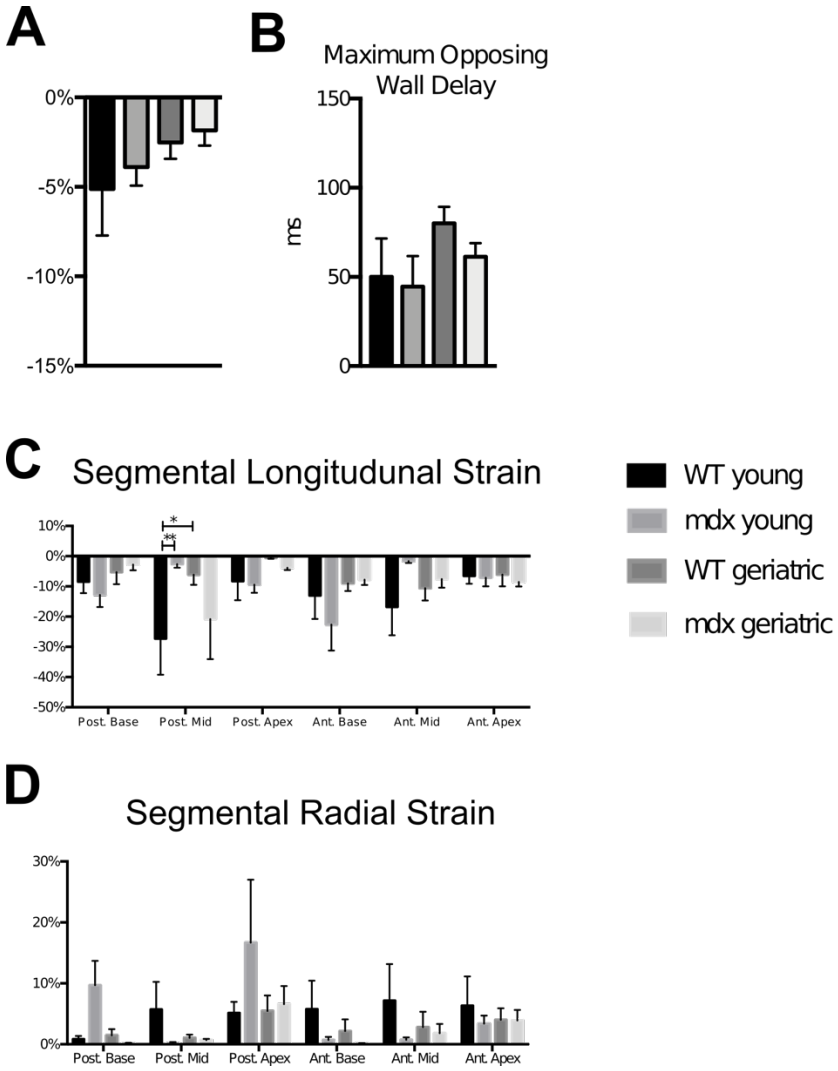

Speckle tracking measurements from conscious WT and mdx mice. A) Global longitudinal strain. B) Desynchrony in left ventricular contraction in terms of peak strain. C) Peak longitudinal strain of the 6 segments. D) Peak radial strain of the 6 segments. A, B) 1-Way ANOVA. Tukey's post-hoc test. C, D) 2-Way ANOVA. Tukey's post-hoc test. Asterisk denote significance. * $P < 0.05$. ** < 0.01.